Geophysical Journal International

Advancing Astronomy and Geophysics

doi: 10.1093/gji/ggab152

Geophys. J. Int. (2021) **226**, 1262–1307 Advance Access publication 2021 April 15 GJI Seismology

Higher-order Hamilton-Jacobi perturbation theory for anisotropic heterogeneous media: dynamic ray tracing in ray-centred coordinates

Einar Iversen, ¹ Bjørn Ursin, ² Teemu Saksala, ³ Joonas Ilmavirta ⁴ and Maarten V. de Hoop ⁵

- ¹University of Bergen, Department of Earth Science, P.O. Box 7803, N-5020 Bergen, Norway. E-mail: einar.iversen@uib.no
- ²Norwegian University of Science and Technology (NTNU), Department of Electronic Systems, O.S. Bragstadsplass 2B, NO-7491 Trondheim, Norway
- ³North Carolina State University, Department of Mathematics, Box 8205, NC State University, Raleigh, NC 27695-8205, USA
- ⁴Tampere University, Unit of Computing Sciences, Kalevantie 4, FI-33014 Tampere University, Finland
- ⁵Rice University, Department of Computational and Applied Mathematics, 6100 Main MS-134, Houston, TX 77005-1892, USA

Accepted 2021 April 13. Received 2021 April 12; in original form 2020 December 22

SUMMARY

Dynamic ray tracing is a robust and efficient method for computation of amplitude and phase attributes of the high-frequency Green's function. A formulation of dynamic ray tracing in Cartesian coordinates was recently extended to higher orders. Extrapolation of traveltime and geometrical spreading was demonstrated to yield significantly higher accuracy—for isotropic as well as anisotropic heterogeneous 3-D models of an elastic medium. This is of value in mapping, modelling and imaging, where kernel operations are based on extrapolation or interpolation of Green's function attributes to densely sampled 3-D grids. We introduce higherorder dynamic ray tracing in ray-centred coordinates, which has certain advantages: (1) such coordinates fit naturally with wave propagation; (2) they lead to a reduction of the number of ordinary differential equations; (3) the initial conditions are simple and intuitive and (4) numerical errors due to redundancies are less likely to influence the computation of the Green's function attributes. In a 3-D numerical example, we demonstrate that paraxial extrapolation based on higher-order dynamic ray tracing in ray-centred coordinates yields results highly consistent with those obtained using Cartesian coordinates. Furthermore, in a 2-D example we show that interpolation of dynamic ray tracing quantities along a wavefront can be done with much better consistency in ray-centred coordinates than in Cartesian coordinates. In both examples we measure consistency by means of constraints on the dynamic ray tracing quantities in the 3-D position space and in the 6-D phase space.

Key words: Numerical approximations and analysis; Numerical modelling; Body waves; Computational seismology; Seismic anisotropy; Wave propagation.

1 INTRODUCTION

Dynamic ray tracing is established in seismology and seismic exploration as a robust and efficient method for computation of amplitude and phase attributes of the high-frequency Green's function (e.g. Červený 1972, 2001; Červený *et al.* 1977, 1984, 2012; Popov & Pšenčík 1978; Červený & Hron 1980; Hanyga 1982; Farra & Madariaga 1987; Gajewski & Pšenčík 1990; Kendall *et al.* 1992; Klimeš 1994; Chapman 2004; Iversen 2004a; Klimeš 2006b; Červený & Moser 2007; Červený & Pšenčík 2010).

The accuracy of the Green's function attributes, in particular regarding traveltime, is key in the construction of an initial velocity model for full-waveform inversion (FWI). Moreover, as shown recently by Djebbi & Alkhalifah (2020), sensitivity kernels computed by dynamic ray tracing can be used in the FWI model update—this is beneficial with respect to the computation speed and the computer memory required to store the Green's function attributes. Another example on the use of ray theory for FWI is Zhou *et al.* (2018), who compute two-way reflection wave paths to update the velocity model.

For the computation of traveltimes only, methods based on the finite-difference solution to the Eikonal equation (e.g. Vidale 1988; Podvin & Lecomte 1991) have been popular due to their simplicity and efficiency. Le Bouteiller *et al.* (2019) describe an efficient and accurate seismic traveltime computation in 3-D anisotropic media by applying the fast-sweeping method to a discontinuous Galerkin based eikonal solver. A limitation of the latter methods, however, is the restriction to compute only the first arrivals. The wavefront construction method (e.g. Vinje *et al.* 1993; Lambaré *et al.* 1996; Gibson *et al.* 2005), which is based on dynamic ray tracing, omits this limitation and provides

an efficient and accurate computation of multi-arrivals in a dense grid of receivers (or image points). On the other hand, the implementation of the method can be challenging.

The dynamic ray tracing quantities, that is the first-order derivatives of perturbations in position and momentum (slowness) with respect to ray parameters at the source, are integrated along a reference ray through a system of ordinary differential equations (ODEs). Dynamic ray tracing is frequently used for *paraxial* computations, which means to obtain wavefield quantities in the vicinity of the reference ray. If we have only one reference ray the paraxial computation is an extrapolation operation—with a system of several reference rays the paraxial computation can be conducted as interpolation.

Dynamic ray tracing in Cartesian coordinates has recently been extended to higher orders (Iversen *et al.* 2019). The motivation is to provide more accurate paraxial computations of the quantities characterizing the high-frequency Green's function: traveltime, geometrical spreading, polarization vectors and so forth. In addition, the higher-order dynamic ray tracing system yields a possibility that does not exist for the leading-order system: to extrapolate the fundamental solution, that is the ray propagator matrix, to a paraxial location.

As follows from the above, dynamic ray tracing has had a role in seismology and seismic exploration for five decades. A classic paper in the history of seismic ray theory is Červený (1972)—it describes kinematic and dynamic ray tracing for arbitrarily anisotropic media, in Cartesian coordinates. Later in the 1970s, one became aware that alternative coordinates could be beneficial with respect to removing the redundancies of the dynamic ray tracing system. In this respect, the introduction of ray-centred coordinates for dynamic ray tracing for isotropic media (Popov & Pšenčík 1978) is a major achievement. From the perspective of differential geometry, ray-centred coordinates are linearized *Fermi coordinates* (e.g. Chavel 2006). To our knowledge, the first report on using ray-centred coordinates for anisotropic media is Kendall *et al.* (1992).

When choosing coordinates for a particular application of dynamic ray tracing, trade-offs are coming into the consideration. With Cartesian coordinates, the dynamic ray tracing system is relatively easy to implement, but on the other hand, there is redundant information in the system, which may yield propagating errors along the reference ray. In ray-centred coordinates, redundancies can be removed and the number of ODEs reduced accordingly. However, with ray-centred coordinates one must include at least one ODE for continuation of the basis vectors along the ray—and, as the subsurface model is often specified in Cartesian coordinates, the method then relies on transformation of spatial derivatives of the model parameters from Cartesian to ray-centred coordinates. This means that the advantage of fewer ODEs can easily be lost in the extra computations required to evaluate the right-hand side of the equations. An additional, important, aspect with respect to computational efficiency is how the evaluation of the ODE's right-hand side is implemented. For an example of in-depth specifications to obtain an optimal implementation, see Vinje *et al.* (1996b).

Concerning which coordinates one should choose for the dynamic ray tracing system, it is not easy to give a straight answer. For many applications the choice of coordinates is not crucial and the results are almost identical—this concerns, for example, forward modelling by classic two-point ray tracing. There are, however, wave propagation and data processing methods for which intrinsic use of ray-centred coordinates would yield added value: We have in mind the methods built directly upon the properties of *wavefronts*. As follows intuitively, it can be very powerful if such methods can use a coordinate system where one coordinate is time and the two other coordinates determine the position on the wavefront.

From the 1970s and onwards a great effort has been invested in the theory of wavefront curvatures of elementary waves pertaining to seismic reflections, referred to by Peter Hubral and colleagues as the *normal wave* (N-wave; exploding reflector wave) and the *normal-incidence point wave* (NIP-wave) (e.g. Hubral 1977; Hubral & Krey 1980; Ursin 1982b; Iversen & Gjøystdal 1984; Bortfeld 1989; Hubral *et al.* 1992, 1993; Iversen 2006a). Later, the pioneering work of Hubral resulted in the common reflection surface (CRS) processing method (Jäger *et al.* 2001; Duveneck 2004; Schleicher *et al.* 2007). Ray-centred coordinates have been essential in the development of the CRS-method—the reason is the close connection between the wavefront curvatures, given in the ray-centred coordinate system, and the *wavefront attributes* (second-order derivatives of traveltime), that can be retrieved from reflection seismic data.

Another example of methods taking advantage of ray-centred coordinates is *wavefront construction* (Vinje *et al.* 1993, 1996a, b). This method is a combination of (1) taking small ray steps from one wavefront to the next and (2) interpolation of kinematic and dynamic ray tracing quantities on the new wavefront to ensure a minimum sampling density before the wavefront is further continued. The dynamic ray tracing step between two consecutive wavefronts can be performed equally well in Cartesian as in ray-centred coordinates, but the latter yield better consistency in the interpolation of the dynamic ray tracing quantities. The degree of *consistency* of the dynamic ray-tracing system along rays and wavefronts is therefore an issue that needs our attention, and to measure it we can use *constraint relations* (Červený 2001).

One of the difficulties with ray-theory based methods is the sampling of the medium. In the wavefront construction method the sampling along the wavefront is adapted as the wavefront is continued. By incorporating higher-order dynamic ray tracing in the wavefront construction method one could allow the ray cells to be wider and still retain the same, high, accuracy. In this way, fewer rays will be needed in the step from one wavefront to the next. Likewise, in areas of the model with only one arrival one could allow the 3-D grid for storage of Green's function attributes to be coarser.

One of the most suitable applications of ray-centred coordinates is time-to-depth mapping—when the coordinate system of the velocity model has one axis corresponding to two-way diffraction time (e.g. Iversen *et al.* 2012). In this case one can estimate a velocity model in depth by the combined use of Dix's (1955) classic method, the concept of the *image ray* (Hubral 1977) and the downward continuation of a dynamic ray tracing system specified in ray-centred coordinates. For references to this combined approach, see, e.g. Hubral & Krey (1980); Cameron *et al.* (2007); Iversen & Tygel (2008); de Hoop *et al.* (2014, 2015).

Motivated by the good results obtained when extending dynamic ray tracing in Cartesian coordinates to higher orders (Iversen *et al.* 2019), we take in this paper yet another step, by introducing higher orders also for dynamic ray tracing in ray-centred coordinates. An important foundation of the paper is the transformation between the ray-centred and the Cartesian phase-space coordinates (Klimeš 1994, 2002b, 2006b), which is also recently developed to higher orders (Iversen *et al.* 2021).

As with the higher-order dynamic ray tracing in Cartesian coordinates (Iversen *et al.* 2019), the corresponding extension for ray-centred coordinates can be useful to many applications in modelling, mapping, processing and imaging (e.g. de Hoop *et al.* 1994; Brandsberg-Dahl *et al.* 2003; Ursin 2004; Iversen 2004b, 2006b; Douma & de Hoop 2006; Stolk & de Hoop 2006; Iversen & Pšenčík 2008). More specifically:

- (i) With the new achievements, it will be possible to do a better, *wavefront consistent*, interpolation of the dynamic ray tracing quantities. This is fundamental in the wavefront construction method (Vinje *et al.* 1993, 1996a, b), and therefore also for applications using it for high-frequency Green's function computation.
- (ii) The new developments have a potential in the modelling and mapping of the elementary (N- and NIP-)waves related to seismic reflections (Iversen 2006a), as well as CRS processing and 'true-amplitude' imaging (Duveneck 2004; Schleicher *et al.* 2007).
- (iii) The higher-order extension is expected to be of particular value in methods where ray-centred coordinates is the most natural choice (e.g. Klimeš 2002a; Goldin & Duchkov 2003; Klimeš 2006a, b; Cameron *et al.* 2007; Iversen & Tygel 2008; de Hoop *et al.* 2014, 2015).

The paper is organized as follows. We start by considering leading-order dynamic ray tracing in ray-centred coordinates, which is based on first-order Hamilton–Jacobi perturbation equations. Thereafter, we derive second- and third-order Hamilton–Jacobi perturbation equations in ray-centred coordinates.

One section is devoted to identify constraints and address intrinsic relations between derivatives of perturbations in ray-centred coordinates. Such relations are important for removal of redundancies from the ODEs for higher-order dynamic ray tracing in ray-centred coordinates. Next, we write transformation formulas between derivatives of perturbations given in ray-centred and Cartesian coordinates, and we provide initial conditions corresponding to a point source and a plane-wave source. In a numerical examples section, we show that paraxial extrapolation based on higher-order dynamic ray tracing in ray-centred coordinates yields results highly consistent with those obtained previously using Cartesian coordinates. We further demonstrate that interpolation of the dynamic ray tracing quantities along a wavefront is achieved with much better consistency in ray-centred coordinates than in Cartesian coordinates. Appendices A–E describe details of the derivations, under the assumption of a homogeneous Hamiltonian of degree two in the momentum components. Appendix F addresses the generalization of the higher-order dynamic ray-tracing equations to an arbitrary degree of the Hamiltonian.

Notes on the nomenclature—We use mostly component notation, but also vector/matrix notation where appropriate. Components of vectors, matrices and tensors are specified by lower- and uppercase subscript indices. The lowercase indices a, b, c, \ldots, p, q run from 1 to 3, unless noted otherwise, while the uppercase indices A, B, C, \ldots, P, Q have only the values 1, 2. The indices r, s, t, \ldots run from 1 to 6; their (reduced) uppercase versions only take the four values 1, 2, 4, 5. For equations in component notation we use Einstein's summation convention. The symbol \dagger is used to signify components of an inverse matrix, $\mathcal{B}^{-1} = \{\mathcal{B}_{ij}^{\dagger}\}$. For overview of the mathematical symbols used in the paper, see Tables 1–5. Explicit results from Iversen *et al.* (2021) are summarized in Tables 6–7.

2 LEADING-ORDER DYNAMIC RAY TRACING IN RAY-CENTRED COORDINATES

In this section, we derive systems for leading-order dynamic ray tracing in ray-centred coordinates pertaining to arbitrarily anisotropic media. The derivations are done directly from a Hamilton–Jacobi equation given in ray-centred coordinates. One novelty aspect of this section is that we use a fully general formulation for the continuation of basis vectors along the reference ray.

We consider a reference ray Ω with traveltime τ as the monotonous variable along the ray. In Cartesian coordinates, phase-space locations along Ω are described by the six-component vector function $\hat{\mathbf{w}}(\tau)$, which represents the concatenation of the position and slowness (momentum) vector functions $\hat{\mathbf{x}}(\tau)$ and $\hat{\mathbf{p}}(\tau)$. When taking the time derivative of $\hat{\mathbf{x}}$ and $\hat{\mathbf{p}}$ along Ω we obtain the *ray-velocity vector* $\mathbf{v} = d\hat{\mathbf{x}}/d\tau$ and the *eta vector* $\mathbf{\eta} = d\hat{\mathbf{p}}/d\tau$. The *phase-velocity vector* along the ray is $\mathbf{c} = c^2\hat{\mathbf{p}}$, where c is the (scalar) phase velocity.

2.1 Ray-centred coordinates

We give a brief review of the concept ray-centred coordinates. For greater technical detail, see Iversen et al. (2021).

The ray-centred coordinate system (q_1, q_2, q_3) is attached to the chosen reference ray Ω . The q_1 and q_2 coordinates refer to straight axes situated in a plane orthogonal to the slowness vector $\hat{\mathbf{p}}(\tau)$. On Ω we have

$$q_1 = q_2 = 0. (1)$$

The q_3 coordinate is curvilinear and chosen here as the traveltime along Ω , that is $q_3 = \tau$.

In ray-centred coordinates we denote the position vector $\mathbf{q} = (q_i)$ and the momentum vector $\mathbf{p}^{(q)} = (p_i^{(q)})$. The latter is not referred to here as a slowness vector, for the reason that all its components do not have the measurement unit of inverse velocity. The vectors (q_i) and $(p_i^{(q)})$ form the phase space in ray-centred coordinates, $\mathbf{w}^{(q)} = (w_r^{(q)}) = (q_i, p_j^{(q)})$, where all six components vary freely.

Table 1. Basic mathematical symbols used in the paper. For multicomponent quantities the dimensions are specified.

Quantity	Dimension	Description	
(x_1, x_2, x_3)	3	Cartesian coordinate system	
$\mathbf{x} = (x_i)$	3	Position vector of the Cartesian coordinate system	
$\mathbf{p} = (p_i)$	3	Slowness vector (momentum vector) of the Cartesian coordinate system	
$\mathbf{w} = (w_x) = (x_i, p_i)$	6	Phase-space vector of the Cartesian coordinate system	
Ω		Reference ray	
$\mathcal{H}(\mathbf{w})$		Hamiltonian	
\mathcal{N}		Degree of the Hamiltonian	
$\{a_{ijkl}\}$	$3 \times 3 \times 3 \times 3$	Density-normalized elastic moduli	
$\Gamma = \{\Gamma_{ij}\}$	3×3	Christoffel matrix	
G		Eigenvalue of the Christoffel matrix	
τ		Traveltime along the ray Ω	
τ_0		Traveltime at the initial point of the ray Ω	
c		Phase velocity	
$\mathbf{c} = (c_i)$	3	Phase-velocity vector	
$\mathbf{n} = (n_i)$	3	Normalized phase-velocity vector	
$\mathbf{v} = (v_i)$	3	Ray-velocity (group-velocity) vector	
$\eta = (\eta_i)$	3	Derivative of slowness vector p with respect to traveltime τ	
(q_1, q_2, q_3)	3	Ray-centred coordinate system	
$\mathbf{q} = (q_i)$	3	Position vector of the ray-centred coordinate system	
$\mathbf{p}^{(q)} = (p_i^{(q)})$	3	Momentum vector of the ray-centred coordinate system	
$\mathbf{w}^{(q)} = (w_x^{(q)})$ $= (q_i, p_j^{(q)})$	6	Phase-space vector of the ray-centred coordinate system	
$\mathcal{E} = \{\mathcal{E}_{iM}\}$	3 × 2	Contra-variant (paraxial) basis of the ray-centred coordinate system	
$= [\mathbf{e}_1 \ \mathbf{e}_2]$ $\mathcal{F} = \{\mathcal{F}_{iM}\}$	3×2	Co-variant (paraxial) basis of the ray-centred coordinate system	
$\tau(\mathbf{x})$		Traveltime function in Cartesian coordinates	
$\tau(\mathbf{q})$		Traveltime function in ray-centred coordinates	
$\{\widetilde{\mathcal{M}}_{IJ}\}$	2×2	Derivatives of traveltime, ray-centred coordinates, second order	
$\{\mathcal{M}_{IJK}\}$	$2 \times 2 \times 2$	Derivatives of traveltime, ray-centred coordinates, third order	
$\{\mathcal{M}_{IJKL}\}$	$2 \times 2 \times 2 \times 2$	Derivatives of traveltime, ray-centred coordinates, fourth order	
s = (a)	3	Course point	
$\mathbf{s} = (s_i)$ $\mathbf{r} = (r_i)$	3	Source point Receiver resint	
\ ·/	3	Receiver point Traveltime as a function of source–receiver coordinates	
$T(\mathbf{r}, \mathbf{s})$			
$\mathcal{L}(\mathbf{r},\mathbf{s})$		Relative geometrical spreading as a function of	
T	6 × 6	source-receiver coordinates Matrix for recommending desiratives in Hemilton's equations	
J	6 × 6 6 × 6	Matrix for rearranging derivatives in Hamilton's equations	
$\{\Lambda_{xr}\}$	$6 \times 6 \times 6$	Coefficients of phase-space coordinate transformation, ray-centred to Cartesian, first order	
$\{\Lambda_{xrs}\}$		Coefficients of phase-space coordinate transformation, ray-centred to Cartesian, second order	
$\{\Lambda_{xrst}\}$	$6 \times 6 \times 6 \times 6$	Coefficients of phase-space coordinate transformation, ray-centred to Cartesian, third order	
$\mathcal{B} = \{\mathcal{B}_{IJ}\}$	2×2	Matrix describing the deviation of the basis ${\cal E}$ from orthonormality	
$\mathcal{A} = \{\mathcal{A}_{IJ}\}$	2×2	Coefficient matrix, phase-velocity formulation for the derivative $d\mathcal{E}/d\tau$	
$\mathcal{K} = \{\mathcal{K}_{IJ}\}$	2×2	Coefficient matrix, ray-velocity formulation for the derivative $d\mathcal{E}/d\tau$	

Table 2. Mathematical symbols: derivatives of perturbations, Cartesian coordinates. For multicomponent quantities the dimensions are specified.

Quantity	Dimension	Description
$\overline{N_{\gamma}}$		Number of parameters specifying a perturbation of the initial
		phase-space location. Possible values are 1 to 6
(γ_a)	$N_{ u}$	Parameters specifying a perturbation
	•	of the initial phase-space location
$\{X_{ra}\}$	$6 \times N_{\nu}$	First-order derivatives
$\{X_{rab}\}$	$6 \times N_{\nu} \times N_{\nu}$	Second-order derivatives
$\{X_{rabc}\}$	$6 \times N_{\nu} \times N_{\nu} \times N_{\nu}$	Third-order derivatives
$\{Q_{iA}\}, \{P_{iA}\}$	3×2	First-order derivatives, Q-P notation, for $N_{\gamma} = 2$
$\{Q_{iAB}\}, \{P_{iAB}\}$	$3 \times 2 \times 2$	Second-order derivatives, Q-P notation, for $N_{\nu} = 2$
$\{Q_{iABC}\}, \{P_{iABC}\}$	$3 \times 2 \times 2 \times 2$	Third-order derivatives, Q-P notation, for $N_{\nu}=2$
${Q_{ia}} = [{Q_{iA}} \{v_i\}]$	3×3	Extension of 3 \times 2 matrix $\{Q_{iA}\}$ to size 3 \times 3, the
(2)		geometrical spreading matrix

Table 3. Mathematical symbols: derivatives of perturbations, ray-centred coordinates. For multicomponent quantities the dimensions are specified.

Quantity	Dimension	Description
$\mathbf{X}^{(q)} = \{X_{ra}^{(q)}\}$	$6 \times N_{\gamma}$	First-order derivatives
$\bar{\mathbf{X}}^{(q)} = \{X_{Ra}^{(q)}\}$	$4 \times N_{\gamma}$	First-order derivatives, reduced version
$ \begin{aligned} \{X_{rab}^{(q)}\} \\ \{X_{rabc}^{(q)}\} \\ \mathbf{S}^{(q)} &= \{S_{rs}\} \end{aligned} $	$6 \times N_{\gamma} \times N_{\gamma}$	Second-order derivatives
$\{X_{rabc}^{(q)}\}$	$6 \times N_{\gamma} \times N_{\gamma} \times N_{\gamma}$	Third-order derivatives
$\mathbf{S}^{(q)} = \{S_{rs}\}$	6×6	Coefficients of ODEs, first order
$\bar{\mathbf{S}}^{(q)} = \{S_{RS}\}$	4×4	Coefficients of ODEs, first order, reduced version
$\{S_{rst}^{(q)}\}$	$6 \times 6 \times 6$	Main coefficients of ODEs, second order
$\{R_{rst}^{(q)}\}$	$6 \times 6 \times 6$	Additional coefficients of ODEs, second order
$\{S_{rstu}^{(q)}\}$	$6 \times 6 \times 6 \times 6$	Main coefficients of ODEs, third order
$\{R_{rstu}^{(q)}\}$	$6 \times 6 \times 6 \times 6$	Additional coefficients of ODEs, third order
$\delta \bar{\mathbf{w}}^{(q)} = (\delta w_R^{(q)})$	4	Perturbation of the reduced phase-space vector
$\delta \mathbf{w}_0^{(q)} = (\delta w_R^{(q)})_0$	4	Perturbation of the reduced phase-space vector
=(a)		at the initial point on Ω
$\bar{\mathbf{\Pi}}^{(q)}(\tau, \tau_0)$	4×4	Ray propagator matrix
$= \{\Pi_{RS}^{(q)}(\tau, \tau_0)\}\$		
$\{Q_{iA}\}, \{P_{iA}\}$	3×2	First-order derivatives, Q-P notation, for $N_{\gamma} = 2$
$\{Q_{iAB}\}, \{\mathcal{P}_{iAB}\}$	$3 \times 2 \times 2$	Second-order derivatives, Q-P notation, for $N_{\gamma} = 2$
$\{Q_{iABC}\}, \{\mathcal{P}_{iABC}\}$	$3 \times 2 \times 2 \times 2$	Third-order derivatives, Q-P notation, for $N_{\gamma} = 2$
$\{\Psi_{RS}\}, \{\Phi_{RS}\}$	4×4	Auxiliary matrices of the ODEs, second-order

Table 4. Mathematical symbols: derivatives of the Hamiltonian, Cartesian coordinates. For multicomponent quantities the dimensions are specified.

Quantity	Dimension	Description
$\mathcal{H}_{,r}$	6	First-order derivatives
$\{\mathcal{H}_{,rs}\}$	6×6	Second-order derivatives
$\{\mathcal{H}_{,rst}\}$	$6 \times 6 \times 6$	Third-order derivatives
$\{\mathcal{H}_{,rstu}\}$	$6 \times 6 \times 6 \times 6$	Fourth-order derivatives
$\{U_{ij}\}$	3×3	Derivatives with respect to position, second order
$\{U_{ijk}\}$	$3 \times 3 \times 3$	Derivatives with respect to position, third order
$\{U_{ijkl}\}$	$3 \times 3 \times 3 \times 3$	Derivatives with respect to position, fourth order
$\{V_{ij}\}$	3 × 3	Derivatives with respect to momentum, second order—the wave-propagation metric tensor
$\{V_{ijk}\}$	$3 \times 3 \times 3$	Derivatives with respect to momentum, third order
$\{V_{iikl}\}$	$3 \times 3 \times 3 \times 3$	Derivatives with respect to momentum, fourth order
$\{W_{ij}^{12} = \partial^2 \mathcal{H} / \partial x_i \partial p_j\}$	3 × 3	Derivatives with respect to position/momentum, second order
$\{W_{ijk}^{\ 112}\}$	$3 \times 3 \times 3$	Derivatives with respect to position/momentum,
$= \partial^3 \mathcal{H} / \partial x_i \partial x_j \partial p_k $		third order
$\{W_{ijk}^{122}\}$	$3 \times 3 \times 3$	Derivatives with respect to position/momentum,
$= \partial^3 \mathcal{H} / \partial x_i \partial p_j \partial p_k $		third order
$\{W_{ijkl}^{\ 1112}$	$3 \times 3 \times 3 \times 3$	Derivatives with respect to position/momentum,
$= \partial^4 \mathcal{H} / \partial x_i \partial x_j \partial x_k \partial p_l $		fourth order
$\{W_{ijkl}^{1122}$	$3 \times 3 \times 3 \times 3$	Derivatives with respect to position/momentum,
$= \partial^4 \mathcal{H} / \partial x_i \partial x_j \partial p_k \partial p_l $		fourth order
$\{W_{ijkl}^{\ 1222}$	$3 \times 3 \times 3 \times 3$	Derivatives with respect to position/momentum,
$= \partial^4 \mathcal{H} / \partial x_i \partial p_j \partial p_k \partial p_l $		fourth order

On the ray Ω the momentum vector components in ray-centred coordinates are

$$p_I^{(q)} = 0, p_3^{(q)} = 1,$$
 (2)

see the initial discussion on the momentum vector in ray-centred coordinates in Iversen *et al.* (2021). Moreover, contra-variant basis vectors denoted \mathbf{e}_1 and \mathbf{e}_2 are assigned, respectively, to the q_1 and q_2 coordinates; the components of these vectors form a 3 × 2 matrix $\mathcal{E} = \{\mathcal{E}_{iM}\}$. The corresponding co-variant basis vectors, denoted \mathbf{f}_1 and \mathbf{f}_2 , form the 3 × 2 matrix $\mathcal{F} = \{\mathcal{F}_{iM}\}$. The matrices \mathcal{E} and \mathcal{F} satisfy the relations

$$\mathcal{E}_{iM}p_i = 0, \qquad \mathcal{F}_{iM}v_i = 0, \tag{3}$$

along the ray Ω . Eq. (3) means that the momentum direction is orthogonal to the directions given by the basis vectors \mathbf{e}_1 and \mathbf{e}_2 . Similar for the ray-velocity vector—it is orthogonal to the vectors \mathbf{f}_1 and \mathbf{f}_2 .

Table 5. Mathematical symbols: derivatives of the Hamiltonian, ray-centred coordinates. For multicomponent quantities the dimensions are specified.

Quantity	Dimension	Description
$\overline{\{\mathcal{H}_{,r}^{(q)}\}}$	6	First-order derivatives
$\{\mathcal{H}_{,rs}^{(q)}\}$	6×6	Second-order derivatives
$\{\mathcal{H}_{,rst}^{(q)}\}$	$6 \times 6 \times 6$	Third-order derivatives
$\{\mathcal{H}_{.rstu}^{(q)}\}$	$6 \times 6 \times 6 \times 6$	Fourth-order derivatives
$\{U_{ij}^{(q)}\}$	3×3	Derivatives with respect to position, second order
$\{U_{ijk}^{(q)}\}$	$3 \times 3 \times 3$	Derivatives with respect to position, third order
$\{U_{iikl}^{(q)}\}$	$3 \times 3 \times 3 \times 3$	Derivatives with respect to position, fourth order
$\{\mathcal{H}_{rst}^{(q)}\}$ $\{\mathcal{H}_{rst}^{(q)}\}$ $\{\mathcal{H}_{ij}^{(q)}\}$ $\{U_{ij}^{(q)}\}$ $\{U_{ijk}^{(q)}\}$ $\{U_{ijk}^{(q)}\}$ $\{V_{ijk}^{(q)}\}$	3 × 3	Derivatives with respect to momentum, second order — the wave-propagation metric tensor
$\{V_{ijk}^{(q)}\}$	$3 \times 3 \times 3$	Derivatives with respect to momentum, third order
$\{V_{ijkl}^{(q)}\}$	$3 \times 3 \times 3 \times 3$	Derivatives with respect to momentum, fourth order
$ \begin{cases} V_{ijk}^{(q)} \\ V_{ijkl}^{(q)} \end{cases} $ $ \{W_{ij}^{(q)}\}^{12} = \partial^2 \mathcal{H} / \partial q_i \partial p_j^{(q)} \} $	3 × 3	Derivatives with respect to position/momentum, second order
$\{W_{ijk}^{(q) \ 112} = \partial^3 \mathcal{H} / \partial q_i \partial q_j \partial p_k^{(q)}\}$	$3 \times 3 \times 3$	Derivatives with respect to position/momentum, third order
	$3 \times 3 \times 3$	Derivatives with respect to position/momentum,
$\{W_{ijkl}^{(q) \ 1112}$	$3 \times 3 \times 3 \times 3$	Derivatives with respect to position/momentum,
$= \partial^{4} \mathcal{H} / \partial q_{i} \partial q_{j} \partial q_{k} \partial p_{l}^{(q)} \}$ $\{W_{ijkl}^{(q)}\}_{ijkl}^{1122}$	$3 \times 3 \times 3 \times 3$	fourth order Derivatives with respect to position/momentum,
$= \frac{\partial^4 \mathcal{H}}{\partial q_i \partial q_j \partial p_k^{(q)} \partial p_l^{(q)}} $ $\{W_{ijkl}^{(q) 1222}$ $= \frac{\partial^4 \mathcal{H}}{\partial q_i \partial p_j^{(q)} \partial p_k^{(q)} \partial p_l^{(q)}} $	$3 \times 3 \times 3 \times 3$	fourth order Derivatives with respect to position/momentum, fourth order

Table 6. First- and second-order coefficients of the transformation from raycentred to Cartesian phase-space coordinates.

Quantity	Dimension	Expression
$\{\partial x_i/\partial q_A\}$	3 × 2	\mathcal{E}_{iA}
$\{\partial x_i/\partial q_3\}$	3	v_i
$\{\partial x_i/\partial p_a^{(q)}\}$	3×3	0
$\{\partial p_i/\partial q_A\}$	3×2	$p_i\eta_j\mathcal{E}_{jA}$
$\{\partial p_i/\partial q_3\}$	3	η_i
$\{\partial p_i/\partial p_A^{(q)}\}$	3×2	\mathcal{F}_{iA}
$\{\partial p_i/\partial p_3^{(q)}\}$	3	p_i
$\{\partial^2 x_i/\partial q_A\partial q_B\}$	$3 \times 2 \times 2$	0
$\{\partial^2 x_i/\partial q_A \partial q_3\}$	3×2	$\dot{\mathcal{E}}_{iA}$
$\{\partial^2 x_i/\partial q_3^2\}$	3	\dot{v}_i
$\{\partial^2 x_i/\partial q_j\partial p_a^{(q)}\}$	$3 \times 3 \times 3$	0
$\{\partial^2 x_i/\partial p_i^{(q)}\partial p_a^{(q)}\}$	$3 \times 3 \times 3$	0
$\{\partial^2 p_i/\partial q_A \partial q_B\}$	$3 \times 2 \times 2$	$2 p_i \eta_j \eta_k \mathcal{E}_{jA} \mathcal{E}_{kB}$
$\{\partial^2 p_i/\partial q_3^2\}$	3	η_i
$\{\partial^2 p_i/\partial q_A \partial q_3\}$	3×2	$\mathrm{d}/\mathrm{d}\tau(p_i\eta_j\mathcal{E}_{jA})$
$\{\partial^2 p_i/\partial p_i^{(q)}\partial p_k^{(q)}\}$	$3 \times 3 \times 3$	0
$\{\partial^2 p_i/\partial q_A \partial p_B^{(q)}\}$	$3 \times 2 \times 2$	$-p_i\mathcal{K}_{AB}$
$\{\partial^2 p_i/\partial q_A \partial p_3^{\overline{(q)}}\}$	3×2	$p_i\eta_j\mathcal{E}_{jA}$
$\{\partial^2 p_i/\partial q_3\partial p_A^{(q)}\}$	3×2	$\dot{\mathcal{F}}_{iA}$
$\{\partial^2 p_i/\partial q_3\partial p_3^{(q)}\}$	3	η_i

2.2 Continuation of contra-variant basis vectors along the reference ray

Klimeš (2006b) provides a fundamental treatment of the continuation of the bases of ray-centred coordinates along a certain reference ray, Ω . Iversen *et al.* (2021) obtain two equivalent sets of ODEs for the contra-variant basis \mathcal{E} —the *phase-velocity formulation*

$$\frac{\mathrm{d}\mathcal{E}_{nI}}{\mathrm{d}\tau} = \mathcal{E}_{nL}\mathcal{A}_{LI} - c_n\eta_k\mathcal{E}_{kI},\tag{4}$$

Table 7. Third- and fourth-order coefficients of the transformation from ray-centred to Cartesian phase-space coordinates. Some trivial expressions are excluded.

Quantity	Dimension	Expression
$\{\partial^3 x_i/\partial q_A \partial q_3^2\}$	3 × 2	$\ddot{\mathcal{E}}_{iA}$
$\{\partial^3 x_i/\partial q_3^3\}$	3	\ddot{v}_i
$\{\partial^3 p_i/\partial q_A \partial q_B \partial q_C\}$	$3 \times 2 \times 2 \times 2$	$6 p_i \eta_j \eta_k \eta_l \mathcal{E}_{jA} \mathcal{E}_{kB} \mathcal{E}_{lC}$
$\{\partial^3 p_i/\partial q_A \partial q_B \partial q_3\}$	$3 \times 2 \times 2$	$2 d/d\tau (p_i \eta_j \eta_k \mathcal{E}_{jA} \mathcal{E}_{kB})$
$\{\partial^3 p_i/\partial q_A \partial q_3^2\}$	3×2	$d^2/d\tau^2 (p_i \eta_j \mathcal{E}_{jA})$
$\{\partial^3 p_i/\partial q_3^3\}$	3	$\ddot{\eta_i}$
$\{\partial^3 p_i/\partial q_A \partial q_B \partial p_C^{(q)}\}$	$3 \times 2 \times 2 \times 2$	$-p_i\eta_j\left(\mathcal{E}_{jA}\mathcal{K}_{BC}+\mathcal{E}_{jB}\mathcal{K}_{AC}\right)$
$\{\partial^3 p_i/\partial q_A \partial q_B \partial p_3^{(q)}\}$	$3 \times 2 \times 2$	$2 p_i \eta_j \eta_k \mathcal{E}_{jA} \mathcal{E}_{kB}$
$\{\partial^3 p_i/\partial q_3\partial q_A\partial p_B^{(q)}\}$	$3 \times 2 \times 2$	$-\mathrm{d}/\mathrm{d} au~(p_i~\mathcal{K}_{AB})$
$\{\partial^3 p_i/\partial q_3\partial q_A\partial p_3^{(q)}\}$	3×2	$\mathrm{d}/\mathrm{d} au\left(p_{i}\eta_{j}\mathcal{E}_{jA} ight)$
$\{\partial^3 p_i/\partial q_3^2 \partial p_A^{(q)}\}$	3×2	$\ddot{\mathcal{F}}_{iA}$
$\{\partial^3 p_i/\partial q_3^2 \partial p_3^{(q)}\}$	3×2	$\dot{\eta_i}$
$\{\partial^4 x_i/\partial q_A \partial q_4^2\}$	3×2	$d^3/d\tau^3 (\mathcal{E}_{iA})$
$\{\partial^4 x_i/\partial q_3^4\}$	3	$d^3/d\tau^3(v_i)$
$\{\partial^4 p_i/\partial q_A \partial q_B \partial q_C \partial q_D\}$	$3 \times 2 \times 2 \times 2 \times 2$	$24 p_i \eta_j \eta_k \eta_l \eta_m \mathcal{E}_{jA} \mathcal{E}_{kB} \mathcal{E}_{lC} \mathcal{E}_{mD}$
$\{\partial^4 p_i/\partial q_A \partial q_B \partial q_C \partial p_D^{(q)}\}$	$3 \times 2 \times 2 \times 2 \times 2$	$-2 p_i \eta_j \eta_k (\mathcal{E}_{jA} \mathcal{E}_{kB} \mathcal{K}_{CD} + \mathcal{E}_{jA} \mathcal{E}_{kC} \mathcal{K}_{BD} + \mathcal{E}_{jB} \mathcal{E}_{kC} \mathcal{K}_{AD})$
	•••	

and the ray-velocity formulation

$$\frac{\mathrm{d}\mathcal{E}_{nI}}{\mathrm{d}\tau} = \mathcal{E}_{nL}\mathcal{K}_{IL} - v_n \eta_k \mathcal{E}_{kI}.\tag{5}$$

Eq. (5) is equivalent to Klimeš (2006b, eq. 25).

Eq. (4) makes use of two 2×2 matrices \mathcal{A} and \mathcal{B} , with components

$$\mathcal{A}_{IJ} = \mathcal{B}_{IK}^{\dagger} \mathcal{E}_{mK} \frac{\mathrm{d} \mathcal{E}_{mJ}}{\mathrm{d} \tau},\tag{6}$$

$$\mathcal{B}_{IJ} = \mathcal{E}_{mI} \mathcal{E}_{mJ}. \tag{7}$$

If matrix \mathcal{A} equals the zero matrix the basis \mathcal{E} is determined entirely by (1) the curvature and torsion of the ray trajectory and (2) the initial condition for \mathcal{E} . Matrix $\mathcal{B} = \mathcal{E}^T \mathcal{E}$ is symmetric. When \mathcal{B} equals the identity matrix the basis \mathcal{E} is orthonormal.

Eq. (5) involves the 2×2 matrix \mathcal{K} (Klimeš 2006b, eq. 24), which has an important role in dynamic ray tracing systems for anisotropic media. It is defined by

$$\mathcal{K}_{IJ} \equiv \frac{\mathrm{d}\mathcal{E}_{nI}}{\mathrm{d}\tau} \mathcal{F}_{nJ} = -\mathcal{E}_{nI} \frac{\mathrm{d}\mathcal{F}_{nJ}}{\mathrm{d}\tau}.$$
 (8)

It is shown in Iversen et al. (2021) that \mathcal{A} , \mathcal{B} and \mathcal{K} are linked through the relation

$$\mathcal{K}_{IJ} = \mathcal{A}_{JI} + \mathcal{E}_{nI} \eta_n v_k \mathcal{E}_{kL} \mathcal{B}_{IJ}^{\dagger}. \tag{9}$$

The *standard option* to dynamic ray tracing in ray-centred coordinates (Červený 2001; Klimeš 2006b, section 5.4; Iversen *et al.* 2021, Appendix A) corresponds to requiring $A_{IJ} = 0$ along the whole ray Ω . This specification yields \mathcal{B}_{IJ} constant along Ω . Hence, if we specify the basis \mathcal{E} orthonormal at the initial point, that is $\mathcal{B}_{IJ} = \delta_{IJ}$, then \mathcal{E} will remain orthonormal along the whole ray. As an example of implementation of the standard option, we refer to the Complete Ray Tracing (CRT) software package (Klimeš 2006c, section 6.2).

When the contra-variant basis \mathcal{E} is known at some point on Ω one can compute the covariant basis \mathcal{F} from an explicit expression. This can also be done the other way around—first integrate \mathcal{F} along Ω and then compute \mathcal{E} by a simple formula. For details, see Iversen *et al.* (2021).

2.3 Hamilton-Jacobi equation

In an arbitrarily anisotropic heterogeneous medium, we consider an elementary P or S wave, which corresponds to a specific eigenvalue $G(\mathbf{x}, \mathbf{p})$ of the Christoffel matrix Γ ,

$$\Gamma_{ik}(\mathbf{x}, \mathbf{p}) = a_{ijkl}(\mathbf{x}) \, p_j \, p_l. \tag{10}$$

Here, a_{ijkl} denotes the tensor of density-normalized elastic moduli.

The foundation of our theoretical development in ray-centred coordinates is given by the Hamilton-Jacobi equation for stationary time,

$$\mathcal{H}(\mathbf{w}^{(q)}) = \text{constant} = \frac{1}{\mathcal{N}},\tag{11}$$

where \mathcal{H} , the *Hamiltonian* is a homogeneous function of degree \mathcal{N} in the momentum components. Eq. (11) yields a constraint in phase space, implying a reduction of the number of degrees of freedom from six to five.

According to Euler's theorem for homogeneous functions we have

$$p_i^{(q)} \frac{\partial \mathcal{H}}{\partial p_i^{(q)}} = \mathcal{N} \mathcal{H}. \tag{12}$$

To make the Hamiltonian satisfy eq. (12) we adopt the approach of Klimeš (2002b, eq. 9),

$$\mathcal{H}(\mathbf{w}^{(q)}) = \frac{1}{\mathcal{N}} \left[G(\mathbf{w}^{(q)}) \right]^{\mathcal{N}/2}, \tag{13}$$

where G is the relevant eigenvalue of the Christoffel matrix (10), expressed in the ray-centred phase-space coordinates. An important property of eq. (13) is that the variable along the ray Ω is traveltime, independently of the value of \mathcal{N} .

In the main text and Appendices A–E of the paper, all derivations are done for a homogeneous Hamiltonian of second degree, $\mathcal{N}=2$, in the momentum components. For some applications, however, a value different from 2 can be more optimal. For example, Bulant & Klimeš (2007) successfully use $\mathcal{N}=-1$ in the context of coupling ray theory for S waves in anisotropic media. In Appendix F the interested reader can find the equations needed to generalize the theory to arbitrary \mathcal{N} .

2.4 Hamilton's equations

In ray-centred coordinates, Hamilton's equations (Hamilton 1837) read

$$\frac{\mathrm{d}q_i}{\mathrm{d}\tau} = \frac{\partial \mathcal{H}}{\partial p_i^{(q)}}, \qquad \frac{\mathrm{d}p_i^{(q)}}{\mathrm{d}\tau} = -\frac{\partial \mathcal{H}}{\partial q_i},\tag{14}$$

or compactly

$$\frac{\mathrm{d}w_r^{(q)}}{\mathrm{d}\tau} = J_{rs} \frac{\partial \mathcal{H}}{\partial w_s^{(q)}},\tag{15}$$

with $\{J_{rs}\} = \mathbf{J}$ as the 6×6 matrix

$$\mathbf{J} = \{J_{rs}\} = \begin{pmatrix} \{0_{ij}\} & \{\delta_{ij}\} \\ -\{\delta_{ij}\} & \{0_{ij}\} \end{pmatrix}. \tag{16}$$

The structure of eqs (12)–(16) is the same in any coordinate system.

It is remarked that eqs (14) are of no value with respect to computing a (reference) ray. The reason is that one has to compute the reference ray before attaching a ray-centred coordinate system to it. The eqs (14) are however useful as a basis for developing dynamic ray tracing systems.

Inserting eqs (2) and (11) in eq. (12) we get, on the ray Ω ,

$$\frac{\partial \mathcal{H}}{\partial p_i^{(q)}} = \delta_{i3}. \tag{17}$$

Moreover, since the momentum vector is constant along Ω , the second subequation of (14) yields

$$\frac{\partial \mathcal{H}}{\partial a} = 0. \tag{18}$$

2.5 System of six Hamilton-Jacobi perturbation equations in ray-centred coordinates

As in Iversen *et al.* (2019) we let perturbations of phase-space locations be dependent on variables contained in a vector $\mathbf{\gamma} = (\gamma_a)$ with dimension (length) N_{γ} . The maximum value of N_{γ} is 6. The variables γ_a describe perturbations in phase space at the initial point, under the assumption of constant initial time, $\tau = \tau_0$. For the reference ray Ω , along which the phase-space perturbations are all zero, the vector $\mathbf{\gamma}$ is constant, signified as $\mathbf{\gamma} = \hat{\mathbf{\gamma}}$.

The quantities γ_a of a particular ray are often referred to as *ray parameters*. When including the variable along the ray, in our case the traveltime τ , we speak of (γ, τ) as the *ray coordinates*. These coordinates yield the points of an arbitrary *paraxial ray*, that is a ray in the vicinity of the reference ray.

Furthermore, to describe perturbed phase-space locations in ray-centred coordinates we introduce the following function of the ray coordinates:

$$w_r^{(q)} = w_r^{(q)}(\boldsymbol{\gamma}, \tau).$$
 (19)

The corresponding function in Cartesian coordinates is written without the superscript (q). In analogy with Iversen et al. (2019, eq. 15) and Klimeš (1994, eq. 27) dynamic ray tracing in ray-centred coordinates then yields the matrix quantity

$$X_{ra}^{(q)}(\tau) = \frac{\partial(\delta w_r^{(q)})}{\partial \gamma_a}(\hat{\boldsymbol{\gamma}}, \tau) = \frac{\partial w_r^{(q)}}{\partial \gamma_a}(\hat{\boldsymbol{\gamma}}, \tau)$$
(20)

as output along Ω . The two forms for $X_{rq}^{(q)}$ in eq. (20) are equivalent, but for clarity reasons we mostly use the expression without the perturbation (δ) symbol.

In complete analogy with the derivation in Cartesian coordinates, we can establish a system of ODEs for continuation of first-order derivatives of phase-space perturbations related to ray-centred coordinates (see also Klimeš 1994, eqs 24 and 28),

$$\frac{\mathrm{d}X_{ra}^{(q)}}{\mathrm{d}\tau}(\tau) = S_{rt}^{(q)}(\tau)X_{ta}^{(q)}(\tau),\tag{21}$$

where

$$S_{rt}^{(q)} = J_{rs} \mathcal{H}_{.st}^{(q)}, \tag{22}$$

and

$$\mathcal{H}_{st}^{(q)} = \frac{\partial^2 \mathcal{H}}{\partial w_s^{(q)} \partial w_s^{(q)}}.$$
 (23)

The second-order derivatives of the Hamiltonian in ray-centred coordinates, $\mathcal{H}_{st}^{(q)}$ are all evaluated on the reference ray. We relate them to corresponding derivatives in Cartesian coordinates,

$$\frac{\partial^2 \mathcal{H}}{\partial w_r^{(q)} \partial w_s^{(q)}} = \frac{\partial^2 \mathcal{H}}{\partial w_x \partial w_y} \frac{\partial w_x}{\partial w_r^{(q)}} \frac{\partial w_y}{\partial w_s^{(q)}} + \frac{\partial \mathcal{H}}{\partial w_x} \frac{\partial^2 w_x}{\partial w_r^{(q)} \partial w_s^{(q)}},\tag{24}$$

$$\mathcal{H}_{rs}^{(q)} = \mathcal{H}_{.xv} \Lambda_{xr} \Lambda_{vs} + \mathcal{H}_{.x} \Lambda_{xrs}. \tag{25}$$

In (25) the Λ -quantities are coefficients of the transformation from ray-centred to Cartesian phase-space coordinates, defined by the convention

$$\Lambda_{xr} \equiv \frac{\partial w_x}{\partial w_r^{(q)}}, \qquad \Lambda_{xrs} \equiv \frac{\partial^2 w_x}{\partial w_r^{(q)} \partial w_s^{(q)}}, \qquad \Lambda_{xrst} \equiv \frac{\partial^3 w_x}{\partial w_r^{(q)} \partial w_s^{(q)} \partial w_r^{(q)}}, \tag{26}$$

and so forth for higher orders. Iversen et al. (2021) derived explicit expressions for all Λ -quantities up to order four of the derivatives—these are listed in Tables 6-7.

2.6 6 x 6 coefficient matrix in ray-centred coordinates

In the Cartesian phase-space coordinates, we assemble the partial second-derivatives of the Hamiltonian in three 3×3 matrices U, V and \mathbf{W}^{12} , with components

$$U_{ij} \equiv \frac{\partial^2 \mathcal{H}}{\partial x_i \partial x_j}, \qquad V_{ij} \equiv \frac{\partial^2 \mathcal{H}}{\partial p_i \partial p_j}, \qquad W_{IJ}^{12} \equiv \frac{\partial^2 \mathcal{H}}{\partial x_i \partial p_j}. \tag{27}$$

Starting with eq. (25) we provide derivations in Appendix A of all second-order partial derivatives of the Hamiltonian with respect to ray-centred phase-space coordinates, that is $\{\mathcal{H}_{rs}^{(q)}\}$. For an equivalent treatment, see the derivation leading to eq. (51) in Klimeš (1994). The evaluated results on the ray Ω are

$$U_{IJ}^{(q)} \equiv \frac{\partial^2 \mathcal{H}}{\partial q_I \partial q_J} = (U_{mn} - \eta_m \eta_n) \, \mathcal{E}_{mI} \mathcal{E}_{nJ}, \tag{28}$$

$$V_{IJ}^{(q)} \equiv \frac{\partial^2 \mathcal{H}}{\partial p_I^{(q)} \partial p_I^{(q)}} = V_{mn} \mathcal{F}_{mI} \mathcal{F}_{nJ}, \tag{29}$$

$$W_{IJ}^{(q) 12} \equiv \frac{\partial^2 \mathcal{H}}{\partial q_I \partial p_I^{(q)}} = W_{mn}^{12} \mathcal{E}_{mI} \mathcal{F}_{nJ} - \mathcal{K}_{IJ}, \tag{30}$$

$$\frac{\partial^2 \mathcal{H}}{\partial q_3 \partial q_j} = 0, \qquad \frac{\partial^2 \mathcal{H}}{\partial q_3 \partial p_j^{(q)}} = 0, \tag{31}$$

$$\frac{\partial^2 \mathcal{H}}{\partial q_3 \partial q_j} = 0, \qquad \frac{\partial^2 \mathcal{H}}{\partial q_3 \partial p_j^{(q)}} = 0,
\frac{\partial^2 \mathcal{H}}{\partial p_3^{(q)} \partial q_J} = 0, \qquad \frac{\partial^2 \mathcal{H}}{\partial p_3^{(q)} \partial p_j^{(q)}} = \delta_{3j}.$$
(31)

Here, the indices I and J can take the values 1, 2. Observe that the quantity \mathcal{K}_{IJ} is defined in eq. (8). Eqs (28)–(32) show that the 6×6 matrix $\{\mathcal{H}_{i,vz}^{(q)}\}$ has the form

$$\{\mathcal{H}_{,yz}^{(q)}\} = \begin{pmatrix} \left\{ U_{IJ}^{(q)} \right\} & \{0_{I1}\} \left\{ W_{IJ}^{(q)} \right\} & \{0_{I1}\} \\ \{0_{1J}\} & 0 & \{0_{1J}\} & 0 \\ \left\{ W_{IJ}^{(q)} \right\}^{T} & \{0_{I1}\} & \left\{ V_{IJ}^{(q)} \right\} & \{0_{I1}\} \\ \{0_{1J}\} & 0 & \{0_{1J}\} & 1 \end{pmatrix}$$

$$(33)$$

when evaluated on Ω . Eq. (33) coincides with Klimeš (1994, eq. 50).

The results in eqs (28)–(32) are very general. The only restrictions applying to the basis vectors \mathbf{e}_1 and \mathbf{e}_2 are (1) that they are not parallel and (2) that they are are both orthogonal to the slowness vector \mathbf{p} on Ω . In the q_1q_2 plane one may eliminate the mixed (ray-centred) position and momentum second derivatives of the Hamiltonian, $W_{IJ}^{(q)}$, by using an option proposed by Klimeš (1994, section 9; 2006b, section 5.6),

$$W_{IJ}^{(q)\,12} = \left(\mathcal{E}_{mI}W_{mn}^{\,12} - \frac{\mathrm{d}\mathcal{E}_{nI}}{\mathrm{d}\tau}\right)\mathcal{F}_{nJ} = 0. \tag{34}$$

The option (34) is very useful for studying the Lyapunov exponents (Klimeš 2002c, eq. 13).

Isolation of $d\mathcal{E}/d\tau$ in (34) yields (Klimeš 1994, eq. 52a)

$$\frac{\mathrm{d}\mathcal{E}_{mI}}{\mathrm{d}\tau} = \left(W_{nm}^{12} + v_m \eta_n\right) \mathcal{E}_{nI}.\tag{35}$$

Eq. (35) is a condition which needs to be satisfied by the basis \mathcal{E} in order to have $W_{IJ}^{(q)}$ = 0. For matrix \mathcal{K} this condition implies (Klimeš 2006b, eq. 115)

$$\mathcal{K}_{MN} = \mathcal{E}_{iM} W_{ii}^{12} \mathcal{F}_{iN}. \tag{36}$$

Remark: The 3 × 3 matrix \mathbf{W}^{12} , which relates to Cartesian coordinates, is determined by the knowledge of position and momentum (slowness) in these coordinates. Assume that the contra- and covariant bases \mathcal{E} and \mathcal{F} are known at the location under consideration on the reference ray Ω . From eqs (30) or (34) we see that the matrix $\mathbf{W}^{(q)}^{12}$ in ray-centred coordinates is obtained from four equations with totally four degrees of freedom for the time derivative of the contra-variant basis, $\dot{\mathcal{E}}$. As a consequence, we cannot require $W_{IJ}^{(q)}^{12} = 0$ and at the same time introduce an additional constraint on the rotation and stretch of \mathcal{E} . This means, for example, that eq. (34) is in general not compatible with a situation where the basis \mathcal{E} is orthonormal along the ray Ω . A special case occurs in an isotropic medium, where the matrix elements $W_{IJ}^{(q)}$ are always zero, regardless of how the basis \mathcal{E} is rotated and stretched along the ray.

2.7 System of four Hamilton-Jacobi perturbation equations in ray-centred coordinates

Above, in the context of eq. (21) describing a system of six Hamilton–Jacobi perturbation equations in ray-centred coordinates, the indices r and t run from 1 to 6. However, the form of the 6×6 matrix in eq. (33) suggests that it is possible to remove two equations from the system of ODEs in (21) and in this way save computation time. It is not necessary to continue the quantities $X_{3a}^{(q)}$ and $X_{6a}^{(q)}$ along the ray Ω . Consequently, we establish a reduced form of the system of ODEs, in which the associated capital indices R and T take the values 1, 2, 4, 5. We have then eliminated the cases r, t = 3 and r, t = 6, which correspond to the third and sixth rows and columns of matrix $S^{(q)}$. The resulting reduced system of differential equations reads

$$\frac{\mathrm{d}X_{Ra}^{(q)}}{\mathrm{d}\tau}(\tau) = S_{RT}^{(q)}(\tau) X_{Ta}^{(q)}(\tau); \qquad \frac{\mathrm{d}\bar{\mathbf{X}}^{(q)}}{\mathrm{d}\tau}(\tau) = \bar{\mathbf{S}}^{(q)}(\tau) \bar{\mathbf{X}}^{(q)}(\tau). \tag{37}$$

Eq. (37) represents a system of four Hamilton–Jacobi perturbation equations for dynamic ray tracing in ray-centred coordinates. The 4 \times 4 coefficient matrix $\bar{\mathbf{S}}^{(q)}$ has the form

$$\bar{\mathbf{S}}^{(q)} = \begin{pmatrix} \{W_{IJ}^{(q)}^{12}\}^T & \{V_{IJ}^{(q)}\} \\ -\{U_{IJ}^{(q)}\} & -\{W_{IJ}^{(q)}^{12}\} \end{pmatrix},\tag{38}$$

where the submatrix components are given by eqs (28)–(30).

When using ray-centred coordinates it is common to split the matrix $\{X_{Ra}^{(q)}\}$ into $2 \times N_{\gamma}$ submatrices $\{Q_{Ma}\}$ and $\{\mathcal{P}_{Ma}\}$,

$$Q_{Ma}(\tau) = \frac{\partial q_M}{\partial \gamma_a}(\hat{\boldsymbol{y}}, \tau), \qquad \mathcal{P}_{Ma}(\tau) = \frac{\partial p_M^{(q)}}{\partial \gamma_a}(\hat{\boldsymbol{y}}, \tau), \tag{39}$$

where M = 1, 2; $a = 1, ..., N_{\gamma}$; $1 \le N_{\gamma} \le 4$. We refer to this as 'Q-P notation' for the derivatives of the phase-space perturbations.

2.8 Fundamental solutions to dynamic ray tracing in ray-centred coordinates

Červený (2001) describes the fundamental solutions to dynamic ray tracing as four *paraxial* solutions, one *ray-tangent* solution and one *non-eikonal* solution. These six solutions correspond to perturbations

$$\gamma = \delta \mathbf{w}_0^{(q)} = \delta \left(q_1, q_2, q_3, p_1^{(q)}, p_2^{(q)}, p_2^{(q)} \right)_{\tau_0} \tag{40}$$

at the initial point of the reference ray Ω .

2.8.1 Paraxial solutions

The reduced ray-centred phase-space perturbation at time τ reads

$$(\delta w_R^{(q)}) = \left(q_1, q_2, p_1^{(q)}, p_2^{(q)}\right)_{\tau},\tag{41}$$

with R = 1, 2, 4, 5. Consider now a corresponding reduced ray-centred phase-space perturbation $(\delta w_R^{(q)})_0$ at the initial point on Ω , for which $\tau = \tau_0$,

$$\delta \bar{\mathbf{w}}_0^{(q)} = \left(q_1, q_2, p_1^{(q)}, p_2^{(q)} \right)_{T_0}. \tag{42}$$

By taking the perturbed phase-space location function in eq. (19) as $w_R^{(q)}(\delta \bar{\mathbf{w}}_0^{(q)}, \tau)$, we can introduce the 4 × 4 ray propagator matrix in ray-centred coordinates,

$$\Pi_{RU}^{(q)}(\tau,\tau_0) = \frac{\partial(\delta w_R^{(q)})}{\partial(\delta w_U^{(q)})_0} (\delta \bar{\mathbf{w}}_0^{(q)} = \mathbf{0}, \tau),\tag{43}$$

where **0** is the four-component zero vector. The ray propagator matrix contains the four fundamental paraxial solutions to the system of ODEs in eq. (37), and it is computed as a solution to the Hamilton–Jacobi perturbation equations

$$\frac{d\Pi_{RU}^{(q)}}{d\tau}(\tau,\tau_0) = S_{RT}^{(q)}(\tau)\,\Pi_{TU}^{(q)}(\tau,\tau_0); \qquad \frac{d\bar{\Pi}^{(q)}}{d\tau}(\tau,\tau_0) = \bar{\mathbf{S}}^{(q)}(\tau)\,\bar{\Pi}^{(q)}(\tau,\tau_0). \tag{44}$$

The integration is initialized by setting

$$\Pi_{gU}^{(q)}(\tau_0, \tau_0) = \delta_{RU}. \tag{45}$$

As with Cartesian coordinates, knowledge of the ray propagator matrix for the segment (τ, τ_0) of Ω implies that any other dynamic ray tracing solution on that segment can be found from the linear combination of fundamental solutions,

$$X_{R_{\sigma}}^{(q)}(\tau) = \Pi_{RT}^{(q)}(\tau, \tau_0) X_{T_{\sigma}}^{(q)}(\tau_0); \qquad \bar{\mathbf{X}}^{(q)}(\tau) = \bar{\mathbf{\Pi}}(\tau, \tau_0) \bar{\mathbf{X}}^{(q)}(\tau_0). \tag{46}$$

2.8.2 Ray-tangent solution

Consider again the full set of initial perturbations (40), where we note that

$$\gamma_3 = (\delta q_3)_{\tau_0} \tag{47}$$

yields a time shift at the initial point. Along the ray Ω this further results in the ray-tangent solution to dynamic ray tracing. This solution is expressed explicitly as

$$\frac{\partial q_i}{\partial \nu_3} = \delta_{i3}, \qquad \frac{\partial p_i^{(q)}}{\partial \nu_3} = 0 \tag{48}$$

in ray-centred coordinates (Klimeš 1994, first sub-eq. 53) and

$$\frac{\partial x_i}{\partial \gamma_3} = v_i, \qquad \frac{\partial x_i}{\partial \gamma_3} = \eta_i \tag{49}$$

in Cartesian coordinates (Klimeš 1994, first sub-eq. 55).

2.8.3 Non-eikonal solution

In eq. (40) the ray parameter

$$\gamma_6 = (\delta p_3^{(q)})_{\tau_0} \tag{50}$$

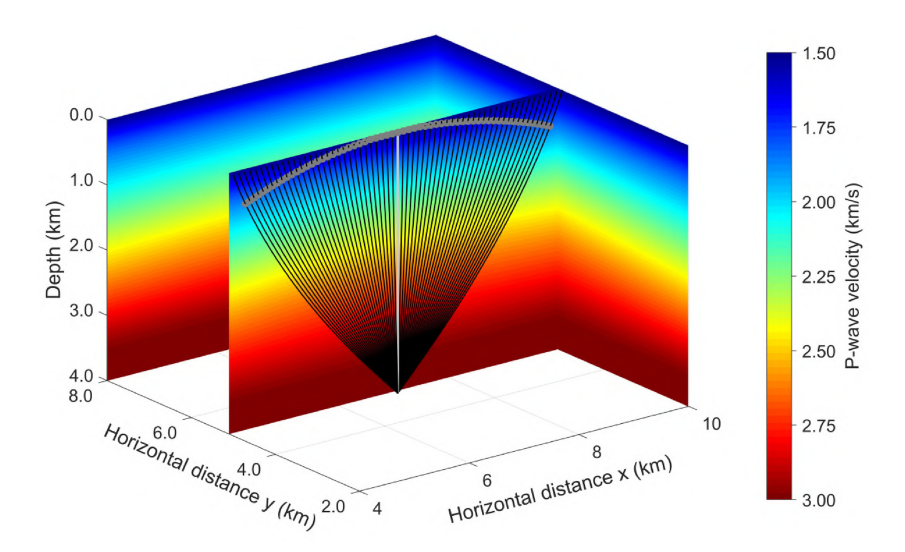


Figure 1. Model 3-D VTI and rays used for comparison of results from dynamic ray tracing in ray-centred and Cartesian coordinates. The colour scale yields the value of the vertical *P*-wave velocity. Data for numerical comparisons is computed along rays (black) from a source point at depth 4 km. Coefficients for paraxial extrapolation are computed along a nearly vertical reference ray (light grey line). A wavefront (grey dots) through the end point of the reference ray is indicated.

yields the non-eikonal solution to dynamic ray tracing. We see that this solution corresponds to a perturbation of the momentum component $p_3^{(q)}$ at the initial point. For the degree $\mathcal{N}=2$ of the Hamiltonian, the non-eikonal solution is given explicitly as

$$\frac{\partial q_i}{\partial \gamma_6} = (\tau - \tau_0)\delta_{i3}, \qquad \frac{\partial p_i^{(q)}}{\partial \gamma_6} = \delta_{i3} \tag{51}$$

in ray-centred coordinates (Klimeš 1994, second sub-eq. 53) and

$$\frac{\partial x_i}{\partial \gamma_6} = (\tau - \tau_0)v_i, \qquad \frac{\partial x_i}{\partial \gamma_6} = p_i + (\tau - \tau_0)\eta_i \tag{52}$$

in Cartesian coordinates (Klimeš 1994, second sub-eq. 55).

Among the six fundamental solutions it is only the non-eikonal solution that depends on the value of \mathcal{N} . For details, see Appendix F.

3 HIGHER ORDER HAMILTON-JACOBI PERTURBATION EQUATIONS IN RAY-CENTRED COORDINATES

In the leading-order approach to dynamic ray tracing in ray-centred coordinates one continues first-order derivatives of phase-space perturbations $X_{Ra}^{(q)}(\tau)$, see equation eq. (20), along the reference ray Ω . In this section we consider an extension of this approach to compute higher-order derivatives of the phase-space perturbations.

3.1 Continuation of second-order derivatives of phase-space perturbations

In an extension of dynamic ray tracing to handle second-order derivatives of phase-space perturbations the full set of quantities to be determined has the form

$$X_{rab}^{(q)}(\tau) = \frac{\partial^2 w_r^{(q)}}{\partial \gamma_a \partial \gamma_b}(\hat{\boldsymbol{\gamma}}, \tau). \tag{53}$$

In O-P notation we write the latter as

$$Q_{iab}(\tau) = \frac{\partial^2 q_i}{\partial \gamma_a \partial \gamma_b}(\hat{\boldsymbol{\gamma}}, \tau), \qquad \mathcal{P}_{iab}(\tau) = \frac{\partial^2 p_i^{(q)}}{\partial \gamma_a \partial \gamma_b}(\hat{\boldsymbol{\gamma}}, \tau). \tag{54}$$

However, as we will become apparent below, the quantities Q_{3ab} and P_{3ab} are redundant in an ODE system for second-order dynamic ray tracing. As in conventional (first-order) dynamic ray tracing, we can therefore introduce reduced phase-space perturbation quantities

$$X_{Rab}^{(q)}(\tau) = \frac{\partial^2 w_R^{(q)}}{\partial \gamma_a \partial \gamma_b} (\hat{\boldsymbol{y}}, \tau), \tag{55}$$

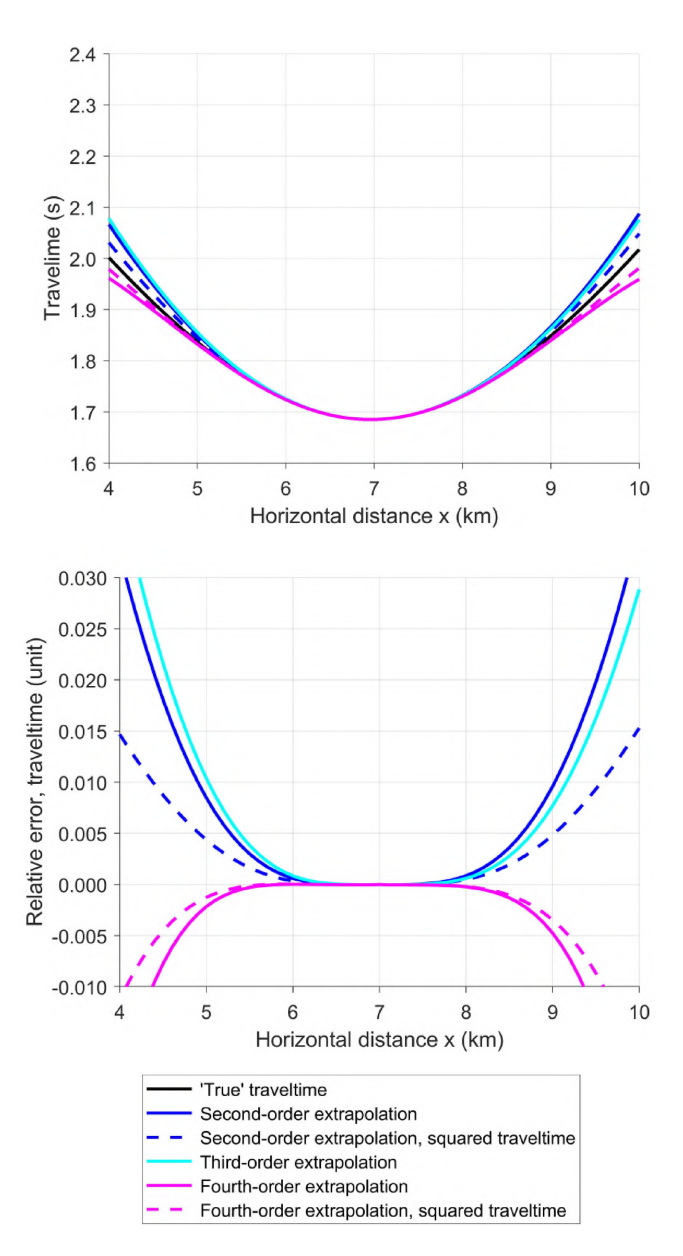


Figure 2. Results of paraxial extrapolation of traveltime based on dynamic ray tracing in ray-centred coordinates. Different extrapolation approaches were applied along the line y = 5 km. The reference point for the extrapolation is at x = 7 km. Top panel: traveltime curves resulting from the extrapolation. Bottom panel: relative error in traveltime for the different approaches.

with index values R = 1, 2, 4, 5. We make use of a three-component coefficient tensor related to the third-order partial phase-space derivatives of the Hamiltonian \mathcal{H} ,

$$S_{RTU}^{(q)}(\tau) = J_{RS} \frac{\partial^3 \mathcal{H}}{\partial w_S^{(q)} \partial w_T^{(q)} \partial w_U^{(q)}} [\mathbf{w}^{(q)}(\hat{\boldsymbol{\gamma}}, \tau)]. \tag{56}$$

For the third-order partial derivatives of the Hamiltonian we obtain (Appendix B)

$$U_{IJK}^{(q)} \equiv \frac{\partial^3 \mathcal{H}}{\partial q_I \partial q_J \partial q_K}$$

$$= \left(U_{mnp} + 2\eta_m U_{np} + 2\eta_n U_{mp} + 2\eta_p U_{mn} - 6\eta_m \eta_n \eta_p \right) \mathcal{E}_{mI} \mathcal{E}_{nJ} \mathcal{E}_{pK}, \tag{57}$$

$$W_{IJK}^{(q) 112} \equiv \frac{\partial^{3} \mathcal{H}}{\partial q_{I} \partial q_{J} \partial p_{K}^{(q)}} = \left(W_{mnp}^{112} + \eta_{m} W_{np}^{12} + \eta_{n} W_{mp}^{12}\right) \mathcal{E}_{mI} \mathcal{E}_{nJ} \mathcal{F}_{pK}, \tag{58}$$

$$W_{IJK}^{(q) 122} \equiv \frac{\partial^{3} \mathcal{H}}{\partial q_{I} \partial p_{J}^{(q)} \partial p_{K}^{(q)}} = W_{mnp}^{122} \mathcal{E}_{mI} \mathcal{F}_{nJ} \mathcal{F}_{pK}, \tag{59}$$

$$W_{IJK}^{(q) 122} \equiv \frac{\partial^3 \mathcal{H}}{\partial q_I \partial p_J^{(q)} \partial p_K^{(q)}} = W_{mnp}^{122} \mathcal{E}_{mI} \mathcal{F}_{nJ} \mathcal{F}_{pK}, \tag{59}$$

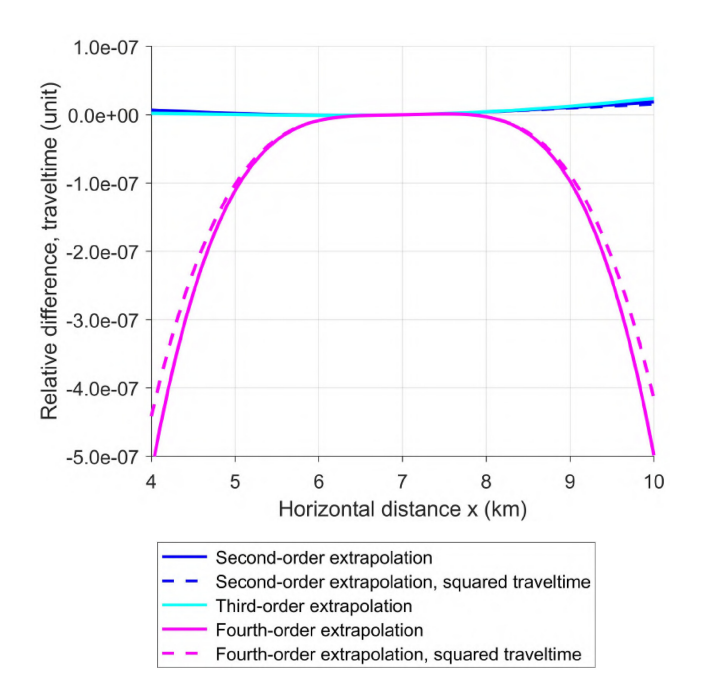


Figure 3. Relative difference between results for extrapolated traveltime when using dynamic ray tracing in ray-centred and Cartesian coordinates. Different extrapolation approaches were applied along the line y = 5 km. The reference point for the extrapolation is at x = 7 km.

$$V_{IJK}^{(q)} \equiv \frac{\partial^3 \mathcal{H}}{\partial p_I^{(q)} \partial p_J^{(q)} \partial p_V^{(q)}} = V_{mnp} \mathcal{F}_{mI} \mathcal{F}_{nJ} \mathcal{F}_{pK}, \tag{60}$$

On the right-hand side of (57)–(60), the quantities U_{mnp} , W_{mnp}^{112} , W_{mnp}^{122} and V_{mnp} are third-order derivatives of the Hamiltonian taken in the Cartesian phase-space coordinates,

$$U_{mnp} \equiv \frac{\partial^{3} \mathcal{H}}{\partial x_{m} \partial x_{n} \partial x_{p}}, \quad W_{mnp}^{112} \equiv \frac{\partial^{3} \mathcal{H}}{\partial x_{m} \partial x_{n} \partial p_{p}},$$

$$W_{mnp}^{122} \equiv \frac{\partial^{3} \mathcal{H}}{\partial x_{m} \partial p_{n} \partial p_{p}}, \quad V_{mnp} \equiv \frac{\partial^{3} \mathcal{H}}{\partial p_{m} \partial p_{n} \partial p_{p}}.$$
(61)

The second-order derivatives of the phase-space perturbations must satisfy a system of ODEs

$$\frac{\mathrm{d}X_{Rab}^{(q)}}{\mathrm{d}\tau}(\tau) = S_{RT}^{(q)}(\tau)X_{Tab}^{(q)}(\tau) + R_{Rab}^{(q)}(\tau),\tag{62}$$

where

$$R_{Rab}^{(q)}(\tau) = S_{RTU}^{(q)}(\tau) X_{Ta}^{(q)}(\tau) X_{Ub}^{(q)}(\tau). \tag{63}$$

We note that the combination of ODEs (37) and (62) can then be integrated to yield the solution (55).

A good alternative is to use an expression for the solution in terms of initial conditions, the ray propagator matrix and a closed-form integral, namely,

$$X_{Rab}^{(q)}(\tau) = \Pi_{RS}^{(q)}(\tau, \tau_0) X_{Sab}^{(q)}(\tau_0) + \int_{\tau_0}^{\tau} \Pi_{RS}^{(q)}(\tau, \tau') R_{Sab}^{(q)}(\tau') d\tau'.$$
(64)

Here, the ray propagator matrix, $\Pi_{RT}^{(q)}(\tau, \tau_0)$, is assumed known along Ω .

As in the case of higher-order dynamic ray tracing in Cartesian coordinates (Iversen *et al.* 2019), it is practical to find formulations where the ray propagator matrix in the integrand corresponds to propagation from $\tau = \tau_0$ to $\tau = \tau'$, rather than from τ' to τ . Using the chain rule for the ray propagator matrix (Červený 2001),

$$\Pi_{RT}^{(q)}(\tau, \tau_0) = \Pi_{RS}^{(q)}(\tau, \tau') \Pi_{ST}^{(q)}(\tau', \tau_0), \tag{65}$$

in combination with its symplectic property, we obtain

$$X_{Rab}^{(q)}(\tau) = \Pi_{RS}^{(q)}(\tau, \tau_0) \left(X_{Sab}^{(q)}(\tau_0) - \int_{\tau_0}^{\tau} J_{SU} \Pi_{TU}^{(q)}(\tau', \tau_0) J_{TV} R_{Vab}^{(q)}(\tau') d\tau' \right). \tag{66}$$

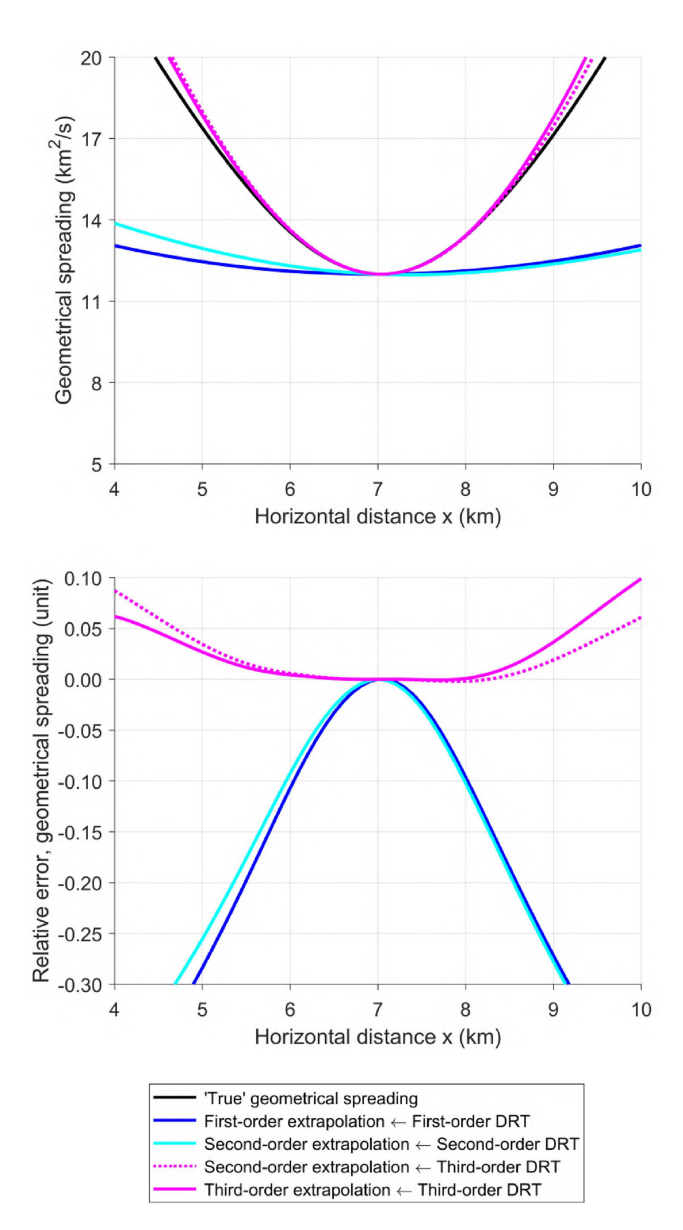


Figure 4. Results of paraxial extrapolation of geometrical spreading based on dynamic ray tracing (DRT) in ray-centred coordinates. Different extrapolation approaches were applied along the line y = 5 km. The reference point for the extrapolation is at x = 7 km. Top panel: geometrical spreading curves resulting from the extrapolation. Bottom panel: relative error in geometrical spreading for the different approaches.

3.2 Continuation of third-order derivatives of phase-space perturbations

We consider third-order derivatives of phase-space perturbations

$$X_{rabc}^{(q)}(\tau) = \frac{\partial^3 w_r^{(q)}}{\partial \gamma_a \partial \gamma_b \partial \gamma_c} (\hat{\boldsymbol{y}}, \tau) \tag{67}$$

and the equivalent *Q*–*P* notation

$$Q_{iabc}(\tau) = \frac{\partial^3 q_i}{\partial \gamma_a \partial \gamma_b \partial \gamma_c} (\hat{\boldsymbol{y}}, \tau), \qquad \mathcal{P}_{iabc}(\tau) = \frac{\partial^3 p_i^{(q)}}{\partial \gamma_a \partial \gamma_b \partial \gamma_c} (\hat{\boldsymbol{y}}, \tau). \tag{68}$$

Similar as for lower orders, the quantities Q_{3abc} and P_{3abc} are redundant—it is not necessary to include differential equations for them. In an ODE system for third-order dynamic ray tracing we therefore only need to continue the reduced set of phase-space perturbation quantities

$$X_{Rabc}^{(q)}(\tau) = \frac{\partial^3 w_R^{(q)}}{\partial \gamma_a \partial \gamma_b \partial \gamma_c} (\hat{\boldsymbol{y}}, \tau) \tag{69}$$

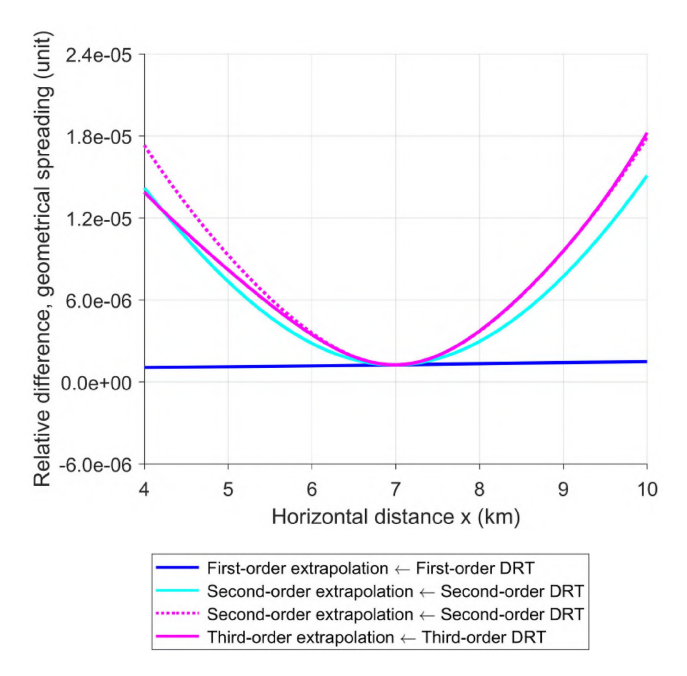


Figure 5. Relative difference between results for extrapolated geometrical spreading when using dynamic ray tracing (DRT) in ray-centred and Cartesian coordinates. Different extrapolation approaches were applied along the line y = 5 km. The reference point for the extrapolation is at x = 7 km.

along the ray Ω . At arbitrary points on Ω it is necessary to compute the four-component coefficient tensor

$$S_{RTUV}^{(q)}(\tau) = J_{RS} \frac{\partial^4 \mathcal{H}}{\partial w_S^{(q)} \partial w_T^{(q)} \partial w_U^{(q)} \partial w_V^{(q)}} [\mathbf{w}^{(q)}(\hat{\boldsymbol{\gamma}}, \tau)], \tag{70}$$

including fourth-order derivatives of the Hamiltonian. These derivatives are given as (Appendix C),

$$U_{IJKL}^{(q)} \equiv \frac{\partial^4 \mathcal{H}}{\partial q_I \partial q_J \partial q_K \partial q_L}$$

$$= \left(U_{mnpq} + 2\eta_m U_{npq} + 2\eta_p U_{mnq} + 2\eta_q U_{mnp} \right)$$

$$+ 6\eta_m \eta_n U_{pq} + 6\eta_m \eta_p U_{nq} + 6\eta_m \eta_q U_{np}$$

$$+ 6\eta_n \eta_p U_{mq} + 6\eta_n \eta_q U_{mp} + 6\eta_p \eta_q U_{mn}$$

$$- 36\eta_m \eta_n \eta_p \eta_q \right) \mathcal{E}_{mI} \mathcal{E}_{nJ} \mathcal{E}_{pK} \mathcal{E}_{qL},$$

$$(71)$$

$$W_{IJKL}^{(q) \, 1112} \equiv \frac{\partial^4 \mathcal{H}}{\partial q_I \partial q_J \partial q_K \partial p_L^{(q)}}$$

$$= \left(W_{mnpq}^{1112} + \eta_m W_{npq}^{112} + \eta_n W_{mpq}^{112} + \eta_p W_{mnq}^{112} + 2\eta_m \eta_n W_{pq}^{12} + 2\eta_m \eta_p W_{nq}^{12} + 2\eta_n \eta_p W_{mq}^{12} \right) \mathcal{E}_{mI} \mathcal{E}_{nJ} \mathcal{E}_{pK} \mathcal{F}_{qL}$$

$$- 2(U_{mn} - \eta_m \eta_n) (\mathcal{E}_{mI} \mathcal{E}_{nJ} \mathcal{K}_{KL} + \mathcal{E}_{mI} \mathcal{E}_{nK} \mathcal{K}_{JL} + \mathcal{E}_{mJ} \mathcal{E}_{nK} \mathcal{K}_{IL}),$$

$$(72)$$

$$W_{IJKL}^{(q) 1122} \equiv \frac{\partial^4 \mathcal{H}}{\partial q_I \partial q_J \partial p_K^{(q)} \partial p_L^{(q)}}$$

$$= W_{mnqp}^{1122} \mathcal{E}_{mI} \mathcal{E}_{nJ} \mathcal{F}_{pK} \mathcal{F}_{qL}$$

$$- W_{mn}^{12} (\mathcal{E}_{mI} \mathcal{F}_{nK} \mathcal{K}_{JL} + \mathcal{E}_{mI} \mathcal{F}_{nL} \mathcal{K}_{JK} + \mathcal{E}_{mJ} \mathcal{F}_{nK} \mathcal{K}_{IL} + \mathcal{E}_{mJ} \mathcal{F}_{nL} \mathcal{K}_{IK})$$

$$+ \mathcal{K}_{IK} \mathcal{K}_{JL} + \mathcal{K}_{IL} \mathcal{K}_{JK},$$

$$(73)$$

$$W_{IJKL}^{(q) 1222} \equiv \frac{\partial^4 \mathcal{H}}{\partial q_I \partial p_J^{(q)} \partial p_K^{(q)} \partial p_L^{(q)}}$$

$$= (W_{mnpq}^{1222} - \eta_m V_{npq}) \mathcal{E}_{mI} \mathcal{F}_{nJ} \mathcal{F}_{pK} \mathcal{F}_{qL}, \tag{74}$$

$$V_{IJKL}^{(q)} \equiv \frac{\partial^4 \mathcal{H}}{\partial p_I^{(q)} \partial p_J^{(q)} \partial p_K^{(q)} \partial p_L^{(q)}}$$

$$= V_{mnpq} \mathcal{F}_{mI} \mathcal{F}_{nJ} \mathcal{F}_{pK} \mathcal{F}_{qL}. \tag{75}$$

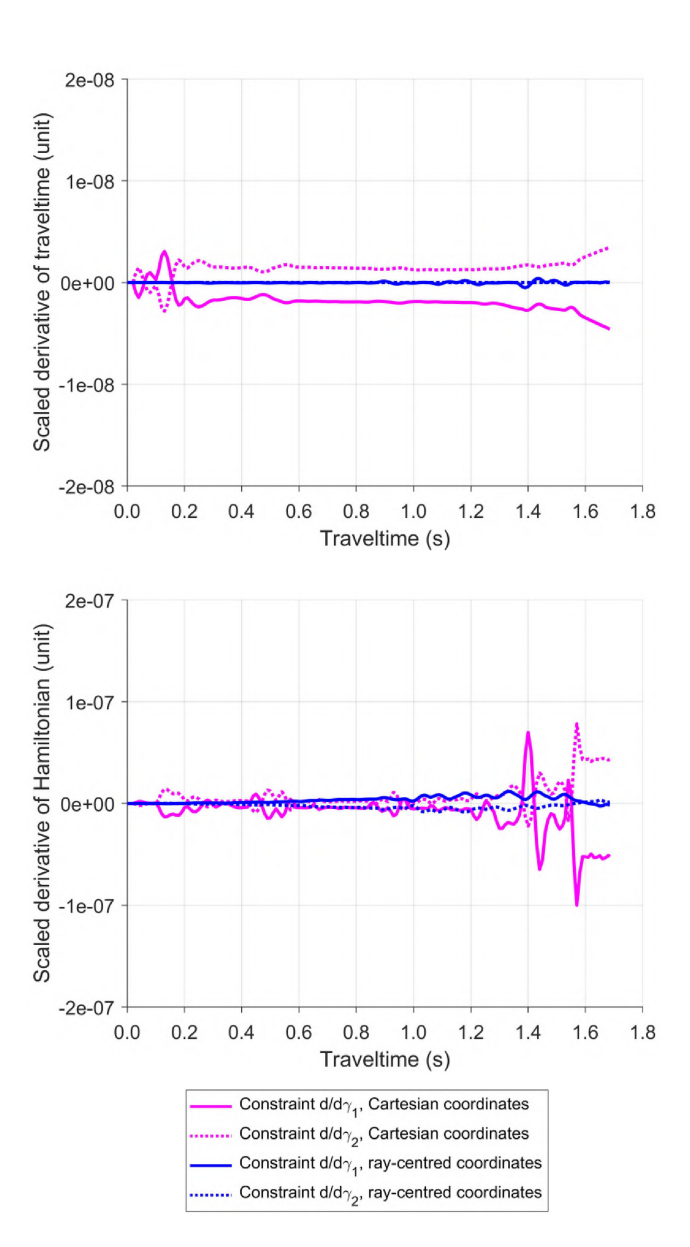


Figure 6. Constraint visualization along the reference ray, for first-order (conventional) dynamic ray tracing in Cartesian and ray-centred coordinates. Top panel: scaled derivatives of traveltime $d\tau/d\gamma_1$ (solid magenta) and $d\tau/d\gamma_2$ (dotted magenta) for dynamic ray tracing in Cartesian coordinates, and corresponding derivatives (solid/dotted blue) estimated from dynamic ray tracing in ray-centred coordinates. The derivatives are scaled by the factor $\delta\gamma/\tau$, where τ is the current traveltime and $\delta\gamma=0.1~{\rm s\,km^{-1}}$. Bottom panel: scaled derivatives of the Hamiltonian $d\mathcal{H}/d\gamma_1$ (solid magenta) and $d\mathcal{H}/d\gamma_2$ (dotted magenta) for dynamic ray tracing in Cartesian coordinates, and corresponding derivatives (solid/dotted blue) estimated from dynamic ray tracing in ray-centred coordinates. The scale factor is $\delta\gamma/\mathcal{H}$, with $\mathcal{H}=1/2$ and $\delta\gamma=0.1~{\rm s/km}$.

The quantities U_{mnpq} , W_{mnpq}^{1112} , W_{mnpq}^{1222} , W_{mnpq}^{1222} and V_{mnpq} , on the right-hand side of (71)–(75), are fourth-order derivatives of the Hamiltonian in the Cartesian phase-space coordinates,

$$U_{mnpq} \equiv \frac{\partial^{4} \mathcal{H}}{\partial x_{m} \partial x_{n} \partial x_{p} \partial x_{q}},$$

$$W_{mnpq}^{1112} \equiv \frac{\partial^{4} \mathcal{H}}{\partial x_{m} \partial x_{n} \partial x_{p} \partial p_{q}}, \quad W_{mnpq}^{1122} \equiv \frac{\partial^{4} \mathcal{H}}{\partial x_{m} \partial x_{n} \partial p_{p} \partial p_{q}}, \quad W_{mnpq}^{1222} \equiv \frac{\partial^{4} \mathcal{H}}{\partial x_{m} \partial p_{n} \partial p_{p} \partial p_{q}},$$

$$V_{mnpq} \equiv \frac{\partial^{4} \mathcal{H}}{\partial p_{m} \partial p_{m} \partial p_{m} \partial p_{m}}.$$

$$(76)$$

We use a system of ODEs for continuation of the third-order derivatives of the phase-space perturbations,

$$\frac{\mathrm{d}X_{Rabc}^{(q)}}{\mathrm{d}\tau}(\tau) = S_{RT}^{(q)}(\tau)X_{Tabc}^{(q)}(\tau) + R_{Rabc}^{(q)}(\tau),\tag{77}$$

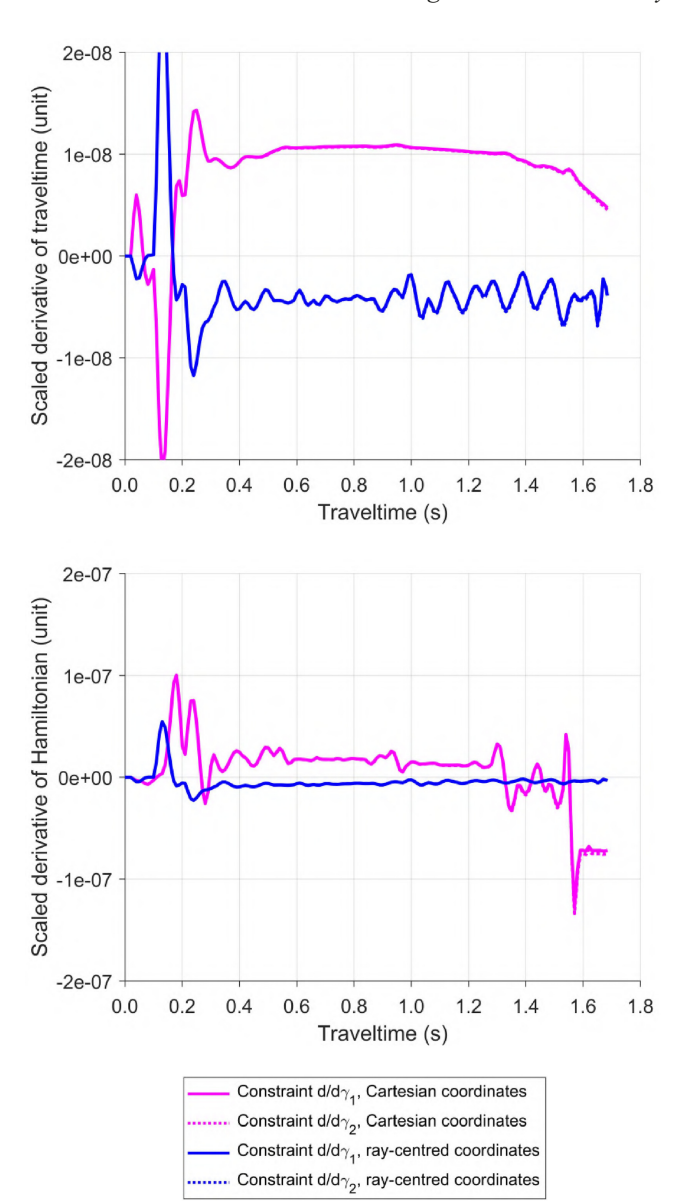


Figure 7. Constraint evaluation along the reference ray, for second-order dynamic ray tracing in Cartesian and ray-centred coordinates. Top panel: scaled derivatives of traveltime $d^2\tau/d\gamma_1^2$ (solid magenta) and $d^2\tau/d\gamma_2^2$ (dotted magenta) for dynamic ray tracing in Cartesian coordinates, and corresponding derivatives (solid/dotted blue) estimated from dynamic ray tracing in ray-centred coordinates. The derivatives are scaled by the factor $(\delta\gamma)^2/(2\tau)$, with τ and $\delta\gamma$ set as in Fig. 6. Bottom panel: scaled derivatives of the Hamiltonian $d^2\mathcal{H}/d\gamma_1^2$ (solid magenta) and $d^2\mathcal{H}/d\gamma_2^2$ (dotted magenta) for dynamic ray tracing in Cartesian coordinates, and corresponding derivatives (solid/dotted blue) estimated from dynamic ray tracing in ray-centred coordinates. The scale factor is $(\delta\gamma)^2/(2\mathcal{H})$, with $\mathcal{H}=1/2$.

where the last term is defined by

$$R_{Rabc}^{(q)}(\tau) = S_{RTUV}^{(q)}(\tau) X_{Ta}^{(q)}(\tau) X_{Ub}^{(q)}(\tau) X_{Vc}^{(q)}(\tau) + S_{RTu}^{(q)}(\tau) \left[X_{Ta}^{(q)}(\tau) X_{ubc}^{(q)}(\tau) + X_{Tb}^{(q)}(\tau) X_{uac}^{(q)}(\tau) + X_{Tc}^{(q)}(\tau) X_{uab}^{(q)}(\tau) \right].$$
(78)

The ODEs given by eqs (37), (62) and (77) can now be integrated to collectively yield the solution (69). We remark that (77)–(78) have a peculiarity compared to the dynamic ray tracing ODEs for lower orders, since the evaluation of the right-hand side requires computation of the second-order perturbation quantities Q_{3ab} and P_{3ab} . The latter are however easily obtained by intrinsic relations to Q_{Ia} , P_{Ia} and their time derivatives—this is shown in Appendix D.

As for lower orders of dynamic ray tracing, one may alternatively compute the solution (69) using its initial condition, the ray propagator matrix and a closed-form integral along the ray Ω ,

$$X_{Rabc}^{(q)}(\tau) = \Pi_{RS}^{(q)}(\tau, \tau_0) X_{Sabc}^{(q)}(\tau_0) + \int_{\tau_0}^{\tau} \Pi_{RS}^{(q)}(\tau, \tau') R_{Sabc}^{(q)}(\tau') d\tau'.$$

$$(79)$$

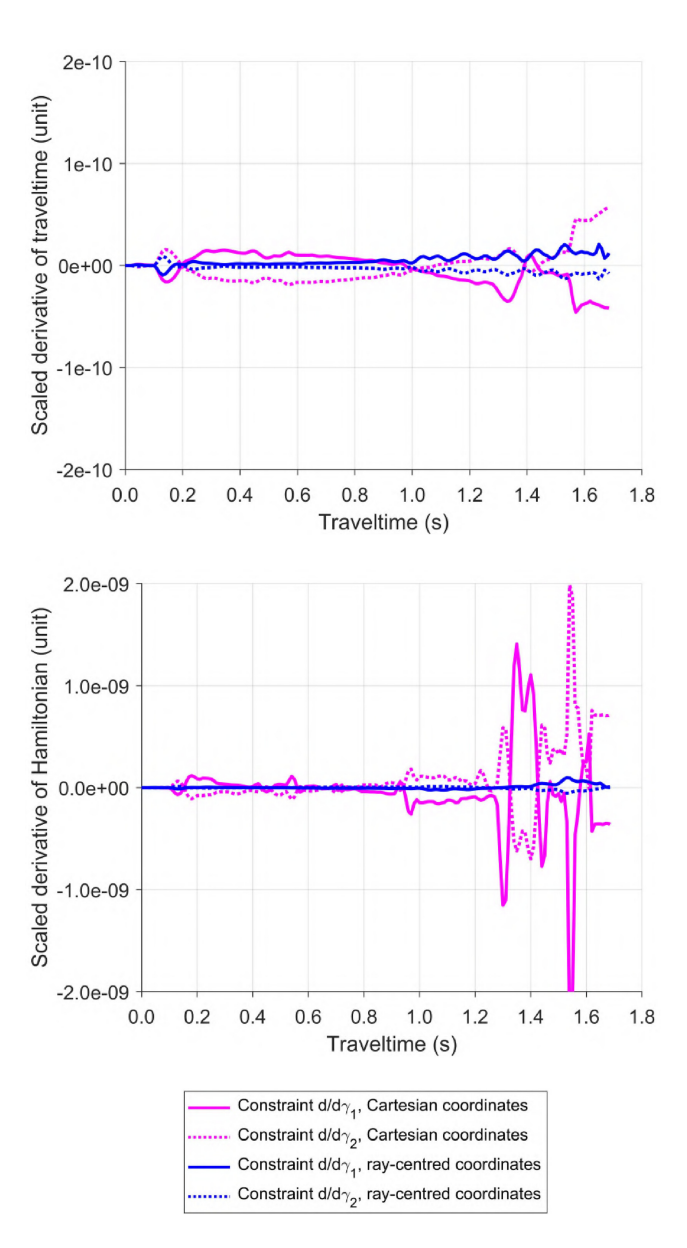


Figure 8. Constraint evaluation along the reference ray, for third-order dynamic ray tracing in Cartesian and ray-centred coordinates. Top panel: scaled derivatives of traveltime $d^3\tau/d\gamma_1^3$ (solid magenta) and $d^3\tau/d\gamma_2^3$ (dotted magenta) for dynamic ray tracing in Cartesian coordinates, and corresponding estimated derivatives (solid/dotted blue) from dynamic ray tracing in ray-centred coordinates. The derivatives are scaled by the factor $(\delta\gamma)^3/(6\tau)$, with τ and $\delta\gamma$ set as in Fig. 6. Bottom panel: scaled derivatives of the Hamiltonian $d^3\mathcal{H}/d\gamma_1^3$ (solid magenta) and $d^3\mathcal{H}/d\gamma_2^3$ (dotted magenta) for dynamic ray tracing in Cartesian coordinates, and corresponding derivatives (solid/dotted blue) estimated from dynamic ray tracing in ray-centred coordinates. The scale factor is $(\delta\gamma)^3/(6\mathcal{H})$, with $\mathcal{H}=1/2$.

Here, the ray propagator matrix $\Pi_{RT}^{(q)}(\tau, \tau_0)$ and the various first- and second-order derivatives of the perturbations must be known on Ω . The chain rule (65) and the symplectic property of the ray propagator matrix yield an important rearrangement

$$X_{Rabc}^{(q)}(\tau) = \Pi_{RS}^{(q)}(\tau, \tau_0) \left(X_{Sabc}^{(q)}(\tau_0) - \int_{\tau_0}^{\tau} J_{SU} \Pi_{TU}^{(q)}(\tau', \tau_0) J_{TV} R_{Vabc}^{(q)}(\tau') d\tau' \right). \tag{80}$$

4 CONSTRAINTS AND INTRINSIC RELATIONS BETWEEN DERIVATIVES OF PHASE-SPACE PERTURBATIONS IN RAY-CENTRED COORDINATES

In this section we focus on *constraints* inherent to conventional and higher-order dynamic ray tracing in ray-centred coordinates. The constraints lead to *intrinsic relations* (Appendix D), which connect various derivatives of the phase-space perturbations, that is the Q-and P-type quantities. The intrinsic relations include M-quantities, which represent derivatives of traveltime of order two and higher, in ray-centred coordinates.

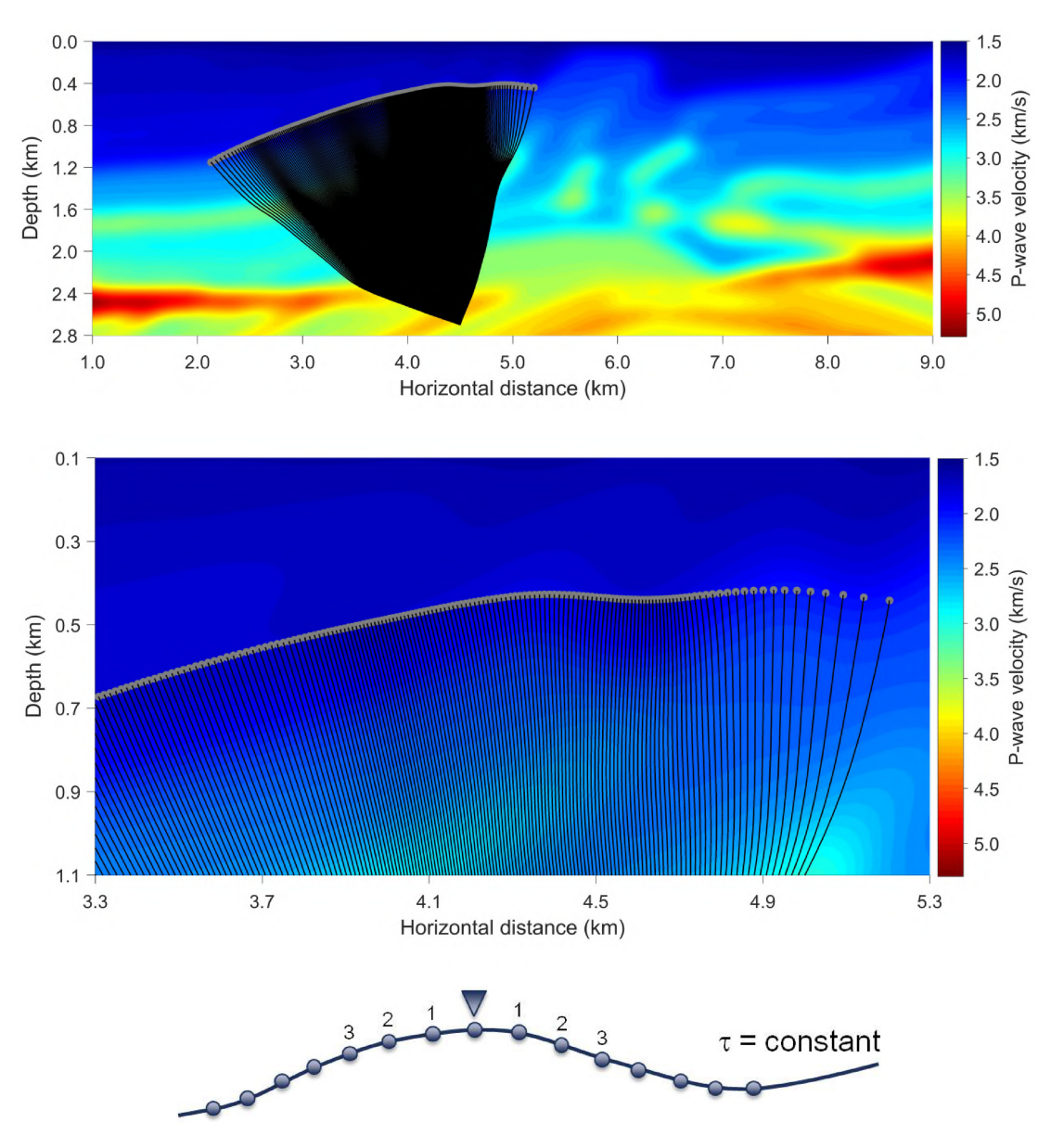


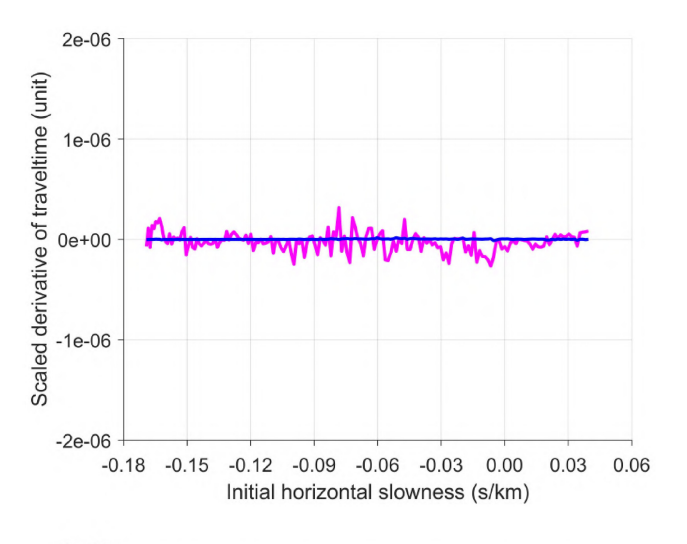
Figure 9. Top panel: the model *Marmousi VTI* and a dense bundle of rays (black) traced from the point (x = 4.5, z = 2.7) km. Grey dots correspond to constant time, $\tau = 0.8$ s. Middle panel: close-up of rays (black) and wavefront points (grey) shown in the top subfigure. Bottom panel: setup for interpolation of dynamic ray tracing results. For any point on the wavefront (signified by the triangle), three cases of interpolation based on neighbouring points are considered. The input points for the three cases are marked 1, 2, 3.

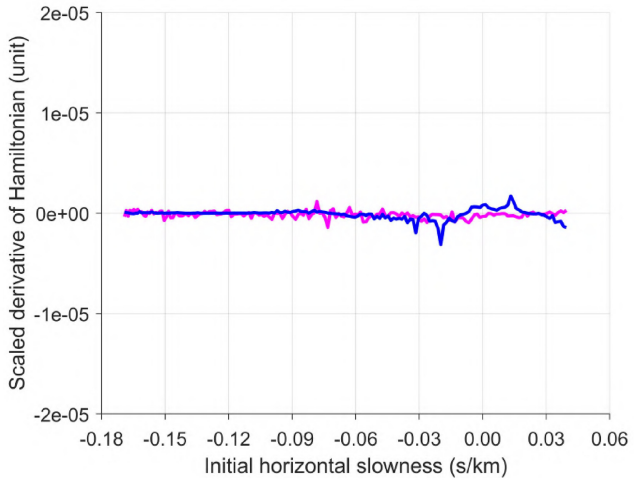
It is not necessary to include dynamic ray tracing ODEs for the quantities Q_{3ab} , \mathcal{P}_{3ab} and Q_{3abc} , \mathcal{P}_{3abc} , but such quantities are needed later, typically at the receiver point, in a transformation of a full set of derivatives of phase-space perturbations from ray-centred to Cartesian coordinates. Also, as mentioned in the previous section, the quantities Q_{3ab} , \mathcal{P}_{3ab} must be computed on the right-hand side of the third-order dynamic ray tracing ODEs.

4.1 The momentum vector as a function of position

Consider here, in addition to Cartesian and ray-centred coordinates, also a 3-D *ray coordinate system* ($\gamma_1, \gamma_2, \gamma_3 = \tau$), in which $\gamma_A, A = 1, 2$, are two paraxial variables. In particular, if there is a one-to-one mapping between ray coordinates and Cartesian coordinates the traveltime can be expressed as a function $\tau(\mathbf{x})$. A fundamental property of ray theory is then that the slowness (momentum) vector \mathbf{p} equals the traveltime gradient at the point \mathbf{x} (Červený 2001),

$$p_i = \frac{\partial \tau}{\partial x_i},\tag{81}$$





Constraint $d/d\gamma_1$, Cartesian coordinates
Constraint $d/d\gamma_1$, ray-centred coordinates

Figure 10. Constraint evaluation along a wavefront, $\tau = 0.8$ s, in the Marmousi VTI model, for first-order (conventional) dynamic ray tracing in Cartesian (magenta) and ray-centred (blue) coordinates. Top panel: scaled derivatives of traveltime $d\tau/d\gamma_1$. The derivatives are scaled by the factor $\delta\gamma/\tau$, with $\delta\gamma = 0.01$ s km⁻¹. Bottom panel: scaled derivatives of the Hamiltonian $d\mathcal{H}/d\gamma_1$. The scale factor is $\delta\gamma/\mathcal{H}$, with $\mathcal{H} = 1/2$ and $\delta\gamma = 0.01$ s km⁻¹.

which means that \mathbf{p} is a function of \mathbf{x} . The property (81) also comes out naturally from the transformation between ray-centred and Cartesian coordinates (Iversen *et al.* 2021).

In ray-centred coordinates we have an analogous form of (81). For a one-to-one correspondence of ray coordinates and ray-centred coordinates the traveltime is a function $\tau(\mathbf{q})$, and the momentum vector $\mathbf{p}^{(q)}$ equals the traveltime gradient at \mathbf{q} ,

$$p_i^{(q)} = \frac{\partial \tau}{\partial q_i},\tag{82}$$

so $\mathbf{p}^{(q)}$ is then a function of \mathbf{q} .

On the reference ray Ω we have $p_I^{(q)} = 0$ and $p_3^{(q)} = 1$, that means, the momentum vector in ray-centred coordinates is constant. As a consequence,

$$\frac{\partial}{\partial q_3} \left(\frac{\partial \tau}{\partial q_i} \right) = 0 \tag{83}$$

on Ω

Derivatives of the momentum component function $p_i^{(q)}(\mathbf{q})$ with respect to ray coordinates γ_A are needed below to establish intrinsic relations between Q- and P-type quantities. Applying the chain rule of differentiation to eq. (82) yields, for the first three orders in γ_A ,

$$\frac{\partial p_i^{(q)}}{\partial \gamma_A} = \frac{\partial p_i^{(q)}}{\partial q_j} \frac{\partial q_j}{\partial \gamma_A} = \frac{\partial^2 \tau}{\partial q_i \partial q_j} \frac{\partial q_j}{\partial \gamma_A},\tag{84}$$

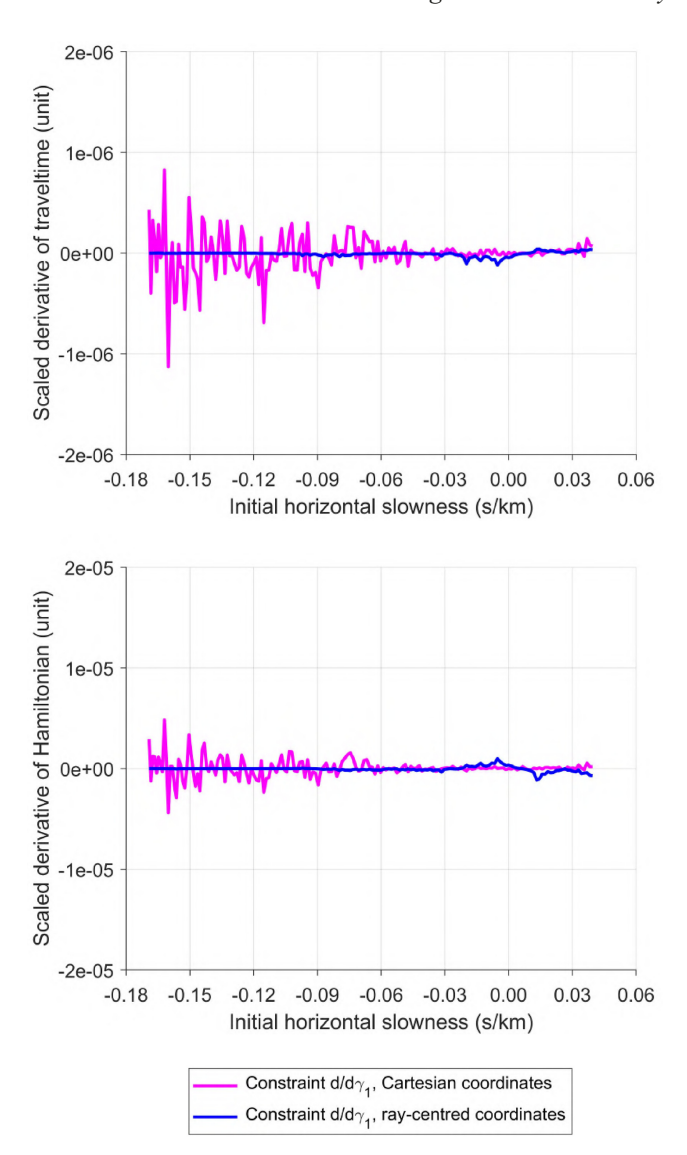


Figure 11. Constraint evaluation along a wavefront, $\tau = 0.8$ s, in the Marmousi VTI model, for second-order dynamic ray tracing in Cartesian (magenta) and ray-centred (blue) coordinates. Top panel: scaled derivatives of traveltime $d^2\tau/d\gamma_1^2$. The derivatives are scaled by the factor $\delta\gamma/\tau$, with $\delta\gamma$ set as in Fig. 10. Bottom panel: scaled derivatives of the Hamiltonian $d^2\mathcal{H}/d\gamma_1^2$. The scale factor is $(\delta\gamma)^2/(2\mathcal{H})$, with $\mathcal{H}=1/2$.

$$\frac{\partial^{2} p_{i}^{(q)}}{\partial \gamma_{A} \partial \gamma_{B}} = \frac{\partial^{3} \tau}{\partial q_{i} \partial q_{j} \partial q_{k}} \frac{\partial q_{j}}{\partial \gamma_{A}} \frac{\partial q_{j}}{\partial \gamma_{B}} + \frac{\partial^{2} \tau}{\partial q_{i} \partial q_{j}} \frac{\partial^{2} q_{j}}{\partial \gamma_{A} \partial \gamma_{B}}, \tag{85}$$

$$\frac{\partial^{3} p_{i}^{(q)}}{\partial \gamma_{A} \partial \gamma_{B} \partial \gamma_{C}} = \frac{\partial^{4} \tau}{\partial q_{i} \partial q_{j} \partial q_{k} \partial q_{l}} \frac{\partial q_{k}}{\partial \gamma_{A}} \frac{\partial q_{l}}{\partial \gamma_{B}} \frac{\partial q_{l}}{\partial \gamma_{C}}$$

$$+ \frac{\partial^{3} \tau}{\partial q_{i} \partial q_{j} \partial q_{k}} \left(\frac{\partial q_{j}}{\partial \gamma_{A}} \frac{\partial^{2} q_{k}}{\partial \gamma_{B} \gamma_{C}} + \frac{\partial q_{j}}{\partial \gamma_{B}} \frac{\partial^{2} q_{k}}{\partial \gamma_{A} \gamma_{C}} + \frac{\partial q_{j}}{\partial \gamma_{C}} \frac{\partial^{2} q_{k}}{\partial \gamma_{A} \gamma_{B}} \right)$$

$$+ \frac{\partial^{2} \tau}{\partial q_{i} \partial q_{j}} \frac{\partial^{3} q_{j}}{\partial \gamma_{A} \partial \gamma_{B} \partial_{C}}.
\tag{86}$$

The form of these equations is the same in Cartesian coordinates (simply replace q_i by x_i and $p_i^{(q)}$ by p_i).

4.2 Constraints on position perturbations

The traveltime τ is constant along any trajectory situated in the wavefront. Therefore, the total derivatives of τ with respect to the ray coordinates γ_A must be zero for any order of these derivatives. We obtain

$$\frac{\mathrm{d}\tau}{\mathrm{d}\gamma_A} = \frac{\partial\tau}{\partial q_i} \frac{\partial q_i}{\partial \gamma_A} = 0,\tag{87}$$

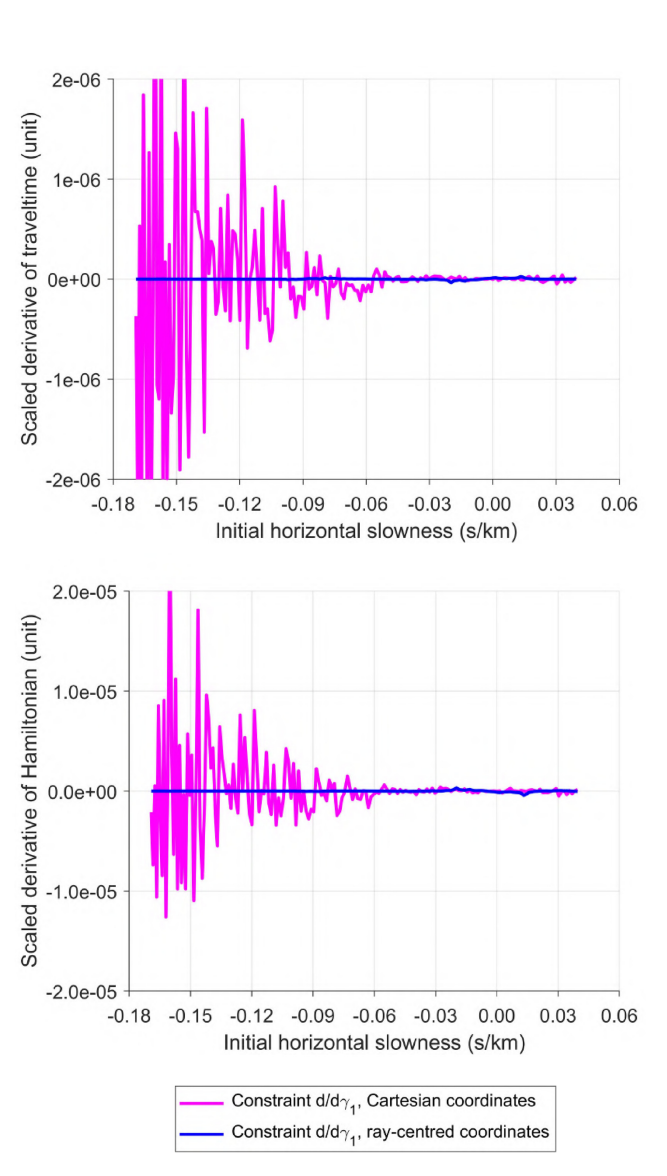


Figure 12. Constraint evaluation along a wavefront, $\tau = 0.8$ s, in the Marmousi VTI model, for third-order dynamic ray tracing in Cartesian (magenta) and ray-centred (blue) coordinates. Top panel: scaled derivatives of traveltime $d^3\tau/d\gamma_1^3$. The derivatives are scaled by the factor $\delta\gamma/\tau$, with $\delta\gamma$ set as in Fig. 10. Bottom panel: scaled derivatives of the Hamiltonian $d^3\mathcal{H}/d\gamma_1^3$. The scale factor is $(\delta\gamma)^3/(6\mathcal{H})$, with $\mathcal{H}=1/2$.

$$\frac{\mathrm{d}^{2}\tau}{\mathrm{d}\gamma_{A}\mathrm{d}\gamma_{B}} = \frac{\partial^{2}\tau}{\partial q_{i}\partial q_{j}} \frac{\partial q_{i}}{\partial \gamma_{A}} \frac{\partial q_{j}}{\partial \gamma_{B}} + \frac{\partial \tau}{\partial q_{i}} \frac{\partial^{2}q_{i}}{\partial \gamma_{A}\partial \gamma_{B}} = 0, \tag{88}$$

$$\frac{\mathrm{d}^{3}\tau}{\mathrm{d}\gamma_{A}\mathrm{d}\gamma_{B}\mathrm{d}\gamma_{C}} = \frac{\partial^{3}\tau}{\partial q_{i}\partial q_{j}\partial q_{k}} \frac{\partial q_{i}}{\partial \gamma_{A}} \frac{\partial q_{j}}{\partial \gamma_{B}} \frac{\partial q_{k}}{\partial \gamma_{C}}$$

$$+ \frac{\partial^{2}\tau}{\partial q_{i}\partial q_{j}} \left(\frac{\partial q_{i}}{\partial \gamma_{A}} \frac{\partial^{2}q_{j}}{\partial \gamma_{B}\partial \gamma_{C}} + \frac{\partial q_{i}}{\partial \gamma_{B}} \frac{\partial^{2}q_{j}}{\partial \gamma_{A}\partial \gamma_{C}} + \frac{\partial q_{i}}{\partial \gamma_{C}} \frac{\partial^{2}q_{j}}{\partial \gamma_{A}\partial \gamma_{B}} \right)$$

$$+ \frac{\partial \tau}{\partial q_{i}} \frac{\partial^{3}q_{i}}{\partial \gamma_{A}\partial \gamma_{B}\partial \gamma_{C}}$$

$$= 0. \tag{89}$$

Eqs (87)–(89) can be referred to as the first-, second- and third-order *position constraint relations* for dynamic ray tracing. The form of the equations remains the same in Cartesian coordinates (replace q_i with x_i).

A remark: If a point (q_i) is perturbed, then the traveltime τ will in general change as well. However, if the point (q_i) is fixed and only the momentum $(p_i^{(q)})$ is varied, the traveltime τ will remain unchanged. As a consequence, eqs (87)–(89) do not include partial derivatives of τ with respect to $p_i^{(q)}$, as all such derivatives are zero.

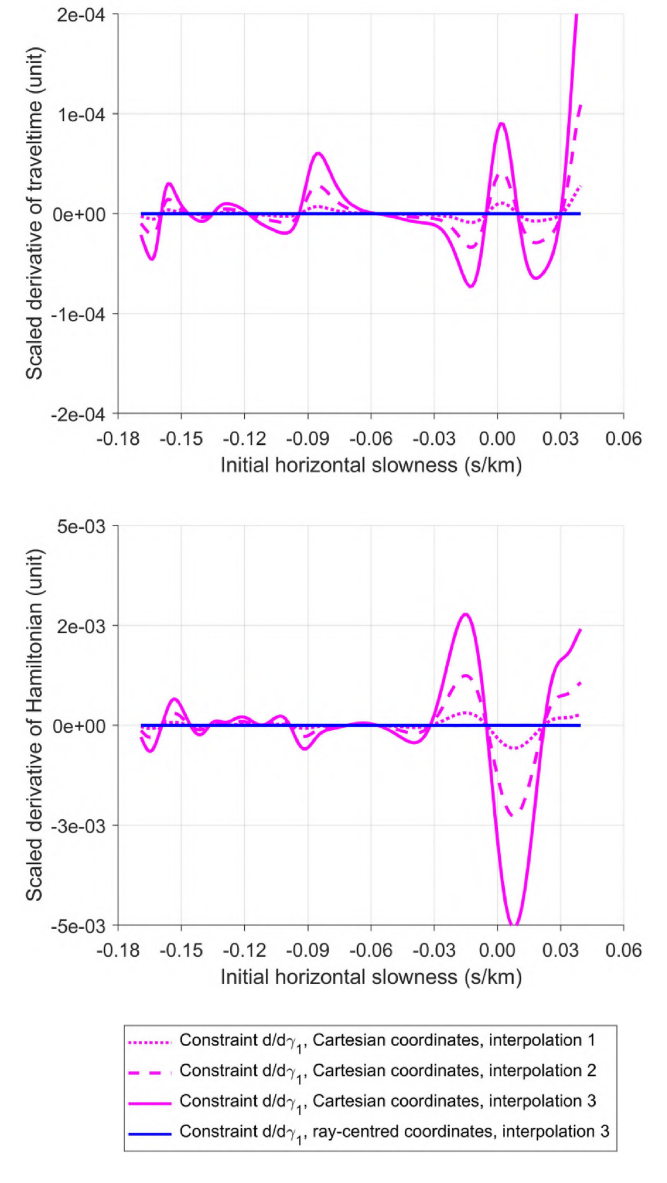


Figure 13. Constraint evaluation along a wavefront, $\tau=0.8$ s, in the Marmousi VTI model, after interpolation of first-order (conventional) dynamic ray tracing results in Cartesian and ray-centred coordinates. Top panel: scaled derivatives of traveltime $d\tau/d\gamma_1$ for three cases of interpolation of dynamic ray tracing results in Cartesian coordinates (magenta) and one interpolation in ray-centred coordinates (blue). The derivatives are scaled by the factor $\delta\gamma/\tau$, with $\delta\gamma=0.01$ s km⁻¹. Bottom panel: scaled derivatives of the Hamiltonian $d\mathcal{H}/d\gamma_1$ for three cases of interpolation of dynamic ray tracing results in Cartesian coordinates (magenta) and one interpolation in ray-centred coordinates (magenta). The scale factor is $\delta\gamma/\mathcal{H}$, with $\mathcal{H}=1/2$ and $\delta\gamma=0.01$ s km⁻¹.

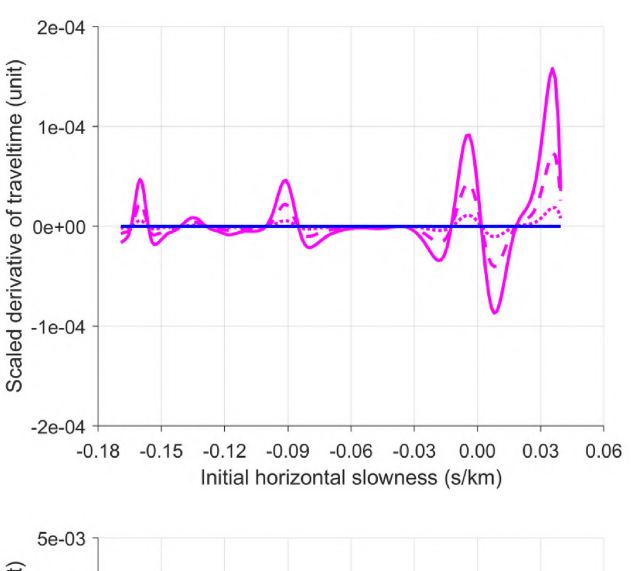
4.3 Constraints on phase-space perturbations

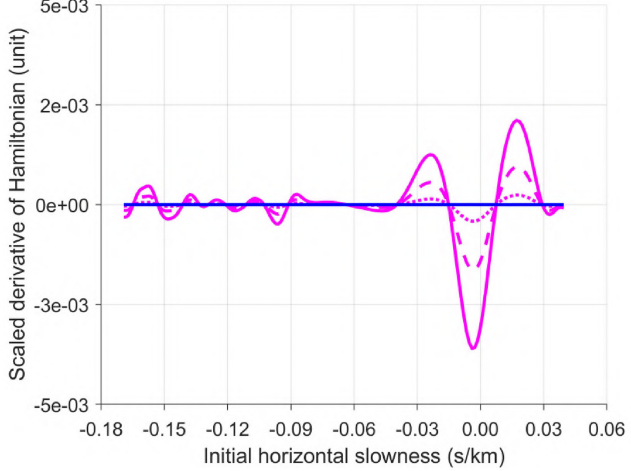
The Hamiltonian in ray-centred phase-space coordinates was introduced in the Hamilton–Jacobi eq. (11). The Hamiltonian is a freely varying function in the six coordinates, but eq. (11) yields a zeroth-order constraint on the domain (manifold) that can give valid ray solutions.

The Hamiltonian is constant along any trajectory in the wavefront. As a consequence, the total derivatives of the Hamiltonian with respect to the ray coordinates γ_A must be zero, to any order. For the first three orders these total derivatives are

$$\frac{\mathrm{d}\mathcal{H}}{\mathrm{d}\gamma_A} = \frac{\partial\mathcal{H}}{\partial w_r^{(q)}} \frac{\partial w_r^{(q)}}{\partial \gamma_A} = 0,\tag{90}$$

$$\frac{\mathrm{d}^{2}\mathcal{H}}{\mathrm{d}\gamma_{A}\mathrm{d}\gamma_{B}} = \frac{\partial^{2}\mathcal{H}}{\partial w_{r}^{(q)}\partial w_{s}^{(q)}} \frac{\partial w_{r}^{(q)}}{\partial \gamma_{A}} \frac{\partial w_{s}^{(q)}}{\partial \gamma_{B}} + \frac{\partial\mathcal{H}}{\partial w_{r}^{(q)}} \frac{\partial^{2}w_{r}^{(q)}}{\partial \gamma_{A}\partial \gamma_{B}} = 0, \tag{91}$$





Constraint $d/d\gamma_1$, Cartesian coordinates, interpolation 1

Constraint $d/d\gamma_1$, Cartesian coordinates, interpolation 2

Constraint $d/d\gamma_1$, Cartesian coordinates, interpolation 3

Constraint $d/d\gamma_1$, ray-centred coordinates, interpolation 3

Figure 14. Constraint evaluation along a wavefront, $\tau=0.8$ s, in the Marmousi VTI model, after interpolation of second-order dynamic ray tracing results in Cartesian and ray-centred coordinates. Top panel: scaled derivatives of traveltime $d^2\tau/d\gamma_1^2$ for three cases of interpolation of dynamic ray tracing results in Cartesian coordinates (magenta) and one interpolation in ray-centred coordinates (blue). The derivatives are scaled by the factor $(\delta \gamma)^2/(2\tau)$ with $\delta \gamma$ set as in Fig. 13. Bottom panel: scaled derivatives of the Hamiltonian $d^2\mathcal{H}/d\gamma_1^2$ for three cases of interpolation of dynamic ray tracing results in Cartesian coordinates (magenta) and one interpolation in ray-centred coordinates (magenta). The scale factor is $(\delta \gamma)^2/(2\mathcal{H})$, with $\mathcal{H}=1/2$.

$$\frac{\mathrm{d}^{3} \mathcal{H}}{\mathrm{d}\gamma_{A} \mathrm{d}\gamma_{B} \mathrm{d}\gamma_{C}} = \frac{\partial^{3} \mathcal{H}}{\partial w_{r}^{(q)} \partial w_{s}^{(q)} \partial w_{t}^{(q)}} \frac{\partial w_{r}^{(q)}}{\partial \gamma_{A}} \frac{\partial w_{s}^{(q)}}{\partial \gamma_{B}} \frac{\partial w_{t}^{(q)}}{\partial \gamma_{C}} + \frac{\partial w_{r}^{(q)}}{\partial \gamma_{B}} \frac{\partial^{2} w_{s}^{(q)}}{\partial \gamma_{A} \partial \gamma_{C}} + \frac{\partial w_{r}^{(q)}}{\partial \gamma_{A}} \frac{\partial^{2} w_{s}^{(q)}}{\partial \gamma_{A} \partial \gamma_{C}} + \frac{\partial w_{r}^{(q)}}{\partial \gamma_{A} \partial \gamma_{C}} + \frac{\partial^{2} w_{s}^{(q)}}{\partial \gamma_{A} \partial \gamma_{C}} + \frac{\partial^{2} w_{s}^{(q)}}{\partial \gamma_{A} \partial \gamma_{B}} \right) + \frac{\partial^{2} \mathcal{H}}{\partial w_{r}^{(q)}} \frac{\partial^{3} w_{r}^{(q)}}{\partial \gamma_{A} \partial \gamma_{B} \partial \gamma_{C}} = 0. \tag{92}$$

The form of the eqs (90)–(92) is the same for Cartesian coordinates (replace $w_r^{(q)}$ with w_r). Eq. (90) is then restated

$$\frac{\mathrm{d}\mathcal{H}}{\mathrm{d}\gamma_A} = \frac{\partial \mathcal{H}}{\partial w_r} \frac{\partial w_r}{\partial \gamma_A} = 0,\tag{93}$$

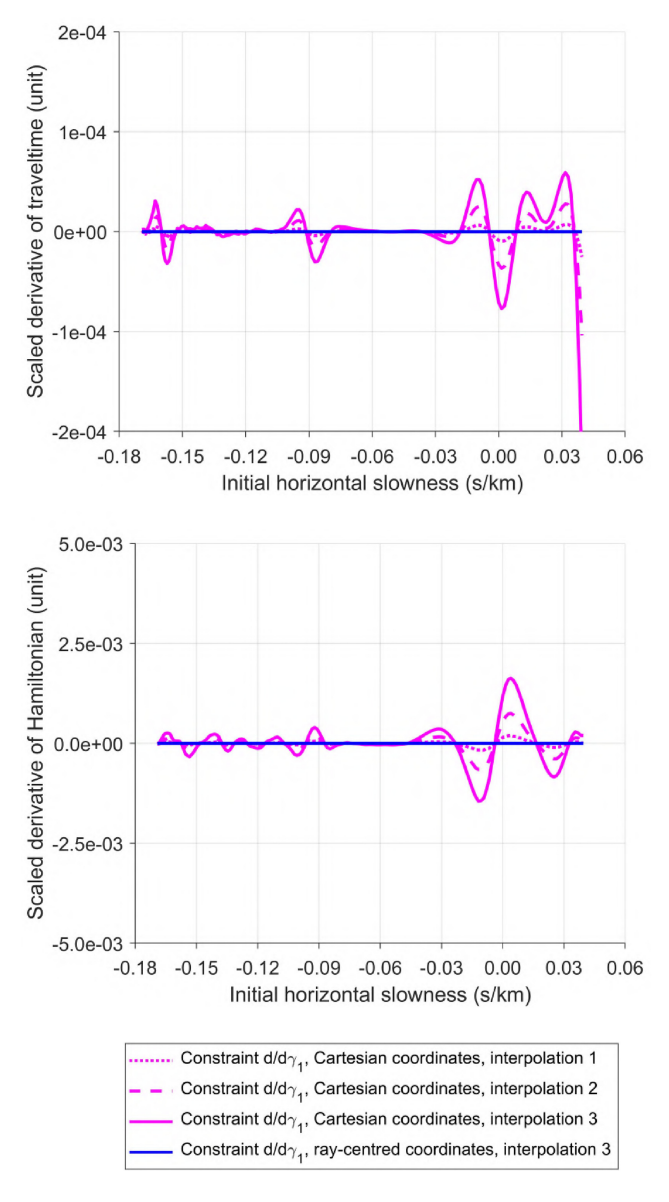


Figure 15. Constraint evaluation along a wavefront, $\tau = 0.8$ s, in the Marmousi VTI model, after interpolation of third-order dynamic ray tracing results in Cartesian and ray-centred coordinates. Top panel: scaled derivatives of traveltime $d^3\tau/d\gamma_1^3$ for three cases of interpolation of dynamic ray tracing results in Cartesian coordinates (magenta) and one interpolation in ray-centred coordinates (blue). The derivatives are scaled by the factor $(\delta \nu)^3/(6\tau)$ with $\delta \gamma$ set as in Fig. 13. Bottom panel: scaled derivatives of the Hamiltonian $d^3\mathcal{H}/d\gamma_1^3$ for three cases of interpolation of dynamic ray tracing results in Cartesian coordinates (magenta) and one interpolation in ray-centred coordinates (magenta). The scale factor is $(\delta \gamma)^3/(6\mathcal{H})$, with $\mathcal{H}=1/2$.

and Červený (2001) refers to it as the *constraint relation* for dynamic ray tracing in Cartesian coordinates. This constraint concept is extended to higher orders by Iversen *et al.* (2019). In the context of the current paper it is natural to refer to equations of the form (90)–(92) as first, second- and third-order *phase-space constraint relations* for dynamic ray tracing.

5 TRANSFORMATION OF DERIVATIVES OF PERTURBATIONS BETWEEN RAY-CENTRED AND CARTESIAN COORDINATES

Consider a field of paraxial rays specified by two variables γ_A , A = 1, 2. For an arbitrary location on the reference ray Ω it is of importance to have access to efficient transformations of derivatives of perturbations given in ray-centred coordinates to derivatives in Cartesian coordinates, and vice versa.

Using the chain rule it is straightforward to state generic relations for derivatives of perturbations in Cartesian coordinates in terms of those given in ray-centred coordinates. For the first, second- and third-order derivatives the transformation relations are

$$X_{xA} = \Lambda_{xx} X_{rA}^{(q)}, \tag{94}$$

$$X_{xAB} = \Lambda_{xr} X_{rAB}^{(q)} + \Lambda_{xrs} X_{rA}^{(q)} X_{sB}^{(q)}, \tag{95}$$

 $X_{xABC} = \Lambda_{xr} X_{rABC}^{(q)} + \Lambda_{xrs} \left(X_{rBC}^{(q)} X_{sA}^{(q)} + X_{rAC}^{(q)} X_{sB}^{(q)} + X_{rAB}^{(q)} X_{sC}^{(q)} \right) + \Lambda_{xrst} X_{rA}^{(q)} X_{sB}^{(q)} X_{rC}^{(q)}.$ (96)

Here, all quantities have been evaluated on the ray Ω . For definition of the Λ -quantities, see eq. (26) and Tables 6–7. The inverse transformation has the same form as (94)–(96) so we do not include it here.

Using eqs (94)–(96) and the results for the Λ -quantities it is straightforward and simple to transform derivatives of perturbations from ray-centred to Cartesian coordinates. However, since there are quite a few zero elements included in the Λ -quantities it can be beneficial, both for efficiency and clarity, to relate explicitly the various Q- and P-quantities in ray-centred coordinates to the corresponding Q- and P-quantities in Cartesian coordinates. For such explicit expressions, the reader is referred to Appendix E.

6 INITIAL CONDITIONS

The described framework of ODEs for higher-order derivatives of perturbations in ray-centred coordinates requires specification of proper initial conditions. Moreover, ray-centred coordinates can be useful for designing initial conditions for continuation of derivatives in Cartesian coordinates. To keep the discussion simple, we consider in the following only the initial conditions for a point source and a plane-wave source. The expressions derived in this section are fully consistent with those obtained in the section on initial conditions in Iversen *et al.* (2019).

6.1 Initial conditions for derivatives of perturbations in ray-centred coordinates

For a point source and a plane-wave source the initial conditions for the derivatives of perturbations in ray-centred coordinates are particularly simple. In fact, in each of these cases all such derivatives will have to be zero, with only one exception. The initial conditions are

$$\mathcal{P}_{IA} = \delta_{IA}$$
; all other derivatives of perturbations = 0; (97)

for a point source, and

$$Q_{IA} = \delta_{IA}$$
; all other derivatives of perturbations = 0; (98)

for a plane-wave source.

6.2 Ray-centred coordinates as a means to specify initial conditions for derivatives of perturbations in Cartesian coordinates

We use ray-centred coordinates as a means to specify initial conditions in Cartesian coordinates. As support for the derivations we use intrinsic relations for the dynamic ray tracing quantities in ray-centred coordinates (Appendix D) and transformations relating the dynamic ray tracing quantities in Cartesian and ray-centred coordinates (Appendix E).

Applying $Q_{IA} = 0$ and $P_{IA} = \delta_{IA}$ in eqs (E2) and (E5) yields an initial condition in Cartesian coordinates for the point-source situation,

$$Q_{iA} = 0, \qquad P_{iA} = \mathcal{F}_{iA}. \tag{99}$$

Likewise, by using $Q_{IA} = \delta_{IA}$ and $\mathcal{P}_{IA} = 0$ in eqs (E2) and (E5) we get a plane-wave initial condition in Cartesian coordinates,

$$Q_{iA} = \mathcal{E}_{iA}, \qquad P_{iA} = p_i \eta_i \mathcal{E}_{iA}. \tag{100}$$

We note that for a point source or a plane-wave source we always have

$$Q_{3AB} = 0, Q_{3ABC} = 0. (101)$$

6.2.1 Point source

For a point source, we use eqs (D6) and (D12) for the second- and third-order derivatives of $\delta p_3^{(q)}$ to obtain

$$\mathcal{P}_{3AB} = -V_{AB}^{(q)}, \qquad \mathcal{P}_{3ABC} = -V_{ABC}^{(q)}. \tag{102}$$

Eqs (E12) and (E18) now become particularly simple,

$$P_{iAB} = p_i \mathcal{P}_{3AB}, \qquad P_{iABC} = p_i \mathcal{P}_{3ABC}, \tag{103}$$

which further yields

$$P_{iAB} = -p_i V_{jk} \mathcal{F}_{jA} \mathcal{F}_{kB}, \tag{104}$$

$$P_{iABC} = -p_i V_{jkl} \mathcal{F}_{jA} \mathcal{F}_{kB} \mathcal{F}_{lC}, \tag{105}$$

in the point-source situation.

6.2.2 Plane-wave source

For a plane-wave source, eqs (D6) and (D12) give the expressions

$$\mathcal{P}_{3AB} = -U_{AB}^{(q)}, \qquad \mathcal{P}_{3ABC} = -U_{ABC}^{(q)}. \tag{106}$$

Eq. (E12) then attains the form

$$P_{iAB} = \frac{\partial^2 p_i}{\partial q_A \partial q_B} + p_i \mathcal{P}_{3AB},\tag{107}$$

which results in

$$P_{i,AB} = -p_i \left(U_{mn} - 3\eta_m \eta_n \right) \mathcal{E}_{mA} \mathcal{E}_{nB}. \tag{108}$$

Moreover, eq. (E18) reduces to

$$P_{iABC} = \frac{\partial^{3} p_{i}}{\partial q_{A} \partial q_{B} \partial q_{C}} + \frac{\partial p_{i}}{\partial q_{A}} \mathcal{P}_{3BC} + \frac{\partial p_{i}}{\partial q_{B}} \mathcal{P}_{3AC} + \frac{\partial p_{i}}{\partial q_{C}} \mathcal{P}_{3AB} + \frac{\partial p_{i}}{\partial p_{i}^{(q)}} \mathcal{P}_{3ABC},$$

$$(109)$$

hence,

$$P_{iABC} = 6p_i \, \eta_m \eta_n \eta_p \mathcal{E}_{mA} \mathcal{E}_{nB} \mathcal{E}_{pC} - p_i \, (\eta_m \mathcal{E}_{mA} U_{RC}^{(q)} + \eta_m \mathcal{E}_{mB} U_{AC}^{(q)} + \eta_m \mathcal{E}_{mC} U_{AR}^{(q)} + U_{ARC}^{(q)}).$$
(110)

Applying eqs (28) and (57) then yields

$$P_{iABC} = p_i \left(15\eta_m \eta_n \eta_p - 3\eta_m U_{np} - 3\eta_n U_{mp} - 3\eta_p U_{mn} - U_{mnp} \right) \mathcal{E}_{mA} \mathcal{E}_{nB} \mathcal{E}_{pC}. \tag{111}$$

7 PARAXIAL EXTRAPOLATION

To prepare for the numerical examples section, we review the main formulas from Iversen *et al.* (2019) for paraxial extrapolation of traveltime and geometrical spreading, in Cartesian coordinates.

We consider a reference ray that connects a source point, \mathbf{s}_0 , and a receiver point, \mathbf{r}_0 . Using the dynamic ray tracing quantities that have been integrated along the reference ray, our objective is to extrapolate traveltime and geometrical spreading to receiver locations \mathbf{r} in the (paraxial) vicinity of \mathbf{r}_0 . Since these operations are done in Cartesian coordinates, we must, as a preparatory step, transform all relevant dynamic ray tracing quantities from ray-centred to Cartesian coordinates.

7.1 Extrapolation of traveltime

Given a fixed source point, \mathbf{s}_0 , the paraxial extrapolation of traveltime from a reference receiver point \mathbf{r}_0 to a general receiver point \mathbf{r} is expressed by means of a Taylor series (Iversen *et al.* 2019, eq. 92)

$$T(\mathbf{r}, \mathbf{s}_{0}) = \tau(\mathbf{r}_{0}, \mathbf{s}_{0}) + p_{i} \, \Delta r_{i} + \frac{1}{2} \frac{\partial^{2} T}{\partial r_{i} \partial r_{j}} \, \Delta r_{i} \Delta r_{j}$$

$$+ \frac{1}{6} \frac{\partial^{3} T}{\partial r_{i} \partial r_{j} \partial r_{k}} \, \Delta r_{i} \Delta r_{j} \Delta r_{k} + \frac{1}{24} \frac{\partial^{4} T}{\partial r_{i} \partial r_{j} \partial r_{k} \partial r_{l}} \, \Delta r_{i} \Delta r_{j} \Delta r_{k} \Delta r_{l} + \dots,$$

$$(112)$$

where $\Delta r_i = r_i - r_{i0}$. The derivatives of traveltime on the right-hand side do all correspond to the reference location, \mathbf{r}_0 . The relations between these derivatives and the dynamic ray tracing quantities, i.e., the derivatives of the phase-space perturbations, are given by eqs (93)–(95) in Iversen *et al.* (2019).

7.2 Extrapolation of geometrical spreading

We extrapolate the 3 \times 3 geometrical spreading matrix in Cartesian coordinates, $\{Q_{ia}\}=\{\partial x_i/\partial \gamma_a\}$, to paraxial locations. The first two columns of $\{Q_{ia}\}$ represent the paraxial solutions arising from the point-source initial condition; the third column is the ray-velocity vector. Eq. (87) in Iversen *et al.* (2019) yields a Taylor series for the elements Q_{ia} ,

$$Q_{ia}(\mathbf{r}, \mathbf{s}_{0}) = Q_{ia}(\mathbf{r}_{0}, \mathbf{s}_{0}) + \frac{\partial Q_{ia}}{\partial r_{k}}(\mathbf{r}_{0}, \mathbf{s}_{0}) \Delta r_{k} + \frac{1}{2} \frac{\partial^{2} Q_{ia}}{\partial r_{k} \partial r_{l}}(\mathbf{r}_{0}, \mathbf{s}_{0}) \Delta r_{k} \Delta r_{l}$$

$$+ \frac{1}{6} \frac{\partial^{3} Q_{ia}}{\partial r_{k} \partial r_{l} \partial r_{m}}(\mathbf{r}_{0}, \mathbf{s}_{0}) \Delta r_{k} \Delta r_{l} \Delta r_{m} + \dots,$$

$$(113)$$

where the first three sets of derivatives are given by their eqs (88)–(90). All indices in eq. (113) and in the underlying computation of Taylor series coefficients run from 1 to 3.

It is important to note that a complete computation of the first-order coefficients $\partial Q_{ia}/\partial r_k$ requires Q_{iab} (second-order dynamic ray tracing), a complete computation of the second-order coefficients $\partial^2 Q_{ia}/\partial r_k \partial r_l$ requires Q_{iabc} (third-order dynamic ray tracing), and a complete computation of the third-order coefficients $\partial^3 Q_{ia}/\partial r_k \partial r_l \partial r_m$ requires Q_{iabcd} (fourth-order dynamic ray tracing). However, in the latter case, even if we do not know Q_{iABCD} ($A, B, \ldots = 1, 2$), we are still able to obtain the remaining elements Q_{iabcd} ($a, b, \ldots = 1, 2, 3$) consisting of time derivatives of the lower-order Q-quantities.

We assume point-source initial conditions for the dynamic ray tracing at the source point \mathbf{s}_0 . For a paraxial ray from \mathbf{s}_0 to the receiver point \mathbf{r} the relative geometrical spreading can then be obtained by (Iversen *et al.* 2019, eq. 91)

$$\mathcal{L}(\mathbf{r}, \mathbf{s}_0) = \left| \frac{1}{c(\mathbf{r})} \det \{ Q_{ia}(\mathbf{r}, \mathbf{s}_0) \} \right|^{1/2}.$$
(114)

Here, $c(\mathbf{r})$ is the phase velocity of the paraxial ray at \mathbf{r} . The quantity \mathcal{L} has the measurement unit of distance/slowness (in SI units, e.g. $\mathrm{km}^2\,\mathrm{s}^{-1}$).

8 NUMERICAL EXAMPLES

We illustrate the above methodology by means of numerical examples in two different subsurface models, named 3-D VTI and Marmousi VTI. As signified by the abbreviation, the anisotropy in both models is transversely isotropic with a vertical axis of symmetry. Other common aspects of the two models: The ratio of of the vertical P-and S-wave velocities is set constant everywhere, to 2, and Thomsen's anisotropy parameters (Thomsen 1986) are defined constant throughout, with $\epsilon = 0.3$ and $\delta = 0.1$. As we consider only P-wave simulations, the value of Thomsen's parameter γ does not influence the results.

Note that the Cartesian model coordinates are referred to in this section as x, y and z.

8.1 Simulations using model 3-D VTI

Iversen *et al.* (2019) tested higher-order dynamic ray tracing in Cartesian coordinates for a 3-D model with weak lateral velocity variation and different situations of anisotropy. We use here the vertical transversely isotropic (VTI) version of that model, for which the vertical *P*-and *S*-wave velocity fields correspond to a gentle anticline structure.

8.1.1 Data

As data for numerical comparisons we use values of traveltime and geometrical spreading, obtained by conventional leading-order kinematic and dynamic ray tracing, in Cartesian coordinates (Iversen *et al.* 2019). We consider a buried source point $\mathbf{s}_0 = (7, 5, 4)$ km to receivers in the plane at zero depth (Fig. 1). The nearly vertical ray (light grey) arriving at the receiver location $\mathbf{r}_0 = (7, 5, 0)$ km is used as a reference for the higher-order dynamic ray tracing computations, in ray-centred as well as Cartesian coordinates.

All computed differences in traveltime and geometrical spreading are relative to the data values obtained previously (Iversen et al. 2019).

8.1.2 Extrapolation of traveltime

We do dynamic ray tracing simulations in ray-centred coordinates along the selected reference ray, which connects the fixed source point, \mathbf{s}_0 , and the chosen reference receiver point, \mathbf{r}_0 . The dynamic ray tracing is conducted for different orders in the derivatives of the phase-space perturbations: first order (conventional dynamic ray tracing), second order and third order.

At the point \mathbf{r}_0 , the dynamic ray tracing quantities are transformed to Cartesian coordinates, and thereby, we obtain coefficients for (paraxial) extrapolation of traveltime away from the reference ray. A Taylor series with terms up to order four is used for this purpose (eq. 112). In addition, as also done in Iversen *et al.* (2019), we compute coefficients in a Taylor series for the *square* of the traveltime, as this extrapolation method often yields good results, in particular for weakly heterogeneous isotropic media.

Fig. 2 shows traveltimes extrapolated at zero depth, along the line y = 5 km, (top) and the corresponding relative errors (bottom). The traveltime extrapolation errors are in general quite small for all the approaches considered. We observe that in the case of second-order extrapolation, which is based on conventional dynamic ray tracing only, the use of Taylor series for squared traveltime (dashed blue) yields a better result than with a plain Taylor series for the traveltime (solid blue). In general, this is however not always the case (Ursin 1982a; Gjøystdal *et al.* 1984). Our fourth-order extrapolations of traveltime (solid magenta) and squared traveltime (dashed magenta) yield better results than the corresponding second-order approaches. Also to fourth order, a Taylor series for squared traveltime give smaller errors than a plain Taylor series for the traveltime. The latter errors are below 0.025 per cent within a 2 km paraxial distance (the lateral distance away from the reference ray).

In Fig. 3 we compare traveltime extrapolation using Taylor series coefficients obtained from dynamic ray tracing in Cartesian coordinates (Iversen *et al.* 2019) and ray-centred coordinates (methodology of this paper). The relative difference between using Cartesian and ray-centred coordinates is larger for the fourth-order than for the lower-order extrapolations, but still below 5e-07 at 3 km paraxial distance. In other words, the traveltime extrapolation results obtained using Cartesian and ray-centred coordinates are highly consistent.

8.1.3 Extrapolation of geometrical spreading

Previously, for dynamic ray tracing in Cartesian coordinates (Iversen *et al.* 2019), we used eq. (113) to extrapolate the geometrical spreading matrix and subsequently eq. (114) to compute the relative geometrical spreading in the (paraxial) receiver point. All coefficients used in the extrapolation were computed in the endpoint of the reference ray (the reference receiver point). We examined extrapolation of the geometrical spreading for the three available sets of dynamic ray tracing quantities—corresponding to first-, second- and third-order dynamic ray tracing.

As explained above, a certain order of the dynamic ray tracing does not permit to compute the full set of coefficients for extrapolation of the geometrical spreading matrix up to the same order. Therefore, for first-order dynamic ray tracing the first-order extrapolation coefficients are incomplete (Q_{iAB} are not known), for second-order dynamic ray tracing the second-order extrapolation coefficients are incomplete (Q_{iABC} are not known), and so forth. In Iversen *et al.* (2019) the unknown coefficients were simply set to zero. Here, we proceed in the same manner when extrapolating the geometrical spreading matrix based on dynamic ray tracing computations in ray-centred coordinates. The results are shown in Fig. 4, where the solid blue, cyan, and magenta curves correspond, respectively, to a first-, second- and third-order Taylor expansion using eq. (113). Among these three, it is only the third-order expansion, with input data from third-order dynamic ray tracing, that yields a satisfactory extrapolation result.

Fig. 4 includes, in addition to the solid magenta curve, also a dotted version. That curve also corresponds to third-order dynamic ray tracing, but now we have lowered the extrapolation order from three to two. As a consequence, the second-order expansion is in this case performed with a complete set of coefficients. We can see that the results for the solid and dotted magenta curves are quite similar: the relative errors are below 1 per cent for paraxial distances 0–1 km and below 5 per cent for paraxial distances 0–2 km. In other words, whether we use a second- or third-order Taylor expansion is not decisive in this situation—what is important is that the dynamic ray tracing is of third order.

Next, we compare in Fig. 5 the extrapolation of geometrical spreading based on dynamic ray tracing in ray-centred coordinates with the corresponding values obtained using Cartesian coordinates (Iversen *et al.* 2019). For the higher-order approaches the relative difference is within 2e-05 at 3 km paraxial distance, so the two dynamic ray tracing approaches must be said to yield very consistent results. Note one particular aspect, that becomes very apparent in Fig. 5 because of the scale: Dynamic ray tracing in ray-centred and Cartesian coordinates are mathematically equivalent, but their numerical implementations result in different values for geometrical spreading on the reference ray. The relative difference is very small though (\approx 1e-06).

8.1.4 Constraints along the reference ray

To get an impression of the numerical errors involved in the integration along the reference ray Ω we monitor the constraints on the perturbations of the position vector (eqs 87–89) and on the phase-space vector (eqs 90–92). The total derivatives in these equations shall ideally be perfectly zero.

For dynamic ray tracing in Cartesian coordinates this monitoring is straightforward. We simply evaluate the constraint relations [eqs (87)–(92)] restated such that $q_i \to x_i$, $w_r^{(q)} \to w_r$.

A similar operation for dynamic ray-tracing in ray-centred coordinates will however just yield zero, in a numerical sense. The reason is that we have already used the constraint relations to remove redundancy from the dynamic ray tracing ODEs. We can however get a measure of the numerical accuracy if we (1) transform the obtained results for the position and phase-space perturbations to Cartesian coordinates and (2) apply relations (87)–(92), again with $q_i \to x_i$, $w_r^{(q)} \to w_r$ (version for Cartesian coordinates). The errors involved in the continuation of the ray-centred coordinate system will then become visible.

Selected graphs corresponding to the involved first-, second- and third-order constraints are shown in Figs 6–8. To facilitate comparison of the graphs the first, second and third total derivatives of the traveltime are multiplied by the scale factors $\delta \gamma / \tau$, $(\delta \gamma)^2 / (2\tau)$ and $(\delta \gamma)^3 / (6\tau)$, respectively, where $\delta \gamma$ is a constant and τ is the traveltime to the current point. Likewise, the first, second and third total derivatives of the Hamiltonian are scaled by the factors $\delta \gamma / \mathcal{H}$, $(\delta \gamma)^2 / (2\mathcal{H})$ and $(\delta \gamma)^3 / (6\mathcal{H})$, where $\mathcal{H} = 1/2$. For all graphs shown we have set $\delta \gamma = 0.01 \text{ s km}^{-1}$.

We summarize our observations.

- (1)A general remark is that the deviations from zero are very small. The largest scaled derivative of the traveltime is \approx 2e-08 (Fig. 7, top panel), while the largest scaled derivative of the Hamiltonian is \approx 1e-07 (Fig. 7, bottom panel).
- (2) The impact on the paraxial deviations of the Hamiltonian seems to be a lot smaller for dynamic ray tracing in ray-centred coordinates than for dynamic ray tracing in Cartesian coordinates.
- (3)The constraint graphs based on dynamic ray tracing in ray-centred coordinates appears somewhat more high frequent than those for Cartesian coordinates. This could be related to the choice of ODE solver (MATLAB's 'ode45') and its settings. However, we must keep in mind that the scale in Figs 6–8 is very small (from 2e-07 down to 2e-10).

8.2 Simulations using model Marmousi VTI

Above, we studied the evolution of the position and phase-space constraint relations along a reference ray in the model 3-D VTI. As a next step, we evaluate and compare the constraint relations along a wavefront. These evaluations and comparisons are conducted for two situations—the as is case where we compare directly the constraint values resulting from higher-order dynamic ray tracing in Cartesian and ray-centred coordinates, and in addition the case when the dynamic ray tracing quantities have been obtained by interpolation. The objective of the latter is to expose eventual differences in the interpolation of dynamic ray tracing quantities given in Cartesian and ray-centred coordinates.

To add some challenges in terms of varying wavefront curvature, the tests are done in a different model, referred to as *Marmousi VTI*. It is the same model as were used by Iversen *et al.* (2021)—a smoothed version of the Marmousi model. The (vertical) *P*-wave velocity was smoothed using the NORSAR software, by applying a Hamming filter with radius 0.3 km.

8.2.1 Data

We wanted to do a test of interpolation of dynamic ray tracing quantities along a wavefront, such that the test results are relevant for the wavefront construction method—however, without invoking the wavefront construction method itself. Our solution to generating a 'true' wavefront reference data set, was to trace a dense system of rays a given time $\tau = 0.8$ s, with all rays starting in the point (x = 4.5, z = 2.7) km. Fig. 9 (top panel) shows shows the *P*-wave velocity field of the *Marmousi VTI* model, overlaid by the traced ray bundle (black) and the resulting wavefront points (grey). A close-up is provided in Fig. 9 (middle panel) to give a better impression of the wavefront geometry.

Along each ray, higher-order dynamic ray tracing was conducted in Cartesian and in ray-centred coordinates. These dynamic ray tracing data sets are used for two purposes: as reference data for numerical comparisons, and as input data to interpolation. The setup for the interpolation tests is outlined in Fig. 9 (bottom panel). For any point on the wavefront (marked by a triangle), three interpolations of dynamic ray tracing quantities based on neighbouring points are conducted. The input points for the three cases are marked in the figure by numbers 1, 2, 3, so that 3 corresponds to the largest interpolation distance.

8.2.2 Constraints along the wavefront

From the generated wavefront data sets, with dynamic ray tracing quantities in Cartesian and ray-centred coordinates stored for each point on the wavefront, we compute the position and phase-space constraints corresponding to first, second and third order in the ray parameters. We are then able to display the constraint values along the wavefront, similarly to what we did earlier along a reference ray.

As before all constraints for ray-centred coordinates are computed *after* transforming the dynamic ray tracing results to Cartesian coordinates. The reason is that we then include errors resulting from the continuation of the ray-centred basis along the rays. Without this operation all evaluated constraint relations for ray-centred coordinates would have been zero (see the comments above related to monitoring constraints along a specific ray).

Figs 10–12 show graphs corresponding to constraint quantities of first-, second- and third-order dynamic ray tracing, performed using Cartesian (magenta) and ray-centred (blue) coordinates. The scaling of the constraint quantities was done in the same way as when monitoring the constraints along a ray (Figs 6–8).

We observe the following.

- (1)For conventional dynamic ray tracing (Fig. 10) the position constraint appears as far more noisy for Cartesian than for ray-centred coordinates. This is also the general impression concerning the phase-space constraint. However, in some parts on the wavefront the phase-space constraint inconsistency is greater in ray-centred than in Cartesian coordinates. These parts have high negative and positive wavefront curvature and are therefore related to the formation of caustics.
- (2)For second-order dynamic ray tracing (Fig. 11) we observe, both for the position and the phase-space constraint, that in the right part the inconsistency of using ray-centred coordinates can be greater than when using Cartesian coordinates. In the left-hand part, the graphs for Cartesian coordinates more noisy, and the noise seems to increase with the increasing obliquity of the rays (away from the vertical).
- (3) For third-order dynamic ray tracing (Fig. 12) we see the same trends as in the second-order case.
- (4)In general, the consistency along the wavefront is much better for ray-centred coordinates than for Cartesian coordinates. However, Cartesian coordinates may do equally well or better in caustic regions.
- (5) The constraint relations for Cartesian coordinates seem quite sensitive to the obliquity of the ray path in this model.

8.2.3 Interpolation along the wavefront

Our setup to do interpolation of dynamic ray tracing results along the wavefront is outlined in Fig. 9(bottom panel). For each dynamic ray tracing coordinate type (Cartesian or ray-centred) we did three linear interpolations of the dynamic ray tracing quantities. The output point of the interpolation was chosen as one of the points we already have on the wavefront, the interpolation was conducted using input data from the first, second and third ray to the left and right (referring to Fig. 9). For the latter case (third ray to the left/right) the interpolation distance along the wavefront varies between 48 and 116 m.

The results for the constraint values, after linear interpolation of the dynamic ray tracing quantities from the ray neighbours, are shown in Figs 13–15. The constraint values, which measure the degree of consistency, appear as quite pronounced for Cartesian coordinates. For ray-centred coordinates, the constraint values are almost insensitive to linear interpolation of the dynamic ray tracing quantities.

Although the latter results are clearly in favour of ray-centred coordinates, it is important to note that the interpolation *error* is not necessarily less in ray-centred coordinates concerning, say, geometrical spreading. For the two coordinate systems the errors distribute on the different components of $\partial q_i/\partial \gamma_A$ and $\partial x_i/\partial \gamma_A$, but in ray-centred coordinates we have by definition $\partial q_3/\partial \gamma_A = 0$. The latter guarantees a better *consistency* along the wavefront. The graphs in Figs 13–15 are therefore very good news with respect to implementation of higher-order dynamic ray-tracing in ray-centred coordinates, as an intrinsic element of the wavefront construction method.

9 DISCUSSION

This work is a follow-up of a previous paper (Iversen *et al.* 2019), where we built a novel framework for higher-order dynamic ray tracing in Cartesian coordinates. No doubt, these coordinates have important advantages, such as the fact that the model coordinates are often also Cartesian, so one can then avoid quite complicated coordinate transformations. In addition, the implementation in Cartesian coordinates is relatively straightforward. However, dynamic ray tracing in Cartesian coordinates is subject to redundancies, and there is little we can do about it. A redundant ODE system increases the risk for numerical inconsistencies, and it is necessary to check the system closely by means of constraint relations. Ray-centred coordinates, on the other hand, yields explicit expressions for the redundant quantities, and it is easy to remove the corresponding ODEs from the system.

For some applications of dynamic ray tracing, it is useful to take the perspective of differential geometry, and ray-centred coordinates is then a natural choice. Here we have in mind approaches where the 'leading' coordinate of the velocity model has the unit of time, and—the corresponding time axis coincides with the reference ray for dynamic ray tracing. An example is the (generalized) Dix inversion problem (Iversen & Tygel 2008; de Hoop *et al.* 2014, 2015).

The number of ODEs for the higher-order fundamental solution of dynamic ray tracing in ray-centred coordinates is substantially reduced as compared to in Cartesian coordinates. We remark, however, that although the equations in Cartesian coordinates include redundancy, the number of independent solutions that we need to compute is the same in ray-centred and Cartesian coordinates. For example, if we want to find the 6×6 ray propagator matrix in Cartesian coordinates it is sufficient to compute the 6×4 system of paraxial solutions corresponding to an initial point source and an initial plane wave. The full 6×6 matrix is obtained by including the ray-tangent and non-eikonal solutions, which are given explicitly—dynamic ray tracing is not needed to computed them. The connections between the 6×4 paraxial system, the associated second-derivatives of traveltime and the 6×6 ray propagator matrix have been known for a long time (see, for example, Klimeš 1994; Červený 2001; Červený & Moser 2007; Červený et al. 2012; Klimeš 2013). Recently this topic has been further illuminated (Koren & Ravve 2021; Ravve & Koren 2021) founded on the properties of parametric functionals (Bliss 1916).

Our numerical tests of interpolation along a wavefront of dynamic ray tracing quantities, in Cartesian and ray-centred coordinates, clearly point in favour of the latter. We emphasize that the conducted interpolation is *linear*, as it typically would be in a practical and efficient ray theory implementation, for example in the wavefront construction method. One could of course consider a more sophisticated, non-linear, interpolation—in order to better honour the dynamic ray tracing quantities in Cartesian coordinates. However, this adds a complication and is therefore by itself an argument supporting to do the interpolation in ray-centred coordinates.

10 CONCLUSIONS

In this paper, we have extended conventional dynamic ray tracing, in ray-centred coordinates, to higher orders. The methodology applies to 3-D anisotropic heterogeneous models. A key application is paraxial extrapolation or interpolation of Green's function attributes, as a kernel operation within mapping, modelling or imaging.

For a 3-D model with VTI anisotropy, model 3-D VTI, we show that the results of higher-order extrapolation of traveltime and geometrical spreading are highly consistent with those obtained in a recent paper using dynamic ray tracing in Cartesian coordinates. Graphs corresponding to constraints along the reference ray confirm our expectation: that higher-order dynamic ray tracing in Cartesian coordinates may be exposed to numerical errors due to redundancies. The numerical inconsistencies resulting in the given model are however very small, both for dynamic ray tracing in Cartesian and in ray-centred coordinates.

In the 2-D model *Marmousi VTI* we tested the evolution of the constraint values along a given wavefront. This model has a much more complicated (vertical) *P*-wave velocity field than model *3-D VTI*, and not surprisingly, the general level of the constraint values is higher.

As a general observation, the consistency along the wavefront is found much better for ray-centred coordinates than for Cartesian coordinates. Moreover, for the model *Marmousi VTI* the constraint relations for Cartesian coordinates seem quite sensitive to the obliquity of the ray path. On the other hand, dynamic ray tracing in Cartesian coordinates is found equally consistent or better in caustic regions.

In a test of interpolation of the dynamic ray tracing quantities along the wavefront, for different interpolation distances, the consistency is far much better with interpolation in ray-centred coordinates than in Cartesian coordinates. This tells us that Cartesian and ray-centred coordinates can be used for dynamic ray tracing in a complementary way: Cartesian coordinates are a good choice when dynamic ray tracing is to be performed with relatively long time steps in a model specified in Cartesian coordinates, while ray-centred coordinates are better suited for approaches where wavefront consistency is important and/or the model is specified in curvilinear (wavefront) coordinates.

With the recent and current introduction of higher-order dynamic ray tracing in Cartesian and ray-centred coordinates, for elementary waves in a smooth anisotropic medium, the natural future extensions are (1) to describe the transformation of higher-order dynamic ray tracing quantities across interfaces, by reflection and transmission and (2) to take into account shear-wave coupling.

ACKNOWLEDGEMENTS

MVdH gratefully acknowledges support from the Simons Foundation under the MATH + X program, the National Science Foundation under grant DMS-1815143 and the corporate members of the Geo-Mathematical Group at Rice University. TS gratefully acknowledges support from the Simons Foundation under the MATH + X program. JI has been supported by the Academy of Finland (decision 295853). BU thanks the Research Council of Norway and the industry partners of the GAMES consortium at NTNU for financial support (grant No. 294404). EI and BU are grateful for being invited to meetings at Rice University. We have used academic software licenses from NORSAR and MathWorks. We are grateful for the feedback from the editorial board of *Geophysical Journal International*, represented by Louise Alexander, Jean Virieux and Michal Malinowski and for the valuable technical reviews by Zvi Koren and Ludek Klimeš.

DATA AVAILABILITY STATEMENT

The input and output data underlying this article will be shared on reasonable request to the corresponding author.

REFERENCES

- Bliss, G.A., 1916. Jacobi's condition for problems of the calculus of variations in parametric form, *Trans. Am. Math. Soc.*, **17**(2), 195–206
- Bortfeld, R., 1989. Geometrical ray theory: rays and traveltimes in seismic systems (second-order approximation of the traveltimes), *Geophysics*, 54, 342–349.
- Brandsberg-Dahl, S., de Hoop, M.V. & Ursin, B., 2003. Focusing in dip and AVA compensation on scatteringangle/azimuth common image gathers, *Geophysics*, **68**(1), 232–254.
- Bulant, P. & Klimeš, L., 2007. Numerical comparison of the isotropic-common-ray and anisotropic-common-ray approximations of the coupling ray theory, *Geophys. J. Int.*, 171(3), 1064–1081.
- Cameron, M.K., Fomel, S. & Sethian, J.A., 2007. Seismic velocity estimation from time migration, *Inverse Problems*, 23, 1329–1369.
- Červený, V., 1972. Seismic rays and ray intensities in inhomogeneous anisotropic media, Geophys. J. R. astr. Soc., 29, 1–13.
- Červený, V., 2001. Seismic Ray Theory, Cambridge Univ. Press.
- Červený, V. & Hron, F., 1980. The ray series method and dynamic ray tracing system for three-dimensional inhomogeneous media, *Bull. seism. Soc. Am.*, 70, 47–77.
- Červený, V. & Moser, T.J., 2007. Ray propagator matrices in threedimensional anisotropic inhomogeneous layered media, *Geophys. J. Int.*, 168, 593–604
- Červený, V. & Pšenčík, I., 2010. Gaussian beams in inhomogeneous anisotropic layered structures, *Geophys. J. Int.*, 180(2), 798–812.
- Červený, V., Molotkov, A. & Pšenčík, I., 1977. Ray Method in Seismology, Charles University.
- Červený, V., Klimeš, L. & Pšenčík, I., 1984. Paraxial ray approximations in the computation of seismic wavefields in inhomogeneous media, *Geo*phys. J. R. astr. Soc., 79, 89–104.
- Červený, V., Iversen, E. & Pšenčík, I., 2012. Two-point paraxial traveltimes in an inhomogeneous anisotropic medium, *Geophys. J. Int.*, **189**(3), 1597–1610.
- Chapman, C.H., 2004. Fundamentals of Seismic Wave Propagation, Cambridge Univ. Press.

- Chavel, I., 2006. Riemannian Geometry: A Modern Introduction, Vol. 98, Cambridge Univ. Press.
- de Hoop, M.V., Burridge, R., Spencer, C. & Miller, D., 1994. Generalized radon transform/amplitude versus angle (GRT/AVA) migration/inversion in anisotropic media, *Proc. SPIE*, 2301, 15–27.
- de Hoop, M.V., Holman, S.F., Iversen, E., Lassas, M. & Ursin, B., 2014. Reconstruction of a conformally euclidean metric from local boundary diffraction travel times, SIAM J. Math. Anal., 46(6), 3705–3726.
- de Hoop, M.V., Holman, S.F., Iversen, E., Lassas, M. & Ursin, B., 2015. Recovering the isometry type of a Riemannian manifold from local boundary diffraction travel times, *J. Math. Pures Appl.*, 103(3), 830–848.
- Dix, C.H., 1955. Seismic velocities from surface measurements, *Geophysics*, **20**(1), 68–86.
- Djebbi, R. & Alkhalifah, T., 2020. Hybrid frequency-domain full-waveform inversion using ray+Born sensitivity kernels, *Geophysics*, 85(4), R339– R347
- Douma, H. & de Hoop, M.V., 2006. Explicit expressions for prestack map time migration in isotropic and VTI media and the applicability of map depth migration in heterogeneous anisotropic media, *Geophysics*, 71(01), S13–S28.
- Duveneck, E., 2004. Velocity model estimation with data-derived wavefront attributes, *Geophysics*, 69(1), 265–274.
- Farra, V. & Madariaga, R., 1987. Seismic waveform modeling in heterogeneous media by ray perturbation theory, J. geophys. Res., 92, 2697–2712.
- Gajewski, D. & Pšenčík, I., 1990. Vertical seismic profile synthetics by dynamic ray tracing in laterally varying layered anisotropic structures, J. geophys. Res., 95(B7), 11 301–11 315.
- Gibson, R.L.Jr, Durussel, V. & Lee, K.-J., 2005. Modeling and velocity analysis with a wavefront-construction algorithm for anisotropic media, *Geophysics*, 70(4), T63–T74.
- Gjøystdal, H., Reinhardsen, J.E. & Ursin, B., 1984. Traveltime and wavefront curvature calculations in three-dimensional inhomogeneous layered media with curved interfaces, *Geophysics*, 49, 1466–1494.
- Goldin, S.V. & Duchkov, A.A., 2003. Seismic wave field in the vicinity of caustics and higher-order travel time derivatives, *Stud. Geophys. Geod.*, 47, 521–544.

- Hamilton, W.R., 1837. Third supplement to an essay on the theory of systems of rays, *Trans. R. Irish Acad.*, **17**, 1–144.
- Hanyga, A., 1982. Dynamic ray tracing in an anisotropic medium, Tectonophysics, 90, 243–251.
- Hubral, P., 1977. Time migration Some ray theoretical aspects, Geophys. Prospect., 25(04), 738–745.
- Hubral, P. & Krey, T., 1980, Interval Velocities from Seismic Reflection Time Measurements, Society of Exploration Geophysicists.
- Hubral, P., Schleicher, J. & Tygel, M., 1992. Three-dimensional paraxial ray properties: basic relations, J. Seismic Explor., 1, 265–279.
- Hubral, P., Schleicher, J. & Tygel, M., 1993. Three-dimensional primary zero-offset reflections, *Geophysics*, 58(5), 692–702.
- Iversen, E., 2004a. Reformulated kinematic and dynamic ray tracing systems for arbitrarily anisotropic media, *Stud. Geophys. Geod.*, **48**, 1–20.
- Iversen, E., 2004b. The isochron ray in seismic modeling and imaging, Geophysics, 69(4), 1053–1070.
- Iversen, E., 2006a. Amplitude, Fresnel zone, and NMO velocity for PP and SS normal-incidence reflections, *Geophysics*, 71(02), W1–W14.
- Iversen, E., 2006b. Velocity rays for heterogeneus anisotropic media: theory and implementation. *Geophysics*, 71(5), T117–T127.
- Iversen, E. & Gjøystdal, H., 1984. Three-dimensional velocity inversion by use of kinematic and dynamic ray tracing, in SEG Technical Program Expanded Abstracts 1984, pp. 643–645, Society of Exploration Geophysicists.
- Iversen, E. & Pšenčík, I., 2008. Ray tracing and inhomogeneous dynamic ray tracing for anisotropy specified in curvilinear coordinates, *Geophys. J. Int.*, 174, 316–330.
- Iversen, E. & Tygel, M., 2008. Image-ray tracing for joint 3D seismic velocity estimation and time-to-depth conversion, *Geophysics*, 73(3), P99–P114.
- Iversen, E., Tygel, M., Ursin, B. & de Hoop, M.V., 2012. Kinematic time migration and demigration of reflections in pre-stack seismic data, *Geophys. J. Int.*, 189(3), 1635–1666.
- Iversen, E., Ursin, B., Saksala, T., Ilmavirta, J. & de Hoop, M.V., 2019. Higher-order Hamilton-Jacobi perturbation theory for anisotropic heterogeneous media: dynamic ray tracing in Cartesian coordinates, *Geophys. J. Int.*, 216(3), 2044–2070.
- Iversen, E., Ursin, B., Saksala, T., Ilmavirta, J. & de Hoop, M.V., 2021. Higher-order Hamilton-Jacobi theory for anisotropic heterogeneous media: transformation between Cartesian and ray-centred coordinates, *Geophys. J. Int.*, doi:10.1093/gji/ggab151.
- Jäger, R., Mann, J., Höcht, G. & Hubral, P., 2001. Common-reflectionsurface stack: Image and attributes, *Geophysics*, 66(1), 97–109.
- Kendall, J.-M., Guest, W.S. & Thomson, C.J., 1992. Ray-theory Green's function reciprocity and ray-centred coordinates in anisotropic media, *Geophys. J. Int.*, 108, 364–371.
- Klimeš, L., 1994. Transformations for dynamic ray tracing in anisotropic media, *Wave Motion*, **20**, 261–272.
- Klimeš, L., 2002a. Second-order and higher-order perturbations of travel time in isotropic and anisotropic media, *Stud. Geophys. Geod.*, 46(2), 213–248.
- Klimeš, L., 2002b. Transformations for dynamic ray tracing in anisotropic media with a homogeneous Hamiltonian of an arbitrary degree, in *Pro*ceeding of the 12th Annual Report of the Seismic Waves in Complex 3-D Structures (SW3D) Consortium, pp. 67–78, Department of Geophysics, Faculty of Mathematics and Physics, Charles University, Praha.

- Klimeš, L., 2002c. Lyapunov exponents for 2-D ray tracing without interfaces, *Pure appl. Geophys.*, 159(7–8), 1465–1485.
- Klimeš, L., 2006a. Spatial derivatives and perturbation derivatives of amplitude in isotropic and anisotropic media, *Stud. Geophys. Geod.*, 50(3), 417–430.
- Klimeš, L., 2006b. Ray-centred coordinate systems in anisotropic media, Stud. Geophys. Geod., 50, 431–447.
- Klimeš, L., 2006c. Common-ray tracing and dynamic ray tracing for S waves in a smooth elastic anisotropic medium, *Stud. Geophys. Geod.*, 50(3), 449–461.
- Klimeš, L., 2013. Relation between the propagator matrix of geodesic deviation and the second-order derivatives of the characteristic function, J. Electromagn. Waves Appl., 27(13), 1589–1601.
- Koren, Z. & Ravve, I., 2021. Eigenrays in 3D heterogeneous anisotropic media, part I: kinematics, Geophys. Prospect., 69(1), 3–27.
- Lambaré, G., Lucio, P.S. & Hanyga, A., 1996. Two-dimensional multivalued traveltime and amplitude maps by uniform sampling of a ray field, *Geophys. J. Int.*, 125(2), 584–598.
- Le Bouteiller, P., Benjemaa, M., Métivier, L. & Virieux, J., 2019. A discontinuous Galerkin fast-sweeping Eikonal solver for fast and accurate traveltime computation in 3D tilted anisotropic media, *Geophysics*, 84(2), C107–C118.
- Podvin, P. & Lecomte, I., 1991. Finite difference computation of traveltimes in very contrasted velocity models: a massively parallel approach and its associated tools, *Geophys. J. Int.*, 105(1), 271–284.
- Popov, M.M. & Pšenčík, I., 1978. Computation of ray amplitudes in inhomogeneous media with curved interfaces, *Stud. Geophys. Geod.*, 22, 248–258.
- Ravve, I. & Koren, Z., 2021. Eigenrays in 3D heterogeneous anisotropic media, part II: dynamics, Geophys. Prospect., 69(1), 28–52.
- Schleicher, J., Tygel, M. & Hubral, P., 2007. Seismic True-Amplitude Imaging, Society of Exploration Geophysicists.
- Stolk, C.C. & de Hoop, M.V., 2006. Seismic inverse scattering in the downward continuation approach, *Wave Motion*, 43(7), 579–598.
- Thomsen, L., 1986. Weak elastic anisotropy, *Geophysics*, **51**, 1954–1966. Ursin, B., 1982a. Quadratic wavefront and travel time approximations in inhomogeneous layered media with curved interfaces, *Geophysics*, **47**,
- Ursin, B., 1982b. Time-to-depth migration using wavefront curvature, Geophys. Prospect., 30(3), 261–280.
- Ursin, B., 2004. Parameter inversion and angle migration in anisotropic elastic media, *Geophysics*, **69**, 1125–1142.
- Vidale, J., 1988. Finite-difference calculation of travel times, Bull. seism. Soc. Am., 78(6), 2062–2076.
- Vinje, V., Iversen, E. & Gjøystdal, H., 1993. Traveltime and amplitude estimation using wavefront construction, *Geophysics*, 58(8), 1157–1166.
- Vinje, V., Iversen, E., Åstebøl, K. & Gjøystdal, H., 1996a. Estimation of multivalued arrivals in 3D models using wavefront construction—part I, *Geophys. Prospect.*, 44(5), 819–842.
- Vinje, V., Iversen, E., Åstebøl, K. & Gjøystdal, H., 1996b. Part II: tracing and interpolation, Geophys. Prospect., 44(5), 843–858.
- Zhou, W., Brossier, R., Operto, S., Virieux, J. & Yang, P., 2018. Velocity model building by waveform inversion of early arrivals and reflections: a 2D case study with gas-cloud effects, *Geophysics*, **83**(2), R141–R157.

APPENDIX A: HAMILTONIAN IN RAY-CENTRED PHASE-SPACE COORDINATES: SECOND-ORDER PARTIAL DERIVATIVES

With reference to eqs (25)–(26) we seek generic expressions for the second-order partial derivatives of the Hamiltonian in the ray-centred phase-space coordinates,

1012-1021.

$$\mathcal{H}_{rs}^{(q)} = \Psi_{rs} + \Phi_{rs},\tag{A1}$$

with

$$\Psi_{rs} = \mathcal{H}_{,xy}\Lambda_{xr}\Lambda_{ys},\tag{A2}$$

$$\Phi_{rs} = \mathcal{H}_{.x} \Lambda_{xrs}. \tag{A3}$$

Here, all indices run from 1 to 6. Explicit expressions for the Λ -quantities are given in Tables 6–7.

A1 Notation remap

We introduce a remap to a lower/upper system of indices so that, e.g. $\Psi_{rs} \to \Psi_{ij}^{i'j'}$, where the new lower indices i and j run from 1 to 3. The corresponding upper (primed) indices i and j may take the values 1 or 2, signifying whether differentiation is performed with respect to a position (1) or momentum (2) variable.

A2 Remap of the second derivatives of the Hamiltonian

Based on the above the remap of eq. (A1) reads

$$\mathcal{H}_{i,j}^{(q),i'j'} = \Psi_{ij}^{i'j'} + \Phi_{ij}^{i'j'}, \tag{A4}$$

with the remap of the quantities Ψ_{st} and Φ_{st} from eqs (A2)–(A3) expressed as

$$\Psi_{ij}^{i'j'} = \mathcal{H}_{,mn}^{,m'n'} \Lambda_{mi}^{m'i'} \Lambda_{nj}^{n'j'}
= \mathcal{H}_{,mn}^{,11i'} \Lambda_{nj}^{1i'} + \mathcal{H}_{,mn}^{,21} \Lambda_{mi}^{2i'} \Lambda_{nj}^{1j'} + \mathcal{H}_{,mn}^{,12} \Lambda_{mi}^{1i'} \Lambda_{nj}^{2j'} + \mathcal{H}_{,mn}^{,22} \Lambda_{mi}^{2i'} \Lambda_{nj}^{2j'},$$
(A5)

$$\Phi_{ij}^{i'j'} = \mathcal{H}_{,m}^{,m'} \Lambda_{mij}^{m'i'j'}
= \mathcal{H}_{,m}^{,1} \Lambda_{mij}^{1i'j'} + \mathcal{H}_{,m}^{,2} \Lambda_{mij}^{2i'j'}.$$
(A6)

We elaborate on specific cases for the individual 3×3 matrix quantities in eqs (A5)–(A6) and utilize that the transformation quantities Λ_{mi}^{12} , Λ_{mii}^{112} , Λ_{mii}^{122} , and Λ_{mii}^{222} are all zero. This yields

$$\Psi_{ij}^{11} = \mathcal{H}_{,mn}^{,m'n'} \Lambda_{mi}^{m'1} \Lambda_{nj}^{n'1}
= \mathcal{H}_{,mn}^{11} \Lambda_{mi}^{11} \Lambda_{ni}^{11} + \mathcal{H}_{,mn}^{,21} \Lambda_{mi}^{21} \Lambda_{ni}^{11} + \mathcal{H}_{,mn}^{,12} \Lambda_{mi}^{11} \Lambda_{ni}^{21} + \mathcal{H}_{,mn}^{,22} \Lambda_{mi}^{21} \Lambda_{ni}^{21},$$
(A7)

$$\Psi_{ij}^{21} = \mathcal{H}_{,mn}^{,m'n'} \Lambda_{mi}^{m'2} \Lambda_{nj}^{n'1}
= \mathcal{H}_{,mn}^{,11} \Lambda_{mi}^{12} \Lambda_{nj}^{11} + \mathcal{H}_{,mn}^{,21} \Lambda_{mi}^{22} \Lambda_{nj}^{11} + \mathcal{H}_{,mn}^{,12} \Lambda_{mi}^{12} \Lambda_{nj}^{21} + \mathcal{H}_{,mn}^{,22} \Lambda_{mi}^{21} \Lambda_{nj}^{21}
= \mathcal{H}_{,mn}^{,21} \Lambda_{mi}^{,22} \Lambda_{ni}^{11} + \mathcal{H}_{,mn}^{,22} \Lambda_{mi}^{,22} \Lambda_{ni}^{,21},$$
(A8)

$$\Psi_{ij}^{12} = \Psi_{ji}^{21},\tag{A9}$$

$$\Psi_{ij}^{22} = \mathcal{H}_{,mn}^{,m'n'} \Lambda_{mi}^{m'2} \Lambda_{nj}^{n'2}
= \mathcal{H}_{,mn}^{,11} \Lambda_{mi}^{12} \Lambda_{nj}^{12} + \mathcal{H}_{,mn}^{,21} \Lambda_{mi}^{22} \Lambda_{nj}^{12} + \mathcal{H}_{,mn}^{,12} \Lambda_{mi}^{12} \Lambda_{nj}^{22} + \mathcal{H}_{,mn}^{,22} \Lambda_{nj}^{22} \Lambda_{nj}^{22}
= \mathcal{H}_{,mn}^{,22} \Lambda_{mi}^{22} \Lambda_{nj}^{22},$$
(A10)

$$\Phi_{ij}^{11} = \mathcal{H}_{,m}^{,m'} \Lambda_{mij}^{m'11}
= \mathcal{H}_{,m}^{1} \Lambda_{mij}^{111} + \mathcal{H}_{,m}^{,2} \Lambda_{mij}^{211},$$
(A11)

$$\Phi_{ij}^{21} = \mathcal{H}_{,m}^{,m'} \Lambda_{mij}^{m'21}
= \mathcal{H}_{,m}^{,1} \Lambda_{mij}^{121} + \mathcal{H}_{,m}^{,2} \Lambda_{mij}^{221}
= \mathcal{H}_{,m}^{,2} \Lambda_{mij}^{221},$$
(A12)

$$\Phi_{ij}^{12} = \Phi_{ji}^{21},\tag{A13}$$

$$\Phi_{ij}^{22} = \mathcal{H}_{,m}^{,m'} \Lambda_{mij}^{m'22}
= \mathcal{H}_{,m}^{,1} \Lambda_{mij}^{122} + \mathcal{H}_{,m}^{,2} \Lambda_{mj}^{222}
= 0.$$
(A14)

A3 Second-order partial derivatives of the Hamiltonian with respect to paraxial coordinates

Consider a reduced form of eqs (A1)–(A3), with indices R, S = 1, 2, 4, 5,

$$\mathcal{H}_{RS}^{(q)} = \Psi_{RS} + \Phi_{RS},\tag{A15}$$

$$\Psi_{RS} = \mathcal{H}_{xy} \Lambda_{xR} \Lambda_{yS},\tag{A16}$$

$$\Phi_{RS} = \mathcal{H}_{x} \Lambda_{xRS}. \tag{A17}$$

The remapping in reduced form reads, e.g. $\mathcal{H}_{,RS}^{(q)} \to \mathcal{H}_{,IJ}^{(q),I'J'}$, where the new lower indices I and J can be 1 or 2, while the corresponding upper (primed) indices signify differentiation in position (1) or momentum (2). Remapping eqs (A16)–(A17) then yields

$$\Psi_{IJ}^{I'J'} = \mathcal{H}_{mn}^{m'n'} \Lambda_{mI}^{m'I'} \Lambda_{nJ}^{n'J'}, \qquad \Phi_{IJ}^{I'J'} = \mathcal{H}_{m}^{m'} \Lambda_{mIJ}^{m'I'J'}. \tag{A18}$$

Now we use eqs (A7)–(A14) to obtain specific reduced forms for the inividual 2 × 2 matrix quantities. Note, in particular, that for eq. (A11) we have $\Lambda_{mLL}^{111} = 0$. The results are,

$$\Psi_{IJ}^{11} = \mathcal{H}_{mn}^{,11} \Lambda_{nI}^{11} \Lambda_{nI}^{11} + \mathcal{H}_{mn}^{,21} \Lambda_{nI}^{21} + \mathcal{H}_{mn}^{,12} \Lambda_{nI}^{11} + \mathcal{H}_{mn}^{,12} \Lambda_{nI}^{11} \Lambda_{nI}^{21} + \mathcal{H}_{mn}^{,22} \Lambda_{nI}^{21} \Lambda_{nI}^{21}, \tag{A19}$$

$$\Psi_{IJ}^{21} = \mathcal{H}_{mn}^{21} \Lambda_{mI}^{22} \Lambda_{nJ}^{11} + \mathcal{H}_{mn}^{22} \Lambda_{mI}^{21} \Lambda_{nJ}^{21}, \tag{A20}$$

$$\Psi_{IJ}^{12} = \Psi_{JI}^{21},\tag{A21}$$

$$\Psi_{IJ}^{22} = \mathcal{H}_{,mn}^{22} \Lambda_{mI}^{22} \Lambda_{nJ}^{22}, \tag{A22}$$

$$\Phi_{IJ}^{11} = \mathcal{H}_{,m}^{2} \Lambda_{mIJ}^{211}, \tag{A23}$$

$$\Phi_{IJ}^{21} = \mathcal{H}_{m}^{2} \Lambda_{mIJ}^{221}, \tag{A24}$$

$$\Phi_{IJ}^{12} = \Phi_{IJ}^{21},\tag{A25}$$

$$\Phi_{IJ}^{22} = 0. (A26)$$

On the ray Ω the different 2 × 2 matrices of type $\Psi^{I'J'}$ and $\Phi^{I'J'}$ have components

$$\Psi_{IJ}^{11} = (U_{mn} - 3\eta_m \eta_n) \mathcal{E}_{mI} \mathcal{E}_{nJ}, \quad \Psi_{IJ}^{22} = V_{mn} \mathcal{F}_{mI} \mathcal{F}_{nJ}, \quad \Psi_{IJ}^{12} = W_{mn}^{12} \mathcal{E}_{mI} \mathcal{F}_{nJ}, \tag{A27}$$

$$\Phi_{IJ}^{11} = 2\eta_m \eta_n \mathcal{E}_{mI} \mathcal{E}_{nJ}, \qquad \Phi_{IJ}^{22} = 0, \qquad \Phi_{IJ}^{12} = -\frac{\mathrm{d}\mathcal{E}_{nI}}{\mathrm{d}\tau} \mathcal{F}_{nJ} = -\mathcal{K}_{IJ}. \tag{A28}$$

This yields the following second derivatives of the Hamiltonian in ray-centred coordinates,

$$U_{IJ}^{(q)} = \frac{\partial^2 \mathcal{H}}{\partial q_I \partial q_J} = (U_{mn} - \eta_m \eta_n) \mathcal{E}_{mI} \mathcal{E}_{nJ}, \tag{A29}$$

$$V_{IJ}^{(q)} = \frac{\partial^2 \mathcal{H}}{\partial p_I^{(q)} \partial p_I^{(q)}} = V_{mn} \mathcal{F}_{mI} \mathcal{F}_{nJ},\tag{A30}$$

$$W_{IJ}^{(q) 12} = \frac{\partial^2 \mathcal{H}}{\partial q_I \partial p_J^{(q)}} = W_{mn}^{12} \mathcal{E}_{mI} \mathcal{F}_{nJ} - \mathcal{K}_{IJ}. \tag{A31}$$

A4 Second-order partial derivatives of the Hamiltonian with respect to time and time stretch

Along the reference ray Ω we consider the particular second-order partial derivatives of the Hamiltonian taken either with respect to the time variable q_3 or the time-stretch variable $p_3^{(q)}$.

The vectors $(\partial \mathcal{H}/\partial p_i^{(q)})$ and $(\partial \mathcal{H}/\partial q_i)$ are both constant along Ω , see eqs (17) and (18). As a consequence, at every point on Ω we have

$$\frac{\partial^2 \mathcal{H}}{\partial q_3 \partial p_i^{(q)}} = \frac{\mathrm{d}}{\mathrm{d}\tau} \left(\frac{\partial \mathcal{H}}{\partial p_i^{(q)}} \right) = 0, \tag{A32}$$

$$\frac{\partial^2 \mathcal{H}}{\partial q_3 \partial q_i} = \frac{\mathrm{d}}{\mathrm{d}\tau} \left(\frac{\partial \mathcal{H}}{\partial q_i} \right) = 0. \tag{A33}$$

Differentiation of eq. (12) with respect to $p_i^{(q)}$ yields

$$p_i^{(q)} \frac{\partial^2 \mathcal{H}}{\partial p_i^{(q)} \partial p_i^{(q)}} = \frac{\partial \mathcal{H}}{\partial p_i^{(q)}}.$$
(A34)

On Ω we use eq. (17) in eq. (A34) to obtain

$$\frac{\partial^2 \mathcal{H}}{\partial p_3^{(q)} \partial p_i^{(q)}} = \delta_{3j}. \tag{A35}$$

When eq. (12) is differentiated with respect to q_i we obtain

$$\frac{\partial^2 \mathcal{H}}{\partial p_3^{(q)} \partial q_j} = \frac{1}{p_3^{(q)}} \left(2 \frac{\partial \mathcal{H}}{\partial q_j} - p_I^{(q)} \frac{\partial^2 \mathcal{H}}{\partial p_I^{(q)} \partial q_j} \right). \tag{A36}$$

Hence, on Ω we have

$$\frac{\partial^2 \mathcal{H}}{\partial p_3^{(q)} \partial q_j} = 0. \tag{A37}$$

APPENDIX B: HAMILTONIAN IN RAY-CENTRED PHASE-SPACE COORDINATES: THIRD-ORDER PARTIAL DERIVATIVES

Consider the third-ordered partial derivatives of Hamiltonian in ray-centred phase-space coordinates, where the indices run from 1 to 6,

$$\mathcal{H}_{,rst}^{(q)} = \mathcal{H}_{,xyz}\Lambda_{xr}\Lambda_{ys}\Lambda_{zt} + \mathcal{H}_{,xy}\left(\Lambda_{xr}\Lambda_{yst} + \Lambda_{xs}\Lambda_{yrt} + \Lambda_{xt}\Lambda_{yrs}\right) + \mathcal{H}_{,x}\Lambda_{xrst}.$$
(B1)

The Λ -quantities are defined in eq. (26); for explicit expressions, see Tables 6–7.

B1 Third-order partial derivatives of the Hamiltonian with respect to paraxial coordinates

Reduction and remap of eq. (B1) yields

$$\mathcal{H}_{,IJK}^{(q),\,l'J'K'} = \mathcal{H}_{,mnp}^{,m'n'p'} \Lambda_{mI}^{m'l'} \Lambda_{nJ}^{n'J'} \Lambda_{pK}^{p'K'}
+ \mathcal{H}_{,mn}^{,m'n'} \left(\Lambda_{mI}^{m'l'} \Lambda_{nJK}^{n'J'} + \Lambda_{mJ}^{m'J'} \Lambda_{nIK}^{n'l'K'} + \Lambda_{mK}^{m'K'} \Lambda_{nIJ}^{n'l'J'} \right)
+ \mathcal{H}_{,m}^{,m'} \Lambda_{mIJK}^{m'l'J'K'}.$$
(B2)

On the way to obtain specific expressions for the third-order derivatives of the Hamiltonian, we loop through the various possible values of I, J, K and eliminate terms that are always zero. The resulting expressions (not stated here) are quite long, but there is room for considerable simplification when we evaluate on the ray Ω .

We observe that some of the transformation quantities (Iversen et al. 2021) Λ_{mI}^{21} , Λ_{mIJ}^{211} , Λ_{mIJ}^{212} , etc. are factored by the component p_m . This is attractive, because one can then, as an example, express the component product $\mathcal{H}_{mnp}^{[m]}\Lambda_{mI}^{21}$ in the form $p_m \mathcal{H}_{mnp}^{[211]}a_I$, where $a_I = \eta_m \mathcal{E}_{mI}$. For the product $p_m \mathcal{H}_{mnp}^{211}$ we can obtain a simpler expression by differentiating twice the fundamental relation $p_i \partial \mathcal{H} / \partial p_i = 2 \mathcal{H}$, which gives

$$p_i \frac{\partial^3 \mathcal{H}}{\partial p_i \partial x_j \partial x_k} = 2 \frac{\partial^2 \mathcal{H}}{\partial x_j \partial x_k} \tag{B3}$$

$$p_i \mathcal{H}_{ijk}^{,211} = 2U_{jk}.$$
 (B4)

The product $\mathcal{H}_{mnn}^{,211} \Lambda_{mI}^{21}$ is therefore simply

$$\mathcal{H}_{,mnp}^{,211} \Lambda_{mI}^{\,21} = 2\eta_m U_{np} \mathcal{E}_{mI}.$$
 (B5)

Next, inspect the component products $\mathcal{H}_{mnp}^{,221} \Lambda_{mI}^{21}$ and $\mathcal{H}_{mnp}^{,221} \Lambda_{mI}^{21}$ using the same strategy as above. We utilize the relations

$$p_i \frac{\partial^3 \mathcal{H}}{\partial p_i \partial p_j \partial x_k} = \frac{\partial^2 \mathcal{H}}{\partial x_k \partial p_j} \tag{B6}$$

$$p_i p_j \frac{\partial^3 \mathcal{H}}{\partial p_i \partial p_j \partial x_k} = 2 \frac{\partial \mathcal{H}}{\partial x_k}$$
 (B7)

to obtain

$$\mathcal{H}_{mnp}^{,221} \Lambda_{mI}^{21} = W_{nn}^{12} \eta_m \mathcal{E}_{mI}$$
(B8)

$$\mathcal{H}_{,mnp}^{,221} \Lambda_{mI}^{21} \Lambda_{nJ}^{21} = -2\eta_m \eta_n \eta_p \mathcal{E}_{mI} \mathcal{E}_{nJ}.$$
 (B9)

Working along such lines, we obtain also the simplifying relations

$$\mathcal{H}_{mn}^{,12} \Lambda_{nJK}^{211} = -4 \eta_m \eta_n \eta_p \mathcal{E}_{nJ} \mathcal{E}_{pK}, \tag{B10}$$

$$\mathcal{H}_{mn}^{,12} \Lambda_{nJK}^{212} = 2\eta_m \mathcal{K}_{JK},$$
 (B11)

$$\mathcal{H}_{mn}^{,22} \Lambda_{ml}^{21} = v_n \eta_m \mathcal{E}_{ml}, \tag{B12}$$

$$\mathcal{H}_{mn}^{,22} \Lambda_{mI}^{21} \Lambda_{nJK}^{211} = 2\eta_m \eta_n \eta_p \mathcal{E}_{mI} \mathcal{E}_{nJ} \mathcal{E}_{pK}, \tag{B13}$$

$$\mathcal{H}_{mn}^{,22} \Lambda_{mI}^{21} \Lambda_{nJK}^{212} = -\eta_m \mathcal{E}_{mI} \mathcal{K}_{JK}, \tag{B14}$$

$$\mathcal{H}_{mn}^{,22} \Lambda_{nK}^{22} \Lambda_{nK}^{211} = 0, \tag{B15}$$

$$\mathcal{H}_{mn}^{,22} \Lambda_{nL}^{212} \Lambda_{nL}^{212} = 0, \tag{B16}$$

$$\mathcal{H}_{m}^{2}\Lambda_{mIJK}^{2111} = 6\eta_{m}\eta_{n}\eta_{p}\mathcal{E}_{mI}\mathcal{E}_{nJ}\mathcal{E}_{pK},\tag{B17}$$

$$\mathcal{H}_{m}^{,2}\Lambda_{mIJK}^{2112} = -\eta_{m}\left(\mathcal{E}_{mI}\mathcal{K}_{JK} + \mathcal{E}_{mJ}\mathcal{K}_{IK}\right). \tag{B18}$$

The above auxiliary results (B5) and (B8)–(B18) enable us to convert eq. (B2) into specific transformation equations for the third-order partial derivatives of the Hamiltonian. We obtain the results

$$\mathcal{H}_{,IJK}^{(q),111} = \left(U_{mnp} + 2\eta_m U_{np} + 2\eta_n U_{mp} + 2\eta_p U_{mn} - 6\eta_m \eta_n \eta_p \right) \mathcal{E}_{mI} \mathcal{E}_{nJ} \mathcal{E}_{pK}, \tag{B19}$$

$$\mathcal{H}_{JJK}^{(q),112} = \left(W_{mnp}^{112} + \eta_m W_{np}^{12} + \eta_n W_{mp}^{12}\right) \mathcal{E}_{mI} \mathcal{E}_{nJ} \mathcal{F}_{pK}, \tag{B20}$$

$$\mathcal{H}_{,IJK}^{(q),122} = W_{mnp}^{122} \mathcal{E}_{ml} \mathcal{F}_{nJ} \mathcal{F}_{pK}, \tag{B21}$$

$$\mathcal{H}_{,IJK}^{(q),222} = V_{mnp} \mathcal{F}_{mI} \mathcal{F}_{nJ} \mathcal{F}_{pK}. \tag{B22}$$

B2 Third-order partial derivatives of the Hamiltonian with respect to time and time stretch

On the reference ray, to take the partial derivative with respect to the coordinate q_3 is equivalent to taking the total derivative with respect to the traveltime τ . Straightforward differentiation of eqs (A29)–(A31) yields

$$\frac{\partial^3 \mathcal{H}}{\partial q_I \partial q_J \partial q_3} = \frac{\mathrm{d}U_{IJ}^{(q)}}{\mathrm{d}\tau} = \frac{\mathrm{d}}{\mathrm{d}\tau} \left[\left(U_{mn} - \eta_m \eta_n \right) \mathcal{E}_{mI} \mathcal{E}_{nJ} \right], \tag{B23}$$

$$\frac{\partial^3 \mathcal{H}}{\partial p_I^{(q)} \partial p_I^{(q)} \partial q_3} = \frac{\mathrm{d}V_{IJ}^{(q)}}{\mathrm{d}\tau} = \frac{\mathrm{d}}{\mathrm{d}\tau} \left[V_{mn} \mathcal{F}_{mI} \mathcal{F}_{nJ} \right],\tag{B24}$$

$$\frac{\partial^3 \mathcal{H}}{\partial q_I \partial p_J^{(q)} \partial q_3} = \frac{\mathrm{d}W_{IJ}^{(q) 12}}{\mathrm{d}\tau} = \frac{\mathrm{d}}{\mathrm{d}\tau} \left[W_{mn}^{12} \mathcal{E}_{mI} \mathcal{F}_{nJ} - \mathcal{K}_{IJ} \right]. \tag{B25}$$

Here, the time derivatives of the quantities U_{ij} , V_{ij} , and W_{ij}^{12} can be computed using

$$\frac{dU_{ij}}{d\tau} = v_k U_{ijk} + \eta_k W_{ijk}^{112}
\frac{dW_{ij}^{12}}{d\tau} = v_k W_{ikj}^{112} + \eta_k W_{ijk}^{122},
\frac{dV_{ij}}{d\tau} = v_k W_{kij}^{122} + \eta_k V_{ijk}.$$
(B26)

For time differentiation of the basis quantities \mathcal{E}_{mI} , \mathcal{F}_{nJ} and \mathcal{K}_{IJ} , see Iversen *et al.* (2021).

Differentiation of the second derivatives of the Hamiltonian with respect to the time stretch variable $p_3^{(q)}$ yields, on the reference ray,

$$\frac{\partial^{3} \mathcal{H}}{\partial q_{I} \partial q_{J} \partial p_{3}^{(q)}} = 2U_{IJ}^{(q)},
\frac{\partial^{3} \mathcal{H}}{\partial p_{I}^{(q)} \partial p_{J}^{(q)} \partial p_{3}^{(q)}} = 0,
\frac{\partial^{3} \mathcal{H}}{\partial q_{I} \partial p_{J}^{(q)} \partial p_{3}^{(q)}} = W_{IJ}^{(q) 12}.$$
(B27)

APPENDIX C: HAMILTONIAN IN RAY-CENTRED PHASE-SPACE COORDINATES: FOURTH-ORDER PARTIAL DERIVATIVES

We elaborate on fourth-order partial derivatives of the Hamiltonian in ray-centred phase-space. Such derivatives have the generic form

$$\mathcal{H}_{,rstu}^{(q)} = \mathcal{H}_{,xyz\phi} \Lambda_{xr} \Lambda_{ys} \Lambda_{zt} \Lambda_{\phi u}$$

$$+ \mathcal{H}_{,xyz} \left(\Lambda_{xrs} \Lambda_{yt} \Lambda_{zu} + \Lambda_{xrt} \Lambda_{ys} \Lambda_{zu} + \Lambda_{xru} \Lambda_{ys} \Lambda_{zt} \right.$$

$$+ \Lambda_{xst} \Lambda_{yr} \Lambda_{zu} + \Lambda_{xsu} \Lambda_{yr} \Lambda_{zt} + \Lambda_{xtu} \Lambda_{yr} \Lambda_{zs} \right)$$

$$+ \mathcal{H}_{,xy} \left(\Lambda_{xrs} \Lambda_{ytu} + \Lambda_{xrt} \Lambda_{ysu} + \Lambda_{xru} \Lambda_{yst} \right.$$

$$+ \Lambda_{xrst} \Lambda_{yu} + \Lambda_{xrsu} \Lambda_{yt} + \Lambda_{xrtu} \Lambda_{ys} + \Lambda_{xstu} \Lambda_{yr} \right)$$

$$+ \mathcal{H}_{,x} \Lambda_{xrstu},$$
(C1)

with all indices running from 1 to 6. For definition of the Λ -quantities and their explicit expressions, see eq. (26) and Tables 6–7.

C1 Fourth-order partial derivatives of the Hamiltonian with respect to paraxial coordinates

We do reduction and remap of eq. (C1), eliminate terms that are always zero, and simplify using a similar strategy as in Appendix B. This yields the following fourth-order partial derivatives with respect to the paraxial coordinates q_I and $p_I^{(q)}$,

$$\mathcal{H}_{,IJKL}^{(q),1111} = \left(U_{mnpq} + 2\eta_{m} U_{npq} + 2\eta_{n} U_{mpq} + 2\eta_{p} U_{mnq} + 2\eta_{q} U_{mnp} \right. \\ + 6\eta_{m} \eta_{n} U_{pq} + 6\eta_{m} \eta_{p} U_{nq} + 6\eta_{m} \eta_{q} U_{np} \\ + 6\eta_{n} \eta_{p} U_{mq} + 6\eta_{n} \eta_{q} U_{mp} + 6\eta_{p} \eta_{q} U_{mn} \\ - 36\eta_{m} \eta_{n} \eta_{n} \eta_{a} \right) \mathcal{E}_{mI} \mathcal{E}_{nJ} \mathcal{E}_{pK} \mathcal{E}_{aL},$$
(C2)

$$\mathcal{H}_{,IJKL}^{(q)}{}^{,1112} = \left(W_{mnpq}^{1112} + \eta_m W_{npq}^{112} + \eta_n W_{mpq}^{112} + \eta_p W_{mnq}^{112} + 2\eta_m \eta_n W_{pq}^{12} + 2\eta_m \eta_p W_{nq}^{12} + 2\eta_n \eta_p W_{mq}^{12}\right) \mathcal{E}_{mI} \mathcal{E}_{nJ} \mathcal{E}_{pK} \mathcal{F}_{qL} - 2(U_{mn} - \eta_m \eta_n) (\mathcal{E}_{mI} \mathcal{E}_{nJ} \mathcal{K}_{KL} + \mathcal{E}_{mI} \mathcal{E}_{nK} \mathcal{K}_{JL} + \mathcal{E}_{mJ} \mathcal{E}_{nK} \mathcal{K}_{IL}),$$
(C3)

$$\mathcal{H}_{,IJKL}^{(q),1122} = W_{mnpq}^{1122} \mathcal{E}_{mI} \mathcal{E}_{nJ} \mathcal{F}_{pK} \mathcal{F}_{qL} - W_{mn}^{12} (\mathcal{E}_{mI} \mathcal{F}_{nK} \mathcal{K}_{JL} + \mathcal{E}_{mI} \mathcal{F}_{nL} \mathcal{K}_{JK} + \mathcal{E}_{mJ} \mathcal{F}_{nK} \mathcal{K}_{IL} + \mathcal{E}_{mJ} \mathcal{F}_{nL} \mathcal{K}_{IK}) + \mathcal{K}_{IK} \mathcal{K}_{JL} + \mathcal{K}_{IL} \mathcal{K}_{JK},$$
(C4)

$$\mathcal{H}_{,IJKL}^{(q),1222} = (W_{mnpq}^{1222} - \eta_m V_{npq}) \,\mathcal{E}_{mI} \mathcal{F}_{nJ} \mathcal{F}_{pK} \mathcal{F}_{qL},\tag{C5}$$

$$\mathcal{H}_{,IJKL}^{(q),2222} = V_{mnpq} \mathcal{F}_{mI} \mathcal{F}_{nJ} \mathcal{F}_{pK} \mathcal{F}_{qL}. \tag{C6}$$

APPENDIX D: INTRINSIC RELATIONS FOR DYNAMIC RAY TRACING IN RAY-CENTRED COORDINATES

We consider intrinsic relations between quantities within the first-, second-, and third-order systems for dynamic ray tracing in ray-centred coordinates.

D1 Intrinsic relations in first-order dynamic ray tracing

Consider the position constraint relation (87). On the reference ray, Ω , we have $\partial \tau / \partial q_i = \delta_{i3}$, and therefore

$$Q_{3A} \equiv \frac{\partial q_3}{\partial \gamma_A} = 0. \tag{D1}$$

Moreover, the phase-space constraint relation (90) yields

$$\frac{\partial \mathcal{H}}{\partial q_i} \frac{\partial q_i}{\partial \gamma_A} + \frac{\partial \mathcal{H}}{\partial p_i^{(q)}} \frac{\partial p_i^{(q)}}{\partial \gamma_A} = 0.$$

Since $\partial \mathcal{H}/\partial q_i = 0$ and $\partial \mathcal{H}/\partial p^{(q)} = \delta_{3i}$ on Ω , we have

$$\mathcal{P}_{3A} \equiv \frac{\partial p_3^{(q)}}{\partial \gamma_A} = 0. \tag{D2}$$

For the first-order derivatives of the momentum components $p_L^{(q)}$ in eq. (84) we find

$$\frac{\partial p_I^{(q)}}{\partial \gamma_A} = \frac{\partial^2 \tau}{\partial q_I \partial q_J} \frac{\partial q_J}{\partial \gamma_A} + \frac{\partial}{\partial q_3} \left(\frac{\partial \tau}{\partial q_I} \right) \frac{\partial q_3}{\partial \gamma_A}.$$

The last term is zero on Ω because of eqs (83) and (D1), hence,

$$\mathcal{P}_{IA} = \mathcal{M}_{IJ} \mathcal{Q}_{JA},\tag{D3}$$

where we have introduced the second-order derivatives of traveltime,

$$\mathcal{M}_{IJ} \equiv \frac{\partial^2 \tau}{\partial q_I \partial q_J}.\tag{D4}$$

D2 Intrinsic relations in second-order dynamic ray tracing

Consider the second-order position constraint (88) when evaluated on Ω ,

$$\frac{\partial^2 \tau}{\partial q_I \partial q_J} \frac{\partial q_I}{\partial \gamma_A} \frac{\partial q_J}{\partial \gamma_B} + \frac{\partial^2 q_3}{\partial \gamma_A \partial \gamma_B} \ = \ 0.$$

Using eqs (D3) and (D4) results in the relation

$$Q_{3AB} \equiv \frac{\partial^2 q_3}{\partial \gamma_A \partial \gamma_B}$$

$$= -\mathcal{M}_{IJ} Q_{IA} Q_{JB} = -Q_{IA} \mathcal{P}_{IB}.$$
(D5)

Then, use the second-order phase-space constraint (91) on Ω , which yields

$$\frac{\partial^2 \mathcal{H}}{\partial w_r^{(q)} \partial w_s^{(q)}} X_{rA}^{(q)} X_{sB}^{(q)} + \frac{\partial^2 p_3^{(q)}}{\partial \gamma_A \partial \gamma_B} = 0.$$

After application of the reduced form of the dynamic ray tracing ODEs (37), we obtain

$$\mathcal{P}_{3AB} \equiv \frac{\partial^2 p_3^{(q)}}{\partial \gamma_A \partial \gamma_B}$$

$$= J_{RS} S_{ST}^{(q)} X_{RA}^{(q)} X_{TB}^{(q)}$$

$$= Q_{LA} \dot{\mathcal{P}}_{LB} - \mathcal{P}_{LA} \dot{\mathcal{Q}}_{LB}.$$
(D6)

The reduced form implies that the indices R, S, T can only have values 1,2,4,5. We can further use eq. (D3) to restate (D6) as

$$\mathcal{P}_{3AB} = \dot{\mathcal{M}}_{IJ} \mathcal{Q}_{IA} \mathcal{Q}_{JB}. \tag{D7}$$

Eqs (D6) and (D7) represent equivalent constraint relations for the second-order derivatives of perturbations in the phase space— the only second-order quantity affected is \mathcal{P}_{3AB} .

Consider the second-order derivatives of the momentum components $p_I^{(q)}$ in eq. (85). On Ω the latter simplifies to

$$\frac{\partial^2 p_I^{(q)}}{\partial \gamma_A \partial \gamma_B} = \frac{\partial^3 \tau}{\partial q_I \partial q_J \partial q_K} \frac{\partial q_J}{\partial \gamma_A} \frac{\partial q_K}{\partial \gamma_B} + \frac{\partial^2 \tau}{\partial q_I \partial q_J} \frac{\partial^2 q_J}{\partial \gamma_A \partial \gamma_B}.$$

This result is conveniently restated

$$\mathcal{P}_{IAB} = \mathcal{M}_{IJK} \mathcal{Q}_{JA} \mathcal{Q}_{KB} + \mathcal{M}_{IJ} \mathcal{Q}_{JAB}, \tag{D8}$$

where \mathcal{M}_{IJK} signifies the third-order derivatives of traveltime,

$$\mathcal{M}_{IJK} \equiv \frac{\partial^3 \tau}{\partial q_I \partial q_J \partial q_K}.\tag{D9}$$

D3 Intrinsic relations in third-order dynamic ray tracing

On Ω the third-order position constraint (89) yields

$$\mathcal{Q}_{3ABC} \equiv \frac{\partial^3 q_3}{\partial \gamma_A \partial \gamma_B \partial \gamma_C}
= -\mathcal{M}_{IJK} \mathcal{Q}_{IA} \mathcal{Q}_{JB} \mathcal{Q}_{KC} - \mathcal{M}_{IJ} (\mathcal{Q}_{IA} \mathcal{Q}_{JBC} + \mathcal{Q}_{IB} \mathcal{Q}_{JAC} + \mathcal{Q}_{IC} \mathcal{Q}_{JAB}).$$
(D10)

One may use eqs (D3) and (D8) to remove the \mathcal{M} -quantities on the right-hand side of eq. (D10). As a result, we obtain the equivalent expression

$$Q_{3ABC} = -Q_{IA}P_{IBC} - P_{IB}Q_{IAC} - P_{IC}Q_{IAB}. \tag{D11}$$

We apply the third-order phase-space constraint (92) on Ω , which results in

$$\begin{split} \frac{\partial^{3} p_{3}^{(q)}}{\partial \gamma_{A} \partial \gamma_{B} \partial \gamma_{C}} &= -\frac{\partial^{3} \mathcal{H}}{\partial w_{r}^{(q)} \partial w_{s}^{(q)} \partial w_{t}^{(q)}} X_{rA}^{(q)} X_{sB}^{(q)} X_{tC}^{(q)} \\ &- \frac{\partial^{2} \mathcal{H}}{\partial w_{r}^{(q)} \partial w_{s}^{(q)}} \left(X_{rA}^{(q)} X_{rBC}^{(q)} + X_{rB}^{(q)} X_{rAC}^{(q)} + X_{rC}^{(q)} X_{rAB}^{(q)} \right) \\ &- 0 \end{split}$$

Introducing the reduced form of the phase-space coordinate indices gives us

$$\mathcal{P}_{3ABC} \equiv \frac{\partial^{3} p_{3}^{(q)}}{\partial \gamma_{A} \partial \gamma_{B} \partial \gamma_{C}}
= J_{SR} S_{RTU}^{(q)} X_{SA}^{(q)} X_{TB}^{(q)} X_{UC}^{(q)}
+ J_{SR} S_{RT}^{(q)} \left(X_{TA}^{(q)} X_{SBC}^{(q)} + X_{TB}^{(q)} X_{SAC}^{(q)} + X_{TC}^{(q)} X_{SAB}^{(q)} \right).$$
(D12)

Using eq. (86) it is straightforward to derive the convenient form

$$\mathcal{P}_{3ABC} = \dot{\mathcal{M}}_{IJK} \mathcal{Q}_{IA} \mathcal{Q}_{JB} \mathcal{Q}_{KC} + \dot{\mathcal{M}}_{IJ} (\mathcal{Q}_{IA} \mathcal{Q}_{JBC} + \mathcal{Q}_{IB} \mathcal{Q}_{JAC} + \mathcal{Q}_{IC} \mathcal{Q}_{JAB}). \tag{D13}$$

Eqs (D12) and (D13) represent equivalent constraint relations for the third-order derivatives of perturbations in the phase space—the only third-order quantity affected is \mathcal{P}_{3ABC} .

We use eq. (86) to obtain third-order derivatives of the momentum components $p_I^{(q)}$ on Ω . As a first result, we obtain

$$\mathcal{P}_{IABC} = \mathcal{M}_{IJKL} \mathcal{Q}_{JA} \mathcal{Q}_{KB} \mathcal{Q}_{LC}$$

$$+ \mathcal{M}_{IJK} (\mathcal{Q}_{JA} \mathcal{Q}_{KBC} + \mathcal{Q}_{JB} \mathcal{Q}_{KAC} + \mathcal{Q}_{JC} \mathcal{Q}_{KAB})$$

$$+ \dot{\mathcal{M}}_{IJ} (\mathcal{Q}_{JA} \mathcal{Q}_{3BC} + \mathcal{Q}_{JB} \mathcal{Q}_{3AC} + \mathcal{Q}_{JC} \mathcal{Q}_{3AB})$$

$$+ \mathcal{M}_{IJ} \mathcal{Q}_{JABC},$$
(D14)

where \mathcal{M}_{IJKL} represent the fourth-order derivatives of traveltime,

$$\mathcal{M}_{IJKL} \equiv \frac{\partial^4 \tau}{\partial q_I \partial q_J \partial q_K \partial q_L}.$$
 (D15)

Applying eq. (D5), we can recast (D14) as

$$\mathcal{P}_{IABC} = (\mathcal{M}_{IJKL} - \dot{\mathcal{M}}_{IJ} \mathcal{M}_{KL} - \dot{\mathcal{M}}_{IK} \mathcal{M}_{JL} - \dot{\mathcal{M}}_{IL} \mathcal{M}_{JK}) \mathcal{Q}_{JA} \mathcal{Q}_{KB} \mathcal{Q}_{LC} + \mathcal{M}_{IJK} (\mathcal{Q}_{JA} \mathcal{Q}_{KBC} + \mathcal{Q}_{JB} \mathcal{Q}_{KAC} + \mathcal{Q}_{JC} \mathcal{Q}_{KAB}) + \mathcal{M}_{IJ} \mathcal{Q}_{JABC}.$$
(D16)

APPENDIX E: TRANSFORMATION OF DYNAMIC RAY TRACING QUANTITIES BETWEEN CARTESIAN AND RAY-CENTRED COORDINATES

We derive expressions that relate the dynamic ray tracing quantities in ray-centred and Cartesian coordinates.

E1 Transformation of first-order derivatives

First-order derivatives of position in ray-centred and Cartesian coordinates are related by

$$\frac{\partial x_i}{\partial \gamma_A} = \frac{\partial x_i}{\partial q_m} \frac{\partial q_m}{\partial \gamma_A}.$$
 (E1)

Since $\partial q_3/\partial \gamma_A = 0$ on Ω we have

$$Q_{iA} = \mathcal{E}_{iM} Q_{MA}, \tag{E2}$$

while the inverse transformation reads

$$Q_{MA} = \mathcal{F}_{iM}Q_{iA}, \qquad Q_{3A} = p_iQ_{iA} = 0. \tag{E3}$$

Furthermore, the derivatives of momentum in Cartesian coordinates are given by

$$\frac{\partial p_i}{\partial \gamma_A} = \frac{\partial p_i}{\partial q_m} \frac{\partial q_m}{\partial \gamma_A} + \frac{\partial p_i}{\partial p_m^{(q)}} \frac{\partial p_m^{(q)}}{\partial \gamma_A}.$$
 (E4)

Using phase-space coordinate transformations from Iversen *et al.* (2021) in combination with $\partial q_3/\partial \gamma_A = 0$ and $\partial p_3^{(q)}/\partial \gamma_A = 0$ on Ω yields

$$P_{iA} = \mathcal{F}_{iM} \mathcal{P}_{MA} + p_i \eta_i \mathcal{E}_{jN} \mathcal{Q}_{NA}. \tag{E5}$$

Conversely, the derivatives of momentum in ray-centred coordinates are expressed by

$$\mathcal{P}_{MA} = \mathcal{E}_{iM} P_{iA}, \qquad \mathcal{P}_{3A} = -\eta_i Q_{iA} + v_i P_{iA} = 0. \tag{E6}$$

The latter sub-equation is recognized as the first-order constraint relation for dynamic ray racing in Cartesian coordinates.

E2 Transformation of second-order derivatives

We differentiate eq. (E1) with respect to γ_R ,

$$\frac{\partial^2 x_i}{\partial \gamma_A \partial \gamma_B} = \frac{\partial^2 x_i}{\partial q_m \partial q_n} \frac{\partial q_m}{\partial \gamma_A} \frac{\partial q_n}{\partial \gamma_B} + \frac{\partial x_i}{\partial q_m} \frac{\partial^2 q_m}{\partial \gamma_A \partial \gamma_B},\tag{E7}$$

which, on the reference ray, becomes

$$Q_{iAB} = \mathcal{E}_{iM} Q_{MAB} + v_i Q_{3AB}. \tag{E8}$$

The inverse result is

$$Q_{MAB} = \mathcal{F}_{iM}Q_{iAB}, \qquad Q_{3AB} = p_i Q_{iAB}. \tag{E9}$$

Using eqs (D5), (E3), and (E6) the second-order derivatives Q_{3AB} in ray-centred coordinates can be expressed solely in terms of first-order derivatives in Cartesian coordinates,

$$Q_{3AB} = -Q_{iA}P_{iB}. \tag{E10}$$

Moreover, we differentiate eq. (E4) with respect to γ_B ,

$$\frac{\partial^{2} p_{i}}{\partial \gamma_{A} \partial \gamma_{B}} = \frac{\partial^{2} p_{i}}{\partial q_{k} \partial q_{l}} \frac{\partial q_{k}}{\partial \gamma_{A}} \frac{\partial q_{l}}{\partial \gamma_{B}} + \frac{\partial^{2} p_{i}}{\partial q_{k} \partial p_{l}^{(q)}} \frac{\partial q_{k}}{\partial \gamma_{A}} \frac{\partial p_{l}^{(q)}}{\partial \gamma_{B}} + \frac{\partial p_{i}}{\partial q_{k}} \frac{\partial^{2} q_{k}}{\partial \gamma_{A}} \frac{\partial^{2} q_{k}}{\partial \gamma_{B}} + \frac{\partial^{2} p_{i}}{\partial q_{k}} \frac{\partial^{2} p_{i}^{(q)}}{\partial \gamma_{A}} \frac{\partial^{2} p_{k}^{(q)}}{\partial \gamma_{A}} \frac{\partial^{2} q_{k}}{\partial \gamma_{A}}$$
(E11)

which gives on Ω ,

$$P_{iAB} = \frac{\partial^{2} p_{i}}{\partial q_{M} \partial q_{N}} \mathcal{Q}_{MA} \mathcal{Q}_{NB} + \frac{\partial^{2} p_{i}}{\partial q_{M} \partial p_{N}^{(q)}} \mathcal{Q}_{MA} \mathcal{P}_{NB}$$

$$+ \frac{\partial p_{i}}{\partial q_{M}} \mathcal{Q}_{MAB} + \eta_{i} \mathcal{Q}_{3AB}$$

$$+ \frac{\partial^{2} p_{i}}{\partial p_{M}^{(q)} \partial q_{N}} \mathcal{P}_{MA} \mathcal{Q}_{NB}$$

$$+ \mathcal{F}_{iM} \mathcal{P}_{MAB} + p_{i} \mathcal{P}_{3AB}. \tag{E12}$$

It is possible to write eq. (E12) differently. As it stands, however, it is simple to directly plug in the values for the transformation coefficients derived in Iversen et al. (2021).

Conversely, to obtain \mathcal{P}_{MAB} in terms of quantities in the Cartesian coordinates we multiply both sides of eq. (E12) with \mathcal{E}_{iM} . This yields,

$$\mathcal{P}_{MAB} = \mathcal{E}_{iM} \left(P_{iAB} - \eta_i p_j Q_{jAB} \right). \tag{E13}$$

We can also relate the quantity \mathcal{P}_{3AB} to Cartesian coordinates, as follows,

$$\mathcal{P}_{3AB} = Q_{iA}\dot{P}_{iB} - P_{iA}\dot{Q}_{iB} + Q_{iA}\dot{\mathcal{E}}_{iK}\mathcal{F}_{jK}P_{jB} + P_{iA}\mathcal{E}_{iK}\dot{\mathcal{E}}_{jK}Q_{jB}. \tag{E14}$$

E3 Transformation of third-order derivatives

Taking the derivative of eq. (E7) with respect to γ_C we obtain, after evaluation on the ray Ω ,

$$Q_{iABC} = \mathcal{E}_{iM} Q_{MABC} + v_i Q_{3ABC} + \dot{\mathcal{E}}_{iM} (Q_{MA} Q_{3BC} + Q_{MB} Q_{3AC} + Q_{MC} Q_{3AB}). \tag{E15}$$

The corresponding expressions for third-order derivatives in ray-centred coordinates are

$$Q_{MABC} = \mathcal{F}_{iM} Q_{iABC} + \mathcal{K}_{KM} \mathcal{F}_{iK} (Q_{iA} Q_{3BC} + Q_{iB} Q_{3AC} + Q_{iC} Q_{3AB}), \tag{E16}$$

$$Q_{3ABC} = p_i \, Q_{iABC} + \eta_i (Q_{iA} Q_{3BC} + Q_{iB} Q_{3AC} + Q_{iC} Q_{3AB}). \tag{E17}$$

Furthermore, differentiation of eq. (E11) with respect to γ_C and subsequent evaluation on Ω yields

$$P_{iABC} = \frac{\partial^{3} p_{i}}{\partial q_{K} \partial q_{L} \partial q_{M}} \mathcal{Q}_{KA} \mathcal{Q}_{LB} \mathcal{Q}_{MC}$$

$$+ \frac{\partial^{3} p_{i}}{\partial q_{K} \partial q_{L} \partial p_{M}^{(q)}} (\mathcal{Q}_{KA} \mathcal{Q}_{LB} \mathcal{P}_{MC} + \mathcal{Q}_{KA} \mathcal{Q}_{LC} \mathcal{P}_{MB} + \mathcal{Q}_{KB} \mathcal{Q}_{LC} \mathcal{P}_{MA})$$

$$+ \frac{\partial^{2} p_{i}}{\partial q_{k} \partial q_{L}} (\mathcal{Q}_{kAB} \mathcal{Q}_{LC} + \mathcal{Q}_{kAC} \mathcal{Q}_{LB} + \mathcal{Q}_{kBC} \mathcal{Q}_{LA})$$

$$+ \frac{\partial^{2} p_{i}}{\partial q_{k} \partial p_{L}^{(q)}} (\mathcal{Q}_{kAB} \mathcal{P}_{LC} + \mathcal{Q}_{kAC} \mathcal{P}_{LB} + \mathcal{Q}_{kBC} \mathcal{P}_{LA}$$

$$+ \mathcal{Q}_{kA} \mathcal{P}_{LBC} + \mathcal{Q}_{kB} \mathcal{P}_{LAC} + \mathcal{Q}_{kC} \mathcal{P}_{LAB})$$

$$+ \frac{\partial p_{i}}{\partial q_{k}} \mathcal{Q}_{kABC} + \frac{\partial p_{i}}{\partial p_{L}^{(q)}} \mathcal{P}_{kABC}.$$
(E18)

Eq. (E18) yields the derivatives $P_{i,ABC}$, after inserting values for the transformation coefficients given in Iversen *et al.* (2021). To find an expression for a corresponding quantity in ray-centred coordinates, \mathcal{P}_{MABC} , we first $P_{i,ABC}$ onto the basis vectors (\mathbf{e}_1 , \mathbf{e}_2),

$$\mathcal{E}_{iK}P_{iABC} = \mathcal{P}_{KABC} + \mathcal{E}_{iK}\eta_{i}\mathcal{Q}_{3ABC} + \mathcal{E}_{iK}\eta_{i}\eta_{j}\mathcal{E}_{jM}\left(\mathcal{Q}_{MA}\mathcal{Q}_{3BC} + \mathcal{Q}_{MB}\mathcal{Q}_{3AC} + \mathcal{Q}_{MC}\mathcal{Q}_{3AB}\right) - \mathcal{K}_{KM}\left(\mathcal{P}_{MA}\mathcal{Q}_{3BC} + \mathcal{P}_{MB}\mathcal{Q}_{3AC} + \mathcal{P}_{MC}\mathcal{Q}_{3AB}\right).$$
(E19)

Based on eq. (E5), the following relation holds in general,

$$\mathcal{K}_{KM}\mathcal{P}_{MC} = \mathcal{E}_{iK}\eta_i\eta_i\mathcal{E}_{iM}\mathcal{Q}_{MC} + \dot{\mathcal{E}}_{iK}P_{iC}. \tag{E20}$$

As a consequence, eq. (E19) can be recast as

$$\mathcal{P}_{MABC} = \mathcal{E}_{iM} (P_{iABC} - \eta_i \mathcal{Q}_{3ABC}) + \dot{\mathcal{E}}_{iM} (P_{iA} \mathcal{Q}_{3BC} + P_{iB} \mathcal{Q}_{3AC} + P_{iC} \mathcal{Q}_{3AB}).$$
 (E21)

In a similar way as in eq. (E14) it is in principle possible to write the quantity \mathcal{P}_{3ABC} in terms of quantities related to Cartesian coordinates. However, to avoid a very long expression we recommend to first transform all relevant quantities to ray-centred coordinates and then apply one of the relations (D12) or (D13).

APPENDIX F: ARBITRARY DEGREE OF THE HAMILTONIAN

In the main text, the Hamiltonian is assumed a homogeneous function of degree $\mathcal{N}=2$ in the momentum components. We describe here a generic approach, valid for any coordinate system, to make the higher-order dynamic ray tracing method correspond to an arbitrary value $\mathcal{N}\neq 0$. Moreover, for dynamic ray tracing in ray-centred coordinates we consider the specific actions needed to generalize the equations of the main text to such arbitrary \mathcal{N} .

In this Appendix we use the Hamiltonian (Klimeš 2002b, eq. 9)

$$\mathcal{H}^{(\mathcal{N})}(\mathbf{w}) = \frac{1}{\mathcal{N}} \left[G(\mathbf{w}) \right]^{\mathcal{N}/2},\tag{F1}$$

where the degree is signified by the superscript (\mathcal{N}) . If the Hamiltonian is a function of ray-centred phase-space coordinates the superscript is extended to $(\mathcal{N})(q)$. In eq. (F1) G is the specific eigenvalue of the Christoffel matrix corresponding to the elementary wave under consideration. From eq. (F1) it is clear that the Hamiltonians of degree 2 and \mathcal{N} are related by

$$\mathcal{H}^{(\mathcal{N})}(\mathbf{w}) = \frac{1}{\mathcal{N}} \left[2\mathcal{H}^{(2)}(\mathbf{w}) \right]^{\mathcal{N}/2}. \tag{F2}$$

F1 Derivatives of the Hamiltonian: Conversion from degree 2 to degree N and vice versa

Using eq. (F2) we relate the derivatives in phase space of the Hamiltonians $\mathcal{H}^{(2)}$ and $\mathcal{H}^{(N)}$. The phase space may correspond to Cartesian coordinates, ray-centred coordinates, or other coordinates. For the first four derivatives the conversion from derivatives of $\mathcal{H}^{(2)}$ to derivatives of $\mathcal{H}^{(N)}$ is stated

$$\mathcal{H}_r^{(\mathcal{N})} = \mathcal{H}_r^{(2)},\tag{F3}$$

$$\mathcal{H}_{rs}^{(\mathcal{N})} = (\mathcal{N} - 2) \,\mathcal{H}_{r}^{(2)} \,\mathcal{H}_{ss}^{(2)} + \,\mathcal{H}_{rs}^{(2)}, \tag{F4}$$

$$\mathcal{H}_{,rst}^{(\mathcal{N})} = (\mathcal{N} - 4)(\mathcal{N} - 2) \,\mathcal{H}_{,r}^{(2)} \,\mathcal{H}_{,s}^{(2)} \,\mathcal{H}_{,t}^{(2)} + (\mathcal{N} - 2) \left(\mathcal{H}_{,r}^{(2)} \,\mathcal{H}_{,st}^{(2)} + \,\mathcal{H}_{,s}^{(2)} \,\mathcal{H}_{,rt}^{(2)} + \,\mathcal{H}_{,t}^{(2)} \,\mathcal{H}_{,rs}^{(2)}\right) + \mathcal{H}_{,rst}^{(2)},$$
(F5)

$$\mathcal{H}_{,rstu}^{(\mathcal{N})} = (\mathcal{N} - 6)(\mathcal{N} - 4)(\mathcal{N} - 2) \,\mathcal{H}_{,r}^{(2)} \,\mathcal{H}_{,s}^{(2)} \,\mathcal{H}_{,t}^{(2)} \,\mathcal{H}_{,u}^{(2)} \\
+ (\mathcal{N} - 4)(\mathcal{N} - 2) \left(\mathcal{H}_{,r}^{(2)} \,\mathcal{H}_{,s}^{(2)} \,\mathcal{H}_{,tu}^{(2)} + \mathcal{H}_{,r}^{(2)} \,\mathcal{H}_{,t}^{(2)} \,\mathcal{H}_{,su}^{(2)} + \mathcal{H}_{,r}^{(2)} \,\mathcal{H}_{,su}^{(2)} + \mathcal{H}_{,s}^{(2)} \,\mathcal{H}_{,st}^{(2)} \\
+ \,\mathcal{H}_{,s}^{(2)} \,\mathcal{H}_{,tu}^{(2)} + \mathcal{H}_{,su}^{(2)} + \mathcal{H}_{,su}^{(2)} \,\mathcal{H}_{,rt}^{(2)} + \mathcal{H}_{,t}^{(2)} \,\mathcal{H}_{,tu}^{(2)} \right) \\
+ (\mathcal{N} - 2) \left(\mathcal{H}_{,rs}^{(2)} \,\mathcal{H}_{,tu}^{(2)} + \mathcal{H}_{,rt}^{(2)} \,\mathcal{H}_{,su}^{(2)} + \mathcal{H}_{,st}^{(2)} \,\mathcal{H}_{,ru}^{(2)} \\
+ \,\mathcal{H}_{,r}^{(2)} \,\mathcal{H}_{,stu}^{(2)} + \mathcal{H}_{,s}^{(2)} \,\mathcal{H}_{,rtu}^{(2)} + \mathcal{H}_{,t}^{(2)} \,\mathcal{H}_{,rsu}^{(2)} + \mathcal{H}_{,u}^{(2)} \,\mathcal{H}_{,rst}^{(2)} \right) \\
+ \,\mathcal{H}_{,rstu}^{(2)}. \tag{F6}$$

The reverse conversion of derivatives is given by

$$\mathcal{H}_r^{(2)} = \mathcal{H}_r^{(\mathcal{N})},\tag{F7}$$

$$\mathcal{H}_{,rs}^{(2)} = (2 - \mathcal{N}) \,\mathcal{H}_{,r}^{(\mathcal{N})} \,\mathcal{H}_{,s}^{(\mathcal{N})} + \,\mathcal{H}_{,rs}^{(\mathcal{N})},\tag{F8}$$

$$\mathcal{H}_{,rst}^{(2)} = (2 - 2\mathcal{N})(2 - \mathcal{N}) \,\mathcal{H}_{,r}^{(\mathcal{N})} \,\mathcal{H}_{,s}^{(\mathcal{N})} \,\mathcal{H}_{,t}^{(\mathcal{N})}$$

$$+ (2 - \mathcal{N}) \left(\mathcal{H}_{,r}^{(\mathcal{N})} \,\mathcal{H}_{,st}^{(\mathcal{N})} + \,\mathcal{H}_{,s}^{(\mathcal{N})} \,\mathcal{H}_{,rt}^{(\mathcal{N})} + \,\mathcal{H}_{,t}^{(\mathcal{N})} \,\mathcal{H}_{,rs}^{(\mathcal{N})} \right)$$

$$+ \,\mathcal{H}_{,rst}^{(\mathcal{N})}, \tag{F9}$$

$$\mathcal{H}_{,rstu}^{(2)} = (2 - 3\mathcal{N})(2 - 2\mathcal{N})(2 - \mathcal{N}) \,\mathcal{H}_{,r}^{(\mathcal{N})} \,\mathcal{H}_{,s}^{(\mathcal{N})} \,\mathcal{H}_{,t}^{(\mathcal{N})} \,\mathcal{H}_{,u}^{(\mathcal{N})} \\
+ (2 - 2\mathcal{N})(2 - \mathcal{N}) \left(\mathcal{H}_{,r}^{(\mathcal{N})} \,\mathcal{H}_{,s}^{(\mathcal{N})} \,\mathcal{H}_{,tu}^{(\mathcal{N})} + \mathcal{H}_{,r}^{(\mathcal{N})} \,\mathcal{H}_{,su}^{(\mathcal{N})} \,\mathcal{H}_{,su}^{(\mathcal{N})} \\
+ \mathcal{H}_{,r}^{(\mathcal{N})} \,\mathcal{H}_{,u}^{(\mathcal{N})} \,\mathcal{H}_{,st}^{(\mathcal{N})} + \mathcal{H}_{,s}^{(\mathcal{N})} \,\mathcal{H}_{,ru}^{(\mathcal{N})} \,\mathcal{H}_{,ru}^{(\mathcal{N})} \\
+ \mathcal{H}_{,s}^{(\mathcal{N})} \,\mathcal{H}_{,u}^{(\mathcal{N})} \,\mathcal{H}_{,rt}^{(\mathcal{N})} + \mathcal{H}_{,t}^{(\mathcal{N})} \,\mathcal{H}_{,u}^{(\mathcal{N})} \,\mathcal{H}_{,rsu}^{(\mathcal{N})} \right) \\
+ (2 - \mathcal{N}) \left(\mathcal{H}_{,rs}^{(\mathcal{N})} \,\mathcal{H}_{,tu}^{(\mathcal{N})} + \mathcal{H}_{,rt}^{(\mathcal{N})} \,\mathcal{H}_{,su}^{(\mathcal{N})} + \mathcal{H}_{,st}^{(\mathcal{N})} \,\mathcal{H}_{,ru}^{(\mathcal{N})} \\
+ \mathcal{H}_{,r}^{(\mathcal{N})} \,\mathcal{H}_{,stu}^{(\mathcal{N})} + \mathcal{H}_{,s}^{(\mathcal{N})} \,\mathcal{H}_{,rtu}^{(\mathcal{N})} + \mathcal{H}_{,t}^{(\mathcal{N})} \,\mathcal{H}_{,rsu}^{(\mathcal{N})} \right) \\
+ \mathcal{H}_{,rstu}^{(\mathcal{N})} . \tag{F10}$$

F2 Conventional dynamic ray tracing in ray-centred coordinates with a Hamiltonian of arbitrary degree

Dynamic ray tracing in ray-centred coordinates with a Hamiltonian of arbitrary degree in the momentum components has been described by Klimeš (2002b). We briefly review the modifications needed, relatively to using a Hamiltonian of the second degree.

F2.1 Coefficients of the conventional (first-order) dynamic ray tracing system

Applying equations (17)–(18) in eq. (F4), it is clear that eq. (33) in the main text transforms to (Klimeš 2002b, eq. 50)

$$\{\mathcal{H}_{,yz}^{(\mathcal{N})(q)}\} = \begin{pmatrix} \left\{ U_{IJ}^{(2)(q)} \right\} & \left\{ 0_{I1} \right\} & \left\{ W_{IJ}^{(2)(q)} \right\}^2 \right\} & \left\{ 0_{I1} \right\} \\ \left\{ 0_{1J} \right\} & 0 & \left\{ 0_{1J} \right\} & 0 \\ \left\{ W_{IJ}^{(2)(q)} \right\}^2 \right\}^T & \left\{ 0_{I1} \right\} & \left\{ V_{IJ}^{(2)(q)} \right\} & \left\{ 0_{I1} \right\} \\ \left\{ 0_{1J} \right\} & 0 & \left\{ 0_{1J} \right\} & \mathcal{N} - 1 \end{pmatrix}.$$
(F11)

Thus, it is clear that

$$U_{IJ}^{(\mathcal{N})(q)} = U_{IJ}^{(2)(q)}, \qquad W_{IJ}^{(\mathcal{N})(q) \, 12} = W_{IJ}^{(2)(q) \, 12}, \qquad V_{IJ}^{(\mathcal{N})(q)} = V_{IJ}^{(2)(q)},$$
 (F12)

and the only coefficient of the (complete) dynamic ray tracing system affected by ${\mathcal N}$ is

$$V_{33}^{(\mathcal{N})(q)} = \mathcal{N} - 1. \tag{F13}$$

In view of the above, the paraxial and ray-tangent solutions of dynamic ray tracing do not depend on the value of \mathcal{N} — only the non-eikonal solution is affected.

F2.2 Non-eikonal solution

The non-eikonal solution for the case $\mathcal{N}=2$ is given by eqs (51)–(52). For a general degree \mathcal{N} of the Hamiltonian, the non-eikonal solution is restated

$$\frac{\partial q_i}{\partial \gamma_6} = (\mathcal{N} - 1)(\tau - \tau_0)\delta_{i3}, \qquad \frac{\partial p_i^{(q)}}{\partial \gamma_6} = \delta_{i3} \tag{F14}$$

in ray-centred coordinates (Klimeš 2002b, second sub-eq. 53) and

$$\frac{\partial x_i}{\partial \gamma_6} = (\mathcal{N} - 1)(\tau - \tau_0)v_i, \qquad \frac{\partial x_i}{\partial \gamma_6} = p_i + (\mathcal{N} - 1)(\tau - \tau_0)\eta_i \tag{F15}$$

in Cartesian coordinates (Klimeš 2002b, second sub-eq. 55).

F2.3 Continuation of basis vectors along the reference ray: Special case

Consider the continuation of the basis vectors $\mathcal{E} = \{\mathcal{E}_{mI}\}$ under the condition $W_{IJ}^{(\mathcal{N})(q)} = 0$. Using eq. (F8) in eq. (35) yields (Klimeš 2002b, eq. 52a)

$$\frac{\mathrm{d}\mathcal{E}_{mI}}{\mathrm{d}\tau} = \left[W_{nm}^{(\mathcal{N}) \ 12} + (\mathcal{N} - 1)v_m \eta_n \right] \mathcal{E}_{nI}. \tag{F16}$$

We note that the left-hand side of this equation is unchanged relatively to the $\mathcal{N}=2$ situation.

For matrix K the condition $W_{IJ}^{(N)(q)} = 0$ implies that eq. (36) is restated (Klimeš 2006b, eq. 115)

$$\mathcal{K}_{MN} = \mathcal{E}_{iM} W_{ij}^{(\mathcal{N}) \, 12} \mathcal{F}_{jN}. \tag{F17}$$

However, even though the quantity \mathcal{N} appears on the right-hand side of (F17), the left-hand side, \mathcal{K}_{MN} , does not depend on \mathcal{N} .

F3 Higher-order dynamic ray tracing in ray-centred coordinates with a Hamiltonian of arbitrary degree

For the higher-order reduced dynamic ray tracing systems in ray-centred coordinates we examine the effect of the quantity \mathcal{N} .

F3.1 Coefficients for second-order dynamic ray tracing

Eq. (F5) yields

$$U_{IJK}^{(\mathcal{N})(q)} = U_{IJK}^{(2)(q)}, W_{IJK}^{(\mathcal{N})(q) \, 112} = W_{IJK}^{(2)(q) \, 112}, W_{IJK}^{(\mathcal{N})(q) \, 122} = W_{IJK}^{(2)(q) \, 122}, V_{IJK}^{(\mathcal{N})(q)} = V_{IJK}^{(2)(q)}. (F18)$$

We observe that the coefficients of the reduced ODE system for second-order dynamic ray tracing do not depend on \mathcal{N} .

F3.2 Coefficients for third-order dynamic ray tracing

We use eq. (F5) to write an expression for third-order derivatives of the Hamiltonian $\mathcal{H}^{(\mathcal{N})(q)}$ included among the coefficients for third-order dynamic ray tracing,

$$\mathcal{H}_{LJ3}^{(\mathcal{N})(q),i'j'2} = (\mathcal{N} - 2) \,\mathcal{H}_{LJ}^{(2)(q),i'j'} + \,\mathcal{H}_{LJ3}^{(2)(q),i'j'2}. \tag{F19}$$

Here we have utilized the auxiliary upper/lower indexing system introduced in Appendix A.

Applying the sub-eqs of (B27) in (F19), we obtain

$$W_{IJ3}^{(\mathcal{N})(q) \, 112} = \mathcal{N} \, U_{IJ}^{(2)(q)}, \tag{F20}$$

$$W_{IJ3}^{(\mathcal{N})(q) \, 122} = (\mathcal{N} - 1) \, W_{IJ}^{(2)(q) \, 12}, \tag{F21}$$

$$V_{IJ3}^{(\mathcal{N})(q)} = (\mathcal{N} - 2) V_{IJ}^{(2)(q)}.$$
 (F22)

Furthermore, using eq. (F6), the effect of \mathcal{N} on the fourth-order derivatives of the Hamiltonian can be expressed compactly as

$$\mathcal{H}_{,IJKL}^{(\mathcal{N})(q),i'j'k'l'} = (\mathcal{N} - 2) \left(\mathcal{H}_{,IJ}^{(2)(q),i'j'} \mathcal{H}_{,KL}^{(2)(q),k'l'} + \mathcal{H}_{,IK}^{(2)(q),i'k'} \mathcal{H}_{,JL}^{(2)(q),j'l'} + \mathcal{H}_{,IL}^{(2)(q),i'l'} \mathcal{H}_{,JL}^{(2)(q),j'l'} + \mathcal{H}_{,IL}^{(2)(q),i'l'} \mathcal{H}_{,JK}^{(2)(q),j'k'} \right) + \mathcal{H}_{IJKI}^{(2)(q),i'j'k'l'}.$$
(F23)

With the help of eq. (F23) we obtain the following specific conversion formulas for the fourth-order coefficients,

$$U_{IJKL}^{(\mathcal{N})(q)} = (\mathcal{N} - 2) \left(U_{IJ}^{(2)(q)} U_{KL}^{(2)(q)} + U_{IK}^{(2)(q)} U_{JL}^{(2)(q)} + U_{IL}^{(2)(q)} U_{JK}^{(2)(q)} \right) + U_{IJKL}^{(2)(q)}, \tag{F24}$$

$$W_{IJKL}^{(\mathcal{N})(q) \, 1112} = (\mathcal{N} - 2) \left(U_{IJ}^{(2)(q)} W_{KL}^{(2)(q) \, 12} + U_{IK}^{(2)(q)} W_{JL}^{(2)(q) \, 12} + U_{JK}^{(2)(q) \, W_{IL}^{(2)(q) \, 12}} \right) + W_{IJKL}^{(2)(q) \, 1112}, \tag{F25}$$

$$W_{IJKL}^{(\mathcal{N})(q) \, 1122} = (\mathcal{N} - 2) \left(U_{IJ}^{(2)(q)} V_{KL}^{(2)(q)} + W_{IK}^{(2)(q) \, 12} W_{JL}^{(2)(q) \, 12} + W_{IL}^{(2)(q) \, 12} W_{JK}^{(2)(q) \, 12} \right) + W_{IJKI}^{(2)(q) \, 1122}, \tag{F26}$$

$$W_{IJKL}^{(\mathcal{N})(q)}^{(2)(q)} = (\mathcal{N} - 2) \left(W_{IJ}^{(2)(q)} V_{KL}^{(2)(q)} + W_{IK}^{(2)(q)} V_{JL}^{(2)(q)} + W_{IL}^{(2)(q)} V_{JK}^{(2)(q)} \right) + W_{IJKL}^{(2)(q)} V_{IJ}^{(2)(q)}$$

$$+ W_{IJKL}^{(2)(q)} V_{IJ}^{(2)(q)} V_{IJ}^{(2)(q)} + W_{IJ}^{(2)(q)} V_{IJ}^{(2)(q)} + W_{IJ}^{(2)(q)} V_{JK}^{(2)(q)}$$
(F27)

$$V_{IJKL}^{(\mathcal{N})(q)} = (\mathcal{N} - 2) \left(V_{IJ}^{(2)(q)} V_{KL}^{(2)(q)} + V_{IK}^{(2)(q)} V_{JL}^{(2)(q)} + V_{JK}^{(2)(q)} V_{IL}^{(2)(q)} \right) + V_{IJKI}^{(2)(q)}.$$
(F28)

We see from eqs (F19)–(F28) that some coefficients of the third-order reduced dynamic ray tracing system depend on the quantity \mathcal{N} . However, one can show, using the theory provided in this paper, that the terms including \mathcal{N} on the right-hand side of the ODEs cancel out. As we would expect, the ODEs for third-order dynamic ray tracing of the paraxial solutions are therefore not influenced by the value of \mathcal{N} . The proof is left as an exercise to the interested reader.